



Search for dark mesons decaying to top and bottom quarks in proton–proton collisions at $\sqrt{s} = 13$ TeV with the ATLAS detector

The ATLAS Collaboration

A search for dark mesons originating from strongly-coupled, $SU(2)$ dark flavor symmetry conserving models and decaying gaugephobically to pure Standard Model final states containing top and bottom quarks is presented. The search targets fully hadronic final states and final states with exactly one electron or muon and multiple jets. The analyzed data sample corresponds to an integrated luminosity of 140 fb^{-1} of proton–proton collisions collected at $\sqrt{s} = 13$ TeV with the ATLAS detector at the Large Hadron Collider. No significant excess over the Standard Model background expectation is observed and the results are used to set the first direct constraints on this type of model. The two-dimensional signal space of dark pion masses m_{π_D} and dark rho-meson masses m_{ρ_D} is scanned. For $m_{\pi_D}/m_{\rho_D} = 0.45$, dark pions with masses $m_{\pi_D} < 940$ GeV are excluded at the 95% CL, while for $m_{\pi_D}/m_{\rho_D} = 0.25$ masses $m_{\pi_D} < 740$ GeV are excluded.

Contents

1	Introduction	2
2	ATLAS detector	5
3	Data and simulated event samples	6
3.1	Signal samples	6
3.2	Background samples	7
4	Object and event selections	9
5	Analysis strategy	12
5.1	All-hadronic channel	12
5.2	One-lepton channel	13
6	Background estimate	15
6.1	All-hadronic channel	15
6.2	One-lepton channel	17
7	Systematic uncertainties	18
7.1	Experimental uncertainties	18
7.2	Modeling uncertainties in background simulations	19
7.3	Data-driven background estimation uncertainties	20
8	Statistical analysis and results	20
8.1	All-hadronic channel	21
8.2	One-lepton channel	22
9	Interpretation	23
10	Conclusion	29

1 Introduction

The Standard Model (SM) can be extended by a new strongly-coupled, confining gauge theory with fermion representation which transforms under the electroweak group. The appeal of such an extension is that dark matter can arise in the form of composite mesons or baryons of the new strongly-coupled theory. In addition, these models often exhibit an automatic accidental symmetry protecting against dark matter decay. Consequently, candidates for strongly-coupled dark matter include dark mesons, dark quarkonia-like states, glueballs and dark baryons [1, 2]. The search presented here targets one set of models incorporating this concept: Stealth Dark Matter [3]. Here, the new strongly-coupled dark sector consists of vector-like fermions that can transform under the new dark group but also interact with both the electroweak sector of the SM and the Higgs boson. The result is the emergence of a quantum chromodynamics (QCD)-like dark sector as the direct analog to the QCD meson and baryon sector. This leads to several intriguing phenomenological consequences: as long as the vector-like mass is dominant over the chiral mass, the new dark sector is only weakly constrained by precision electroweak or Higgs coupling measurements,

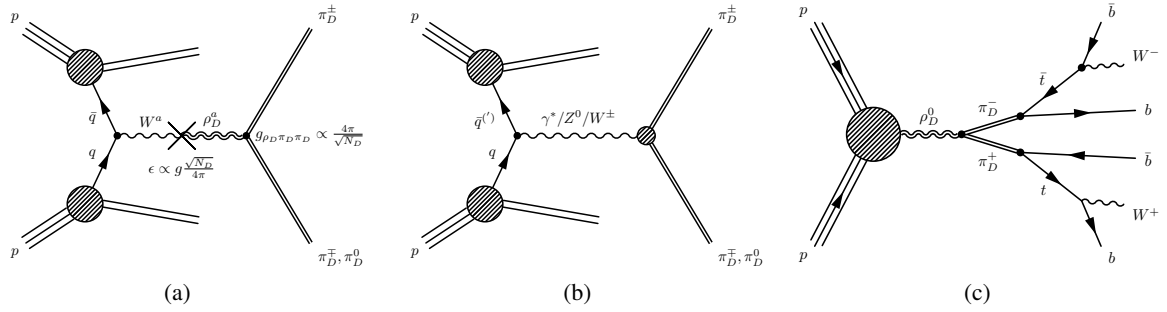


Figure 1: Examples of leading Feynman diagrams of dark pion pair production. The diagram in (a) shows resonant production via kinetic mixing with the W -field resulting in either a neutral or charged dark rho meson, a mixing with the B -field that can only result in a neutral dark rho meson is also possible, (b) shows Drell–Yan-type pair production of dark pions, and (c) shows an illustrative diagram of the dark pion decay into a top and a bottom quark for dark pion production.

while the Higgs interactions break the dark sector global symmetry and thus allow dark mesons to decay into pure SM states [4]. This search focuses on the low-energy effective theories developed in Ref. [5], which incorporate the leading interactions between dark mesons of a strongly-coupled $SU(2)$ dark flavor symmetry preserving dark sector and the SM. These models contain a stable dark scalar baryon which could account for the stable dark matter observed in cosmological measurements [3].

The simplified model targeted in this search contains only the two phenomenologically relevant sets of dark mesons: a lighter pseudoscalar triplet of dark pions, π_D , and an additional triplet of dark rho vector mesons, ρ_D , which are both expected at a scale around or slightly above the electroweak scale. Following standard theoretical assumptions, the triplets are completely mass-degenerate and the dark sector can be fully described by three parameters: the mass of the dark pions m_{π_D} , the mass of the dark rho mesons m_{ρ_D} , and the number of dark colors N_D . Since the phenomenological consequences remain unchanged for values of N_D that are not excessively large, N_D is fixed to $N_D = 4$ throughout this search following the typical choice made for Stealth Dark Matter [3].

Contrary to QCD, the vector-like nature of the dark sector allows to either gauge the full $SU(2)_L$ weak interaction symmetry group or just the underlying $U(1)$ group, which leads to two distinct models of kinetic mixing of dark mesons with the SM, $SU(2)_L$ and $SU(2)_R$. The phenomenological consequences manifest themselves in the allowed decay channels and production cross-sections of dark pions, where the $SU(2)_L$ models result in considerably larger cross sections than the $SU(2)_R$ models. Dark pions are always pair-produced either via Drell–Yan-type processes or resonantly via kinetic mixing of SM electroweak gauge bosons with the ρ_D that then subsequently decays into a pair of dark pions, as shown in Figure 1. The kinetic mixing parameter ϵ depends on the number of dark colors as shown in Figure 1(a) (see also Ref. [4]). Throughout nearly all of the parameter space investigated in this search, the resonant production dominates the production of dark pions. Once the choice of $N_D = 4$ is made, the production cross-section depends trivially on the ratio of the dark pion and dark rho-meson masses, for which the symbol $\eta_D = m_{\pi_D}/m_{\rho_D}$ is used, equivalent to the η defined in Ref. [4]. For gaugephobic $SU(2)_L$ models, a given dark pion mass and η_D -parameter fully specify the model, including the dark pion decay branching fractions.

This search considers only models with $\eta_D < 0.5$ where the decay $\rho_D^{\pm,0} \rightarrow \pi_D^{\pm} \pi_D^{0,\mp}$ has a branching fraction of nearly 1.0, while for models with $\eta_D > 0.5$ this decay is kinematically forbidden and the dark rho meson can only decay to pairs of leptons or quarks. Previous searches for resonances in the dilepton spectrum

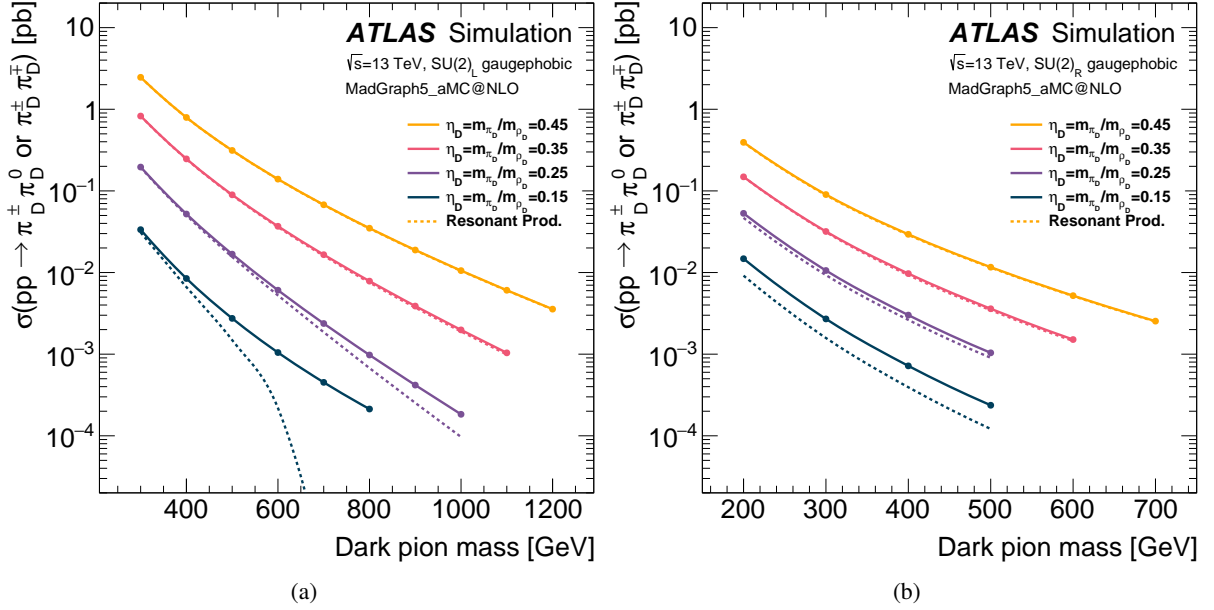


Figure 2: Pair-production cross-sections for dark pions as a function of dark pion mass for four different values of η_D in (a) an $SU(2)_L$ model and (b) an $SU(2)_R$ model. The dashed colored lines indicate the contribution of the resonant production mode to the total dark pion production cross-section.

both in ATLAS [6] and CMS [7] have placed strong constraints on such models [4]. The bounds for models with $\eta_D < 0.5$ are considerably weaker [2]. This is the first search in any collider experiment optimized for this specific type of model.

Figure 2 shows the pair-production cross-sections for dark pions in $SU(2)_L$ and $SU(2)_R$ models. The contribution of resonant production to the total production cross-section is indicated by the dashed lines. A variety of different decay channels are open to dark pions in the available parameter space. The most relevant channels and their branching fractions are shown in Figure 3. For gaugephobic models the decay to top and bottom quarks dominates at high masses, while decays to bottom and charm quarks, τ -leptons and gauge bosons are relevant at lower dark pion masses.

This search is the result of the analysis of 140 fb^{-1} of proton–proton (pp) collisions collected by the ATLAS detector during Run 2 of the Large Hadron Collider (LHC). Since the dark pions are pair-produced in the model considered, the experimental signatures are either three top quarks and one bottom quark ($tttb$) or two top quarks and two bottom quarks ($ttbb$)¹. About one third of dark pions in the $SU(2)_L$ models are neutral, resulting in the $tttb$ event signature being twice as likely as the $ttbb$ signature. These processes can give rise to several different final states depending on the hadronic or semileptonic decay mode of each of the top quarks. The search is performed in the *all-hadronic* channel, targeting fully hadronic top quark decays where the signal results in eight to ten jets of which at least four originate from bottom quarks, and in the *one-lepton* channel, corresponding to final states with exactly one electron or muon in addition to up to four jets from b-quarks.

The results are interpreted as limits on the production cross-section of dark pion pairs as a function of m_{π_D} and η_D .

¹ The label " $tttb$ " is used to indicate both $t\bar{t}b$ as well as its charge conjugate, $t\bar{t}\bar{b}$; whereas " $ttbb$ " refers to $t\bar{t}b\bar{b}$.

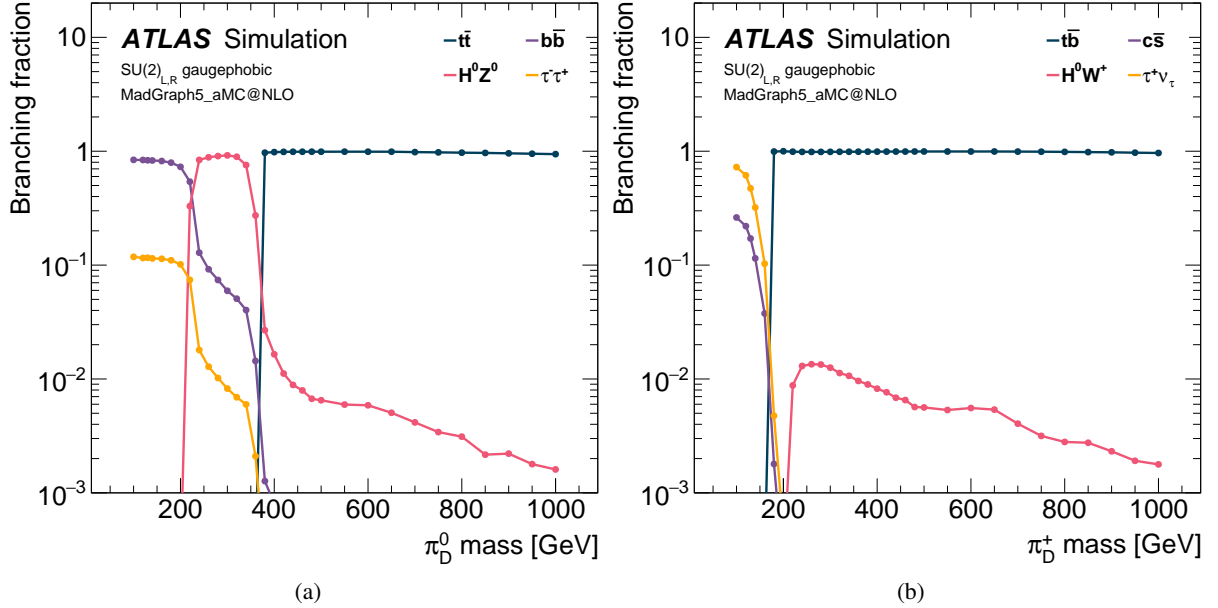


Figure 3: Branching fractions of the available decays of dark pions from gaugephobic $SU(2)_L$ and $SU(2)_R$ models are shown for (a) neutral dark pions and (b) positively charged dark pions. Channels with small branching fractions are suppressed for clarity.

2 ATLAS detector

The ATLAS detector [8] at the LHC covers nearly the entire solid angle around the collision point.² It consists of an inner tracking detector surrounded by a thin superconducting solenoid, electromagnetic and hadronic calorimeters, and a muon spectrometer incorporating three large superconducting air-core toroidal magnets.

The inner-detector system (ID) is immersed in a 2 T axial magnetic field and provides charged-particle tracking in the range $|\eta| < 2.5$. The high-granularity silicon pixel detector covers the vertex region and typically provides four measurements per track, the first hit generally being in the insertable B-layer (IBL) installed before Run 2 [9, 10]. It is followed by the SemiConductor Tracker (SCT), which usually provides eight measurements per track. These silicon detectors are complemented by the transition radiation tracker (TRT), which enables radially extended track reconstruction up to $|\eta| = 2.0$. The TRT also provides electron identification information based on the fraction of hits (typically 30 in total) above a higher energy-deposit threshold corresponding to transition radiation.

The calorimeter system covers the pseudorapidity range $|\eta| < 4.9$. Within the region $|\eta| < 3.2$, electromagnetic calorimetry is provided by barrel and endcap high-granularity lead/liquid-argon (LAr) calorimeters, with an additional thin LAr presampler covering $|\eta| < 1.8$ to correct for energy loss in material

² ATLAS uses a right-handed coordinate system with its origin at the nominal interaction point (IP) in the center of the detector and the z -axis along the beam pipe. The x -axis points from the IP to the center of the LHC ring, and the y -axis points upwards. Polar coordinates (r, ϕ) are used in the transverse plane, ϕ being the azimuthal angle around the z -axis. The pseudorapidity is defined in terms of the polar angle θ as $\eta = -\ln \tan(\theta/2)$ and is equal to the rapidity $y = \frac{1}{2} \ln \left(\frac{E+p_z c}{E-p_z c} \right)$ in the relativistic limit. Angular distance is measured in units of $\Delta R \equiv \sqrt{(\Delta y)^2 + (\Delta \phi)^2}$.

upstream of the calorimeters. Hadronic calorimetry is provided by the steel/scintillator-tile calorimeter, segmented into three barrel structures within $|\eta| < 1.7$, and two copper/LAr hadronic endcap calorimeters. The solid angle coverage is completed with forward copper/LAr and tungsten/LAr calorimeter modules optimized for electromagnetic and hadronic energy measurements respectively.

The muon spectrometer (MS) comprises separate trigger and high-precision tracking chambers measuring the deflection of muons in a magnetic field generated by the superconducting air-core toroidal magnets. The field integral of the toroids ranges between 2.0 and 6.0 T m across most of the detector. Three layers of precision chambers, each consisting of layers of monitored drift tubes, cover the region $|\eta| < 2.7$, complemented by cathode-strip chambers in the forward region, where the background is highest. The muon trigger system covers the range $|\eta| < 2.4$ with resistive-plate chambers in the barrel, and thin-gap chambers in the endcap regions.

The luminosity is measured mainly by the LUCID-2 [11] detector that records Cherenkov light produced in the quartz windows of photomultipliers located close to the beam pipe.

Events are selected by the first-level trigger system implemented in custom hardware, followed by selections made by algorithms implemented in software in the high-level trigger [12]. The first-level trigger accepts events from the 40 MHz bunch crossings at a rate below 100 kHz, which the high-level trigger further reduces in order to record complete events to disk at about 1 kHz.

A software suite [13] is used in data simulation, in the reconstruction and analysis of real and simulated data, in detector operations, and in the trigger and data acquisition systems of the experiment.

3 Data and simulated event samples

This analysis is performed using data from pp collisions with $\sqrt{s} = 13$ TeV recorded by the ATLAS detector in 2015–2018. Only events for which all relevant subsystems were operational are considered. The data correspond to an integrated luminosity of $140.1 \pm 1.2 \text{ fb}^{-1}$ [14].

Monte Carlo (MC) simulated event samples are used for the estimate of background from SM processes and to model the targeted signal models. The details of the event generation are provided in Sections 3.1 and 3.2 for signal and background samples, respectively. The generation of all simulated event samples includes the effect of multiple pp interactions per bunch crossing, as well as changes in detector response due to interactions in bunch crossings before or after the one containing the hard interaction, modeled by overlaying simulated inelastic events on the physics event. These two effects are referred to as pileup. The simulated event samples are processed with the GEANT4-based ATLAS detector simulation [15, 16]. All samples are weighted to match the pileup distribution observed in data and are processed with the same reconstruction algorithms as data.

3.1 Signal samples

Signal samples are generated in a grid over a two-dimensional space, varying the dark pion mass m_{π_D} between 300 – 1200 GeV and the η_D -parameter between 0.15 – 0.45. The matrix element calculation for the pair production of dark pions is performed at next-to-leading order (NLO) in QCD based on the model described in Ref. [4] using MADGRAPH5_aMC@NLO v2.4.3 [17] interfaced with PYTHIA8.212 [18] for the

Table 1: Overview of the configuration of all nominal background samples used in the analysis; details and definitions are provided in the text.

Process	Generator	PDF	Showering	Tune	Cross section
$t\bar{t}$	POWHEGBOX v2	NNPDF3.0NLO	PYTHIA8	A14	NNLO+NNLL
$t\bar{t}b\bar{b}$	POWHEG BOX RES	NNPDF3.0NLO	PYTHIA8	A14	NLO
$V + \text{jets}$	SHERPA v2.2.11	NNPDF3.0NNLO	SHERPA	Def.	NLO
Single top	POWHEGBOX v2	NNPDF3.0NLO	PYTHIA8	A14	NLO+NNLL
$t\bar{t}t\bar{t}$	MADGRAPH5_aMC@NLO v2.4.3	NNPDF3.1NLO	PYTHIA8	A14	NLO
$t\bar{t}V$	MADGRAPH5_aMC@NLO v2.3.3	NNPDF3.0NLO	PYTHIA8	A14	NLO
$t\bar{t}H$	POWHEGBOX v2	NNPDF3.0NLO	PYTHIA8	A14	NLO
Other $t\bar{t}+X$	MADGRAPH5_aMC@NLO	NNPDF2.3LO	PYTHIA8	A14	NLO
Multiboson	SHERPA v2.2.1/v2.2.2	NNPDF3.0NNLO	SHERPA	Def.	NLO

modeling of parton showering, hadronization and underlying event using the A14 set of tuned parameters ("tune") [19] and the NNPDF2.3LO [20] set of parton distribution functions (PDF).

The decays of bottom and charm hadrons are simulated using the EVTGEN v1.6.0 program [21]. An additional set of signal samples, with parameter values near the expected exclusion contour of the all-hadronic channel, is generated at NLO in QCD using MADGRAPH5_aMC@NLO v2.9.9 [17] interfaced with PYTHIA8.306 [22] using the A14 tune and NNPDF2.3LO PDF set. Kinematic distributions match in both setups. All signal cross-sections are extracted from MADGRAPH5_aMC@NLO v2.9.9. The number of dark colors N_D is set to 4 for all signal points. The dark pion decays are simulated using the narrow width approximation and contain all possible decay channels from Figure 3.

3.2 Background samples

The dominant SM background process in the all-hadronic channel is multijet production. This background is estimated with data-driven methods while MC simulation is used to estimate the remaining SM processes. The background in the one-lepton channel is estimated from MC simulations and is dominated by top quark pair-production ($t\bar{t}$), often in association with heavy-flavor quarks ($t\bar{t}+HF$). Other important backgrounds are the production of a vector boson in association with jets ($V + \text{jets}$) and single top-quark production (single top) which is dominated by the associated production of a top quark with a W boson but also contains single top-quark production in the s - and t -channels. Smaller background contributions stem from $t\bar{t}$ produced in association with additional bosons or quarks ($t\bar{t}t\bar{t}$, $t\bar{t}V$, $t\bar{t}H$, and other $t\bar{t}+X$) and multiboson production. The configurations used to produce the background samples are described below and are summarized in Table 1. For all background samples, except those generated with SHERPA, the EVTGEN v.1.6.0 or v1.7.0 program is used to simulate the decays of bottom and charm hadrons.

3.2.1 $t\bar{t}$ background

The production of $t\bar{t}$ events is modeled using the POWHEGBOX v2 [23–26] generator that provides matrix elements at NLO in QCD with the NNPDF3.0NLO [27, 28] set PDFs and the h_{damp} parameter, which controls the matching in POWHEG and effectively regulates the high- p_T radiation against which the $t\bar{t}$ system recoils, set to $1.5 m_{\text{top}}$ [29]. The functional form of the renormalization and factorization scales

are set to the default scale $\sqrt{m_{\text{top}}^2 + p_{\text{T}}^2}$. The events are interfaced with PYTHIA8.230 for the parton shower and hadronization, using the A14 set of tuned parameters and the NNPDF2.3LO PDF set. The $t\bar{t}$ sample is normalized to the cross section prediction at next-to-next-to-leading order (NNLO) in QCD including the resummation of next-to-next-to-leading-logarithmic (NNLL) soft-gluon terms calculated using TOP++2.0 [30–36]. For pp collisions at a center-of-mass energy of $\sqrt{s} = 13$ TeV, this cross section corresponds to $\sigma(t\bar{t})_{\text{NNLO+NNLL}} = 832 \pm 51$ pb using a top-quark mass of $m_{\text{top}} = 172.5$ GeV.

The inclusive $t\bar{t}$ sample described above is complemented by a dedicated sample in which a pair of top quarks is produced in association with two b -quarks. Events are simulated with the POWHEG BOX RES [37] generator and OPENLOOPS 1 [38–40], using a pre-release of the implementation of this process in POWHEG BOX RES provided by the authors [41], with the NNPDF3.0NLO PDF set. It is interfaced with PYTHIA8.240, using the A14 set of tuned parameters and the NNPDF2.3LO PDF set. The four-flavor scheme is used with the b -quark mass set to 4.95 GeV. The factorization scale and h_{damp} parameter are both set to $0.5 \times \sum_{i=\bar{t}, \bar{t}, b, \bar{b}, j} m_{\text{T}, i}$, and the renormalization scale is set to $\sqrt[4]{m_{\text{T}}(t) \cdot m_{\text{T}}(\bar{t}) \cdot m_{\text{T}}(b) \cdot m_{\text{T}}(\bar{b})}$. This $t\bar{t}b\bar{b}$ sample is used in the one-lepton channel where the dominant background comes from $t\bar{t}$ production, whereas the multijet-dominated all-hadronic channel relies on the five-flavor scheme inclusive sample alone.

Previous studies have seen improved agreement between data and prediction in $t\bar{t}$ events, particularly for the top-quark p_{T} distribution, when comparing with NNLO calculations [42]. Top-quark pair differential calculations at NNLO QCD accuracy including electroweak (EW) corrections have become available [43]. Hence, a small improvement to the modeling is incorporated by correcting the $t\bar{t}$ and the $t\bar{t}b\bar{b}$ samples to match their top/antitop-quark p_{T} and the top-quark mass distribution to the accuracy predicted at NNLO in QCD and NLO in EW.

Events in the $t\bar{t}$ and $t\bar{t}b\bar{b}$ samples are classified according to the flavor of the particle jets not originating from the top quark. The particle jets are reconstructed from the simulated stable particles using the anti- k_t algorithm [44, 45] with a radius parameter $R = 0.4$, and are required to have $p_{\text{T}} > 15$ GeV and $|\eta| < 2.5$. Events are labeled as $t\bar{t} + \geq 1b$ if at least one particle jet is matched within $\Delta R < 0.4$ to b -hadrons with $p_{\text{T}} > 5$ GeV that do not arise from the decay of top quarks. In the remaining events, if at least one particle jet is matched within $\Delta R < 0.4$ to additional c -hadrons with $p_{\text{T}} > 5$ GeV, the events are classified as $t\bar{t} + \geq 1c$. All other events are labeled as $t\bar{t} + \text{light}$. The $t\bar{t}b\bar{b}$ sample is used for the $t\bar{t} + \geq 1b$ category meaning that all $t\bar{t} + \text{light}$ and $t\bar{t} + \geq 1c$ events are rejected from this sample. Likewise, only the $t\bar{t} + \text{light}$ and $t\bar{t} + \geq 1c$ events are retained from the inclusive $t\bar{t}$ sample.

3.2.2 Other backgrounds

The production of $V + \text{jets}$ is simulated with the SHERPA v2.2.11 [46] generator using NLO matrix elements for up to two partons, and leading-order (LO) matrix elements for up to five partons calculated with the Comix [47] and OPENLOOPS 1 libraries. They are matched with the SHERPA parton shower [48] using the MEPS@NLO prescription [49–52] and the set of tuned parameters developed by the SHERPA authors. The HESSIAN NNPDF3.0NNLO PDF set is used and the samples are normalized to a prediction that is NNLO in QCD [53].

The associated production of a top quark with a W bosons (tW) is modeled using the POWHEGBOX v2 [24–26, 54] generator at NLO in QCD using the five-flavor scheme and the NNPDF3.0NLO PDF set. The diagram removal scheme [55] is used to remove interference and overlap with $t\bar{t}$ production. The related uncertainty

is estimated by comparing with an alternative sample generated using the diagram subtraction scheme [29, 55]. Single top-quark t -channel production is modeled using the POWHEGBOX v2 [24–26, 56] generator at NLO in QCD using the four-flavor scheme and the corresponding NNPDF3.0_{NLO} PDF set. Single top-quark s -channel production is modeled using the POWHEGBOX v2 [24–26, 57] generator at NLO in QCD in the five-flavor scheme with the NNPDF3.0_{NLO} PDF set. All single top-quark events are processed through PYTHIA8.230 using the A14 tune and the NNPDF2.3_{LO} PDF set.

The production of $t\bar{t}\bar{t}$ events is modeled using the MADGRAPH5_aMC@NLO v2.4.3 generator which provides matrix elements at NLO in QCD with the NNPDF3.1_{NLO} [27] PDF set. The functional form of the renormalization and factorization scales is set to $0.25 \times \sum_i \sqrt{m_i^2 + p_{T,i}^2}$, where the sum runs over all the particles generated from the matrix element calculation, following Ref. [58]. Top quarks are decayed at LO using MADSPIN [59, 60] to preserve all spin correlations. The events are interfaced with PYTHIA8.230 for the parton shower and hadronization, using the A14 set of tuned parameters and the NNPDF2.3_{LO} PDF set.

The production of $t\bar{t}V$ events is modeled using the MADGRAPH5_aMC@NLO v2.3.3 generator at NLO in QCD with the NNPDF3.0_{NLO} PDF set. The events are interfaced to PYTHIA8.210 using the A14 tune and the NNPDF2.3_{LO} PDF set.

The production of $t\bar{t}H$ events is modeled using the POWHEGBOX v2 [23–26, 61] generator at NLO in QCD with the NNPDF3.0_{NLO} PDF set. The events are interfaced to PYTHIA8.230 using the A14 tune and the NNPDF2.3_{LO} PDF set.

Further rare top-quark-pair backgrounds ttt , $t\bar{t}ZZ$, $t\bar{t}WW$, $t\bar{t}WZ$, $t\bar{t}WH$ and $t\bar{t}HH$ are all produced using the NLO in QCD MADGRAPH5_aMC@NLO generator interfaced with PYTHIA8 using the A14 set of tuned parameters and scaled to NLO cross sections [62].

Samples of diboson final states (VV) are simulated with the SHERPA v2.2.1 or v2.2.2 [46] generator depending on the process, including off-shell effects and Higgs-boson contributions, where appropriate. Semileptonic final states, where one boson decays leptonically and the other hadronically, are generated using matrix elements at NLO accuracy in QCD for up to one additional parton and at LO accuracy for up to three additional parton emissions. Samples for the loop-induced processes $gg \rightarrow VV$ are generated using LO-accurate matrix elements for up to one additional parton emission. The matrix element calculations are matched and merged with the SHERPA parton shower based on Catani–Seymour dipole factorization [47, 48] using the MEPS@NLO prescription. The virtual QCD corrections are provided by the OPENLOOPS 1 library. The NNPDF3.0_{NLO} PDF set is used, along with the dedicated set of tuned parton-shower parameters developed by the SHERPA authors.

4 Object and event selections

For each event, interaction vertices are reconstructed from ID charged particle tracks, where the tracks are required to have transverse momenta (p_T) greater than 500 MeV [63]. Candidates for the primary vertex are required to have at least two associated tracks. If multiple vertices are reconstructed, the vertex with the largest sum of the squares of the transverse momenta of associated tracks is taken as the primary vertex. Events that fail the primary vertex reconstruction are rejected.

Electrons are reconstructed from energy deposits in the electromagnetic calorimeter that are matched to charged-particle tracks in the ID [64]. They are identified using a likelihood-based (LH) identification

which employs calorimeter and tracking information to discriminate between electrons and jets and that combines this likelihood and the likelihood of it originating from background processes into a single discriminant. Only electron candidates with $p_T > 10$ GeV within $|\eta| < 1.37$ or $1.52 < |\eta| < 2.47$ are considered. Electrons are required to be well isolated using criteria based on the properties of the topological clusters in the calorimeter and of ID tracks around the reconstructed electron. Further requirements of $|z_0 \sin \theta| < 0.5$ mm and $|d_0|/\sigma(d_0) < 5$ are placed on the longitudinal and transverse impact parameters to select electrons originating from the primary vertex. Electrons are further categorized as “baseline” or “signal”. For the all-hadronic channel, baseline electrons are identified by the *LooseAndBLayer* likelihood-based identification working point and are required to fulfill the *Loose* isolation criteria [64, 65]. Events containing a baseline electron candidate satisfying these baseline criteria are rejected. For the one-lepton channel, baseline electrons are identified with the *Medium* working point [64] and are not subject to any isolation requirement. Signal electrons are identified by the *Tight* working point and are subject to the *Tight* track-based isolation criteria [64]. The p_T -requirement of the signal electrons is increased to $p_T > 28$ GeV. Signal electrons constitute a subset of the baseline electrons.

Muon candidates are reconstructed by combining tracks in the MS with tracks in the ID and are subject to cut-based identification criteria which are based on the numbers of hits in the different ID and MS subsystems, and on the significance of the charge-to-momentum ratio q/p [66]. All muon candidates are required to be within the acceptance region of the ID at $|\eta| < 2.5$ and to have $p_T > 10$ GeV. Muons are required to satisfy isolation requirements based on the properties of ID tracks around the reconstructed muon [66]. Similarly to electrons, requirements on the longitudinal and transverse impact parameters, $|z_0 \sin \theta| < 0.5$ mm and $|d_0|/\sigma(d_0) < 3$, are also applied. Baseline muons are identified in the all-hadronic channel by the *Loose* quality working point and are required to fulfill the *Loose* isolation criteria [66]. Events containing a muon candidate satisfying these baseline criteria are rejected. In the one-lepton channel, baseline muons are identified by the *Medium* quality working point [66] and are not subject to any isolation criteria. For the selection of signal muons the *Medium* quality working point is applied and the muon candidates are required to fulfill the *Tight* isolation criteria based on the $p_T^{\text{varcone30}}$ variable defined in Ref. [66] and have $p_T > 28$ GeV. Signal muons constitute a subset of the baseline muons. Events are selected for the one-lepton channel if they contain exactly one signal and no additional baseline leptons (electrons or muons).

Jet candidates are reconstructed using a particle-flow reconstruction algorithm [67] combining charged particle tracks from the ID and three-dimensional topological energy clusters [68] in the calorimeter. Jets are reconstructed using the anti- k_r algorithm [44] implemented in the FastJet package [45] with a fixed radius parameter $R = 0.4$ using charged constituents associated with the primary vertex and neutral particle flow objects as inputs. In order to minimize the contribution from pileup jets, a requirement on the jet-vertex tagger [69] is made for jets with p_T below 60 GeV.

Slight differences in the efficiency of the association of jets to vertices in data and simulation are addressed by applying scale factors to simulation. Jet energy scale corrections, derived from MC simulation, are used to calibrate the average energies of jet candidates to the scale of their constituent particles [70]. Remaining differences between data and simulated events are evaluated and corrected for using in situ techniques, which exploit the transverse momentum balance between a jet and a reference object such as a photon, Z boson, or multijet system in data. After these calibrations, all jets in the event with $p_T > 20$ GeV must satisfy a set of loose jet-quality requirements [71] designed to reject jets originating from sporadic bursts of detector noise, large coherent noise or isolated pathological cells in the calorimeter system, hardware issues, beam-induced background or cosmic-ray muons [72]. In the one-lepton channel, the jets are required to

satisfy $|\eta| < 2.5$, while in the all-hadronic channel, they are required to satisfy $|\eta| < 2.8$ to match the η range of the H_T trigger. If these jet requirements are not met, the jet is discarded.

Jets are tagged as containing a b -hadron (b -tagged) by a deep neural network algorithm trained on a simulated hybrid sample composed of $t\bar{t}$ and $Z' \rightarrow t\bar{t}$ events [73, 74] at a working point corresponding to a 77% b -jet efficiency, as measured on an inclusive $t\bar{t}$ sample. This working point has a rejection factor of 5 and 170 on charm and light-flavored jets, respectively. Flavor-tagging efficiency differences between data and simulation are corrected by a reweighting procedure detailed in Refs. [75–77].

To resolve any reconstruction ambiguities between electrons, muons and jets, an overlap removal procedure is applied in a prioritized sequence, based on baseline leptons and jets, as follows. First, if an electron shares the same ID track with another electron, the electron with lower p_T is discarded, and then any electron sharing the same ID track with a muon is rejected. Next, jets are rejected if they lie within $\Delta R = 0.2$ of an electron. Similarly, jets within $\Delta R = 0.2$ of a muon are rejected if the jet has fewer than three associated tracks or if the muon is matched to the jet through ghost association [44]. Finally, electrons that are close to a remaining jet are discarded if their distance from the jet is $\Delta R < 0.4$, while for muons the distance is $\Delta R < \min(0.4, 0.04 + 10 \text{ GeV}/p_T)$.

Large- R jets are reclustered from the calibrated $R = 0.4$ jets described above using the anti- k_t algorithm with a fixed radius parameter of $R = 1.2$ [78]. The large- R jets aim to fully contain the dark pion decay products and the R parameter is optimized for the dark pion mass range of the targeted signal points. For the one-lepton channel the signal lepton is added to the $R = 0.4$ jet collection before the reclustering, which then proceeds in the same way as in the all-hadronic channel. After reclustering, the large- R jet containing the lepton is referred to as J^{lep} and the leading fully hadronic large- R jet J^{had} . Both large- R jets originate from the same reclustering procedure, ensuring there is no overlap between the two.

Events are selected for the all-hadronic channel using triggers on H_T , defined as the scalar sum of the transverse momenta of all the reconstructed jets in the event with $|\eta_{\text{jet}}| < 2.8$ [79]. The H_T -trigger threshold was 850 GeV in 2015 and the first half of 2016, and was increased to 1000 GeV in the latter half of 2016 for the remainder of Run 2. Since the trigger decision is based on H_T computed from trigger-level jet momenta (which lack a detailed calibration), the triggers show a slow onset behavior with respect to H_T computed from jet momenta of fully calibrated jets. A requirement of $H_T > 1150$ GeV ensures that the trigger is fully efficient to minimize systematic uncertainties resulting from imprecise modeling of the onset behavior in simulation. The H_T variable computed from fully calibrated jets is used for the remainder of this search.

Events are selected for the one-lepton channel using a combination of single-lepton triggers [80–83]. The single-lepton triggers require the presence of a muon or an electron with p_T higher than a certain threshold and, in some cases, impose identification and lepton-isolation requirements. The lowest p_T threshold was 24 (20) GeV for electrons (muons) during the 2015 data-taking period and 26 GeV for both electrons and muons in the data-taking periods from 2016 to 2018. The efficiencies of the single-lepton triggers range between 20% and 50% in the simulated signal samples. To account for small differences in the single-lepton trigger efficiency between data and simulation, all triggered simulated events receive an event weight to match data.

The analysis strategy relies on the reconstruction of each dark pion using a large- R jet. In the all-hadronic channel, events are required to have six or more $R = 0.4$ jets with $p_T > 25$ GeV, in addition to the $H_T > 1150$ GeV requirement and the lepton veto. At least three jets within the ID acceptance ($|\eta| < 2.5$) must be b -tagged. At least two large- R jets with jet mass $m_{\text{jet}, R=1.2} > 190$ GeV are required in all events. Events for the one-lepton channel are required to have at least five jets, out of which at least three have to be b -tagged, and to have $H_T > 300$ GeV. Here the H_T is defined similar to the all-hadronic channel,

Table 2: Summary of the preselection criteria for the all-hadronic and one-lepton channels, in terms of the number of baseline and signal leptons, $R = 0.4$ and $R = 1.2$ jets, number of b -jets, and H_T . The definitions of the physics objects for the two channels are given in the text. Signal leptons constitute a subset of the baseline leptons.

Variable	All-hadronic channel	One-lepton channel
$N_{\text{lep}}(\text{baseline})$	0	1
$N_{\text{lep}}(\text{signal})$	-	1
$N_{\text{jets}}(R = 0.4)$	≥ 6	≥ 5
$N_{\text{jets}}(R = 1.2)$	≥ 2	-
$N_{b\text{-jets}}$	≥ 3	≥ 3
H_T	≥ 1150 GeV	≥ 300 GeV

however only jets with $|\eta_{\text{jet}}| < 2.5$ are considered. Events passing all selection requirements listed here are considered preselected for the analysis. The preselection requirements are summarized for both the analysis channels in Table 2.

5 Analysis strategy

Preselected events are separated into signal, control, and validation regions based on the properties of the large- R and small- R jets in the event, as well as the signal lepton for the one-lepton channel. Signal regions (SRs) are signal-enriched regions while the control regions (CRs) are used to estimate the SM background contributions. The validation regions (VRs) are used to validate the background estimation methods. The analysis strategies for the all-hadronic and one-lepton channels are detailed below.

5.1 All-hadronic channel

In the all-hadronic channel, the leading two large- R jets define the overall SR, where the leading large- R jet satisfies $m_{\text{jet},R=1.2} > 300$ GeV and the sub-leading large- R jet satisfies $m_{\text{jet},R=1.2} > 250$ GeV as shown in Figure 4 for distributions after preselection. To suppress multijet events containing, for example, gluon to $b\bar{b}$ splitting, a selection on $m_{bb}/p_{T,bb}$, defined as the ratio of the mass to the transverse momentum of the pair of b -tagged jets closest to the center of the large- R jet, is applied to both large- R jets. In signal events $m_{bb}/p_{T,bb}$ is expected to take on larger values than in background events, thus a cut of $m_{bb}/p_{T,bb} > 0.25$ is required. Further, both large- R jets must satisfy a bb_i tag, where the ΔR between the leading ($i = 1$) or sub-leading ($i = 2$) large- R jet and the second closest b -tagged jet, defined as $\Delta R(j, b_2)$, is less than 1.0 and thus both b -tagged jets are well contained within the volume of the large- R jet. This variable is designed to suppress $t\bar{t}$ events where the second closest b -jet arises from the other top quark in the event and can thus have a large ΔR with the large- R jet. In signal, on the other hand, the decay products of the dark pion always include two b -quarks no matter whether the $t\bar{t}b$ or $t\bar{t}bb$ final state is considered and the ΔR therefore tends to be small. The overall SR is then subdivided into nine separate bins in the leading versus sub-leading large- R jet mass plane. A large- R jet is considered $\pi_{D,i}$ tagged if its mass falls into one of the nine mass bins. The SR requires both large- R jets to satisfy both tagging selections (i.e. both jets must be bb_i and $\pi_{D,i}$ tagged). The events where the two leading large- R jets satisfy only one or two out of the four possible tags form the CRs used for the data-driven multijet extrapolation; events that satisfy three tags allow for a validation of the method and thus form the VRs. The SR selection criteria are summarized in Table 3.

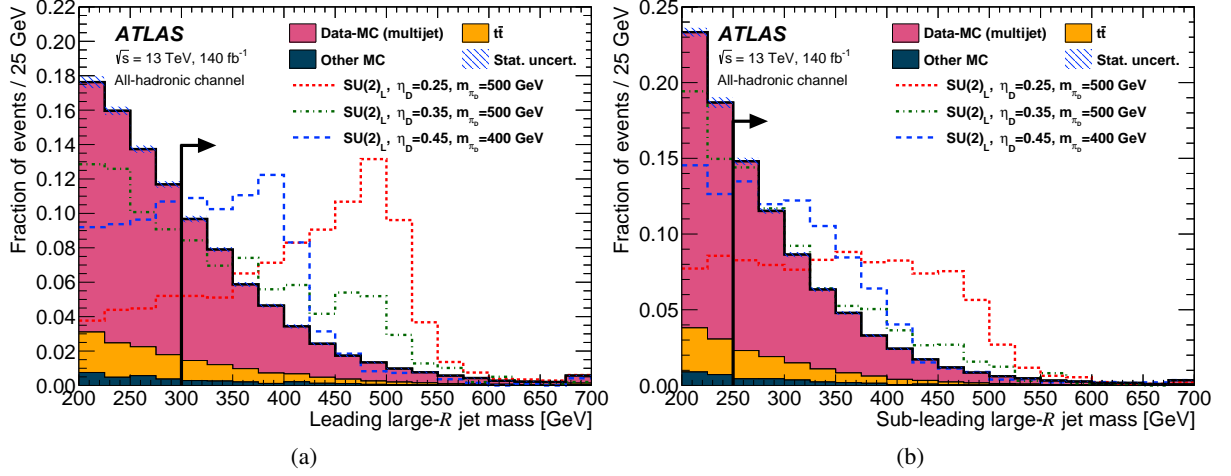


Figure 4: Mass of the (a) leading and (b) sub-leading large- R jet for all simulated backgrounds overlaid with three example distributions for various signal points after preselection in the all-hadronic channel. Also shown is a simplified data-driven estimate of the multijet background which was created by taking the event yields for data and subtracting all simulated backgrounds from it. Statistical uncertainties stemming from MC are indicated by the shaded region. The SR is to the right of the vertical line in both the subfigures. Individual SR bins select sub-regions of leading and sub-leading large- R jet mass for improved background discrimination. The last bin contains the overflow.

Table 3: Summary of selection criteria for the SR (“Tag selection”). Nine bins are defined in the leading large- R jet vs. sub-leading large- R jet mass plane. The inverted selection (“Anti-tag selection”) is also defined for use in the data-driven multijet extrapolation described in Section 6.1.

	Tag	Variable	Tag selection	Anti-tag selection
Both large- R jets		$m_{bb}/p_{T,bb}$	> 0.25	> 0.25
Leading large- R jet	bb_1	$\Delta R(j, b_2)$	< 1.0	≥ 1.0
Sub-leading large- R jet	bb_2	$\Delta R(j, b_2)$	< 1.0	≥ 1.0
Leading large- R jet	$\pi_{D,1}$	$m_{\text{jet},R=1.2}$	[300 – 325 GeV, 325 – 400 GeV, > 400 GeV]	≤ 300 GeV
Sub-leading large- R jet	$\pi_{D,2}$	$m_{\text{jet},R=1.2}$	[250 – 300 GeV, 300 – 350 GeV, > 350 GeV]	≤ 250 GeV

5.2 One-lepton channel

Events satisfying the preselection requirements for the one-lepton channel are categorized into SRs, CRs and VRs based on two kinematic variables defined in terms of the properties of the small- R and large- R jets. The first variable, $\Delta R(\ell, b_2)$, is defined as the angle between the lepton in the event and the second closest b -jet to this lepton and aims to suppress $t\bar{t}$ background similar to $\Delta R(j, b_2)$ in the all-hadronic channel. The kinematics of the second b -jet as distinguishing characteristic of signal events is also utilized for the

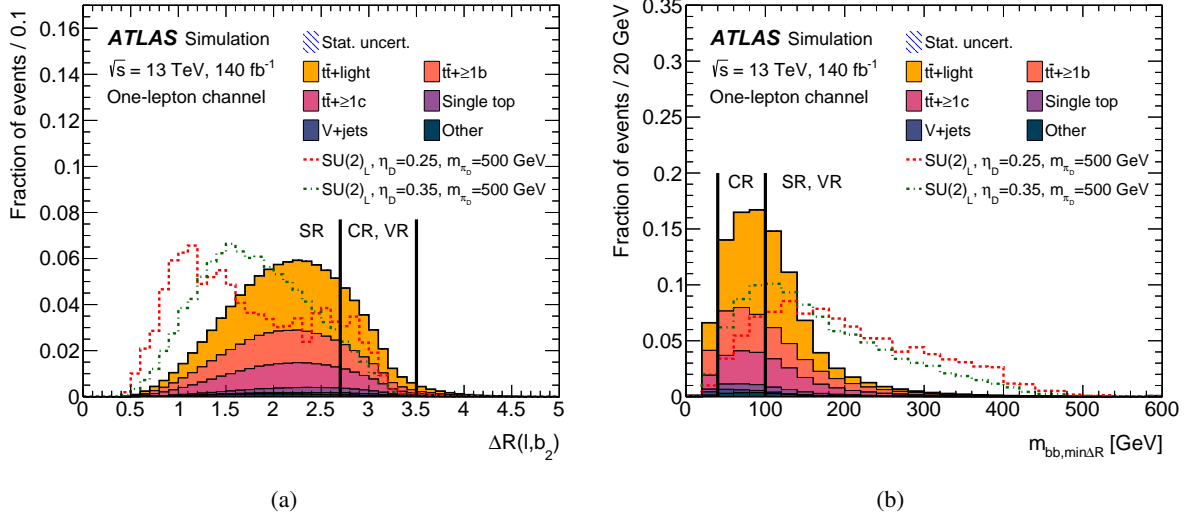


Figure 5: Normalized distributions of (a) $\Delta R(\ell, b_2)$ and (b) $m_{bb, \min \Delta R}$ for all simulated backgrounds with two example signal distributions overlaid after the one-lepton channel preselection. Statistical uncertainties stemming from MC are indicated by a shaded region, but are not visible on the scale of the y-axis. The vertical dashed lines indicate the selection requirements applied to events in the SR, CR and VR, as indicated by the labels.

second variable, $m_{bb, \min \Delta R}$, defined as the invariant mass of the two b -jets in the event that are closest to each other. This is effective for discriminating high dark pion mass signal points against background in which the two b -quarks closest to each other come e.g. from gluon splitting. The distributions of these variables in signal and background MC simulations are shown in Figure 5 for preselected events.

The SR is defined by requiring $\Delta R(\ell, b_2) < 2.7$ and $m_{bb, \min \Delta R} > 100$ GeV. A CR for the $t\bar{t}$ +HF background is defined by the requirements $2.7 < \Delta R(\ell, b_2) < 3.5$, and $40 \text{ GeV} < m_{bb, \min \Delta R} < 100$ GeV, thus ensuring orthogonality to the SR. This region is used to correct for mismodeling in $t\bar{t}$ +HF events and has a background composition similar to that in the SR. Typical signal contamination in the CR, from signal points that are not already excluded through re-interpretation of other collider searches [2], is below 1%. The $t\bar{t}$ +HF background estimate is validated in a VR defined by the requirements $2.7 < \Delta R(\ell, b_2) < 3.5$, and $m_{bb, \min \Delta R} > 100$ GeV, making it orthogonal to both the SR and the CR while also exhibiting a background composition similar to that of the SR and CR.

The statistical analysis in the one-lepton channel relies on a profile-likelihood fit to the distribution of the sum of the masses of the reclustered jets, described in Section 4, $m_{\text{jhad}} + m_{\text{jlep}}$. This discriminating variable is shown in Figure 6 for preselected events. For the fit, all events are further classified into regions split into bins based on the number of jets and b -jets in the event. Six bins are defined labeled XR_5j3b, XR_5j4b, XR_6j3b, XR_6j4b, XR_7j3b and XR_7j4b, where the number before the 'j' indicates the number of jets, the number before the 'b' the number of b -jets and 'X' can take on the values 'S' for an SR, 'C' for a CR and 'V' for a VR bin. In all cases, the highest jet or b -jet multiplicity is inclusive, e.g. the region CR_7j4b is a CR that contains events with ≥ 7 jets and ≥ 4 b -jets.

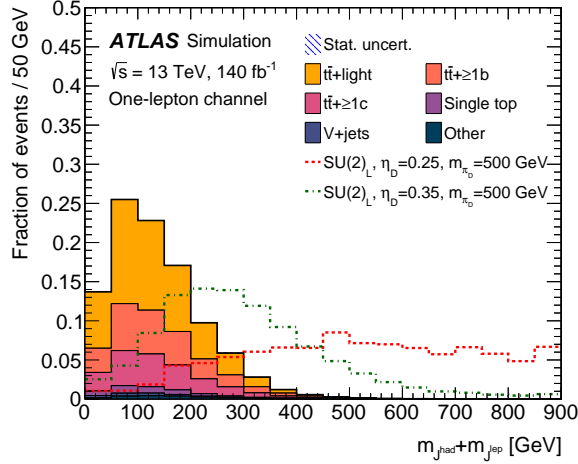


Figure 6: Normalized distributions of $m_{\text{jhad}} + m_{\text{jlep}}$ for all simulated backgrounds overlaid with two example distributions for various signal points after the one-lepton channel preselection. Statistical uncertainties stemming from MC are indicated by a shaded region, but are not visible on the scale of the y-axis.

6 Background estimate

6.1 All-hadronic channel

The dominant background for the analysis in the all-hadronic channel originates from multijet events and constitutes about 75% – 85% of the total background in each SR bin. A data-driven method is used to estimate this background, while MC simulation is used to account for the remaining sub-dominant SM processes as described in Section 3. Typical ABCD multijet extrapolations are based on two discriminating variables. Here, however, an extended ABCD method is employed that relies on four instead of two discriminating variables, which allows the correction of correlations between pairs of discriminating variables and provide validation regions close to the SR selection.

The multijet background is estimated by extrapolating from regions with small leading and sub-leading $m_{\text{jet},R=1,2}$ and large $\Delta R(j, b_2)$ to SR bins with large leading and sub-leading $m_{\text{jet},R=1,2}$ and small $\Delta R(j, b_2)$. The method is similar to the one detailed in Ref. [84]. To this end, two additional anti-tags denoted by a slashed tag label (with orthogonal selections to the already described bb_i and $\pi_{D,i}$ tags) are defined. The tag bb_i inverts the bb_i selection, while $\pi_{D,i}$ places upper requirements on the large- R jet mass, as summarized in Table 3. The combinations of possible tags and anti-tags in an event result in 16 separate regions shown in Figure 7. The extended ABCD method extrapolates from regions with one tag to each of the nine SR bins. Two-tag regions are used to determine correlation correction factors and three-tag regions are used for validation of the multijet estimate.

The concept of the extended ABCD method is detailed here by explicitly stating the computations for one VR, however, analogous derivations have to be carried out for all SRs and VRs. Considering only region K in Figure 7, a 2-variable ABCD estimate for this region would be computed in the standard way through $\hat{K} = \frac{J \cdot D}{B}$, where J , D and B are the number of data events minus the number of simulated events in the respective regions. If $\pi_{D,1}$ and $\pi_{D,2}$ are uncorrelated, \hat{K} would be a valid estimate. However, if $\pi_{D,1}$ and $\pi_{D,2}$ are correlated, then \hat{K} needs to be corrected by a correlation factor (k -factor). As long as there is

		Leading large-R jet			
		$\pi_{D,1}bb_1$	$\pi_{D,1}bb_1$	$\pi_{D,1}bb_1$	$\pi_{D,1}bb_1$
Sub-leading large-R jet	$\pi_{D,2}bb_2$	J	K	L	S
	$\pi_{D,2}bb_2$	B	D	H	N
	$\pi_{D,2}bb_2$	E	F	G	M
	$\pi_{D,2}bb_2$	A	C	I	O

Figure 7: Region labels for the 16 regions used in the data-driven multijet estimate in the all-hadronic channel. Region S labels the SR, regions B , C , E and I are used for the ABCD extrapolation, regions D , F , G , H , J and O are used to compute correlation correction factors, and regions K , L , M and N are validation regions. The background estimate is performed independently for all nine SR bins.

no significant additional three-tag correlation with the bb_2 tag, this correlation factor, $k_{\pi_{D,1},\pi_{D,2}}$, can be measured from $\frac{F \cdot A}{C \cdot E}$ since $\frac{K \cdot B}{J \cdot D} = \frac{F \cdot A}{C \cdot E}$. Thus,

$$\hat{K} = \frac{J \cdot D}{B} \cdot \frac{F \cdot A}{C \cdot E} = \frac{J \cdot D}{B} \cdot k_{\pi_{D,1},\pi_{D,2}}. \quad (1)$$

One can also consider the estimate of region K using a three-variable ABCD estimate computed with two correlation correction factors:

$$\hat{K} = \frac{J \cdot C}{A} \cdot k_{\pi_{D,1},\pi_{D,2}} \cdot k_{\pi_{D,1},bb_2}, \quad (2)$$

where $k_{\pi_{D,1},bb_2} = \frac{D \cdot A}{B \cdot C}$. Substituting this correlation factor into Eq. (2) yields once again Eq. (1). All other k -factors can be defined according to the same principle as $k_{\pi_{D,1},\pi_{D,2}}$ and $k_{\pi_{D,1},bb_2}$.

The final multijet background estimate requires a four-variable ABCD estimate \hat{S}' that is computed from data minus event counts from MC simulated backgrounds in the regions B , C , E , and I where exactly one tag is applied and region A with no applied tags according to

$$\hat{S}' = \frac{B \cdot C \cdot E \cdot I}{A^3}. \quad (3)$$

This estimate is then multiplied by six k -factors to correct for correlations between tags,

$$\hat{S} = \hat{S}' \cdot k_{\pi_{D,1},bb_1} \cdot k_{\pi_{D,2},bb_2} \cdot k_{\pi_{D,1},bb_2} \cdot k_{\pi_{D,2},bb_1} \cdot k_{\pi_{D,1},\pi_{D,2}} \cdot k_{bb_1,bb_2}. \quad (4)$$

If the selection criteria defined by these tags are independent from each other then the expectation value of the corresponding k -factor will be 1. Correlation factors around 1.5 are observed between the $\pi_{D,1}$ and bb_1 tags as well as the $\pi_{D,2}$ and bb_2 tags. The bb_1 and bb_2 tags are highly correlated with a k -factor of 0.1 due to the preselection requirement of three b -tagged jets. This could be mitigated by requiring four b -tagged jets, however, this would result in low statistics and high signal contamination for the four-variable ABCD extrapolation regions.

Typical signal contaminations in the extrapolation regions are less than 5% and small compared to the uncertainty applied to the multijet background discussed in Section 7. The method is validated through the closure of the estimate in the four 3-tag validation regions K , L , M and N . Figure 8 compares data to estimated background yields for each validation region in each bin of the SR. If significant 3-tag correlations occurred, a discrepancy between multijet estimate and data yields should be visible in the validation

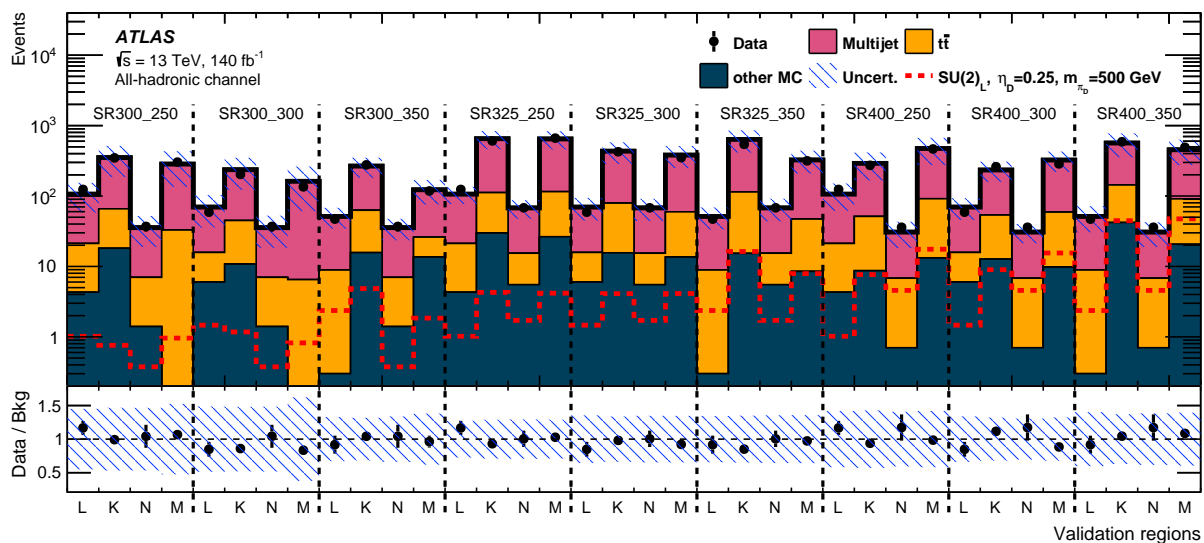


Figure 8: The four all-hadronic channel validation regions K , L , M and N from Figure 7 for each of the nine SR mass bins with the following naming convention: the leading large- R jet lower mass boundary in GeV is followed by the sub-leading large- R jet lower mass boundary. The shaded region indicates the uncertainty on the background estimate in each bin that includes the statistical uncertainties from the limited sample sizes in data and simulation as well as a multijet non-closure systematic uncertainty, as detailed in Section 7.

regions. However, all data yields are compatible with the background estimate within the uncertainty bands for all validation regions. The uncertainty includes a non-closure systematic uncertainty, which by design covers non-linear correlations and the impact of multijet estimation regions with low statistics. It ranges between 33% and 57% and is derived and discussed in Section 7. The procedure was further validated by performing signal injection tests as well as stability tests over time, under variation of the selection criteria and with scaled simulated background contributions. In all cases the resulting background estimates were stable and thus consistent with the nominal estimate.

6.2 One-lepton channel

The background in the one-lepton channel is estimated from MC simulations using the samples described in Section 3 and is dominated by $t\bar{t}$ production in association with light-flavor or heavy-flavor quarks. This background is estimated by using the inclusive $t\bar{t}$ sample complemented by the dedicated $t\bar{t}b\bar{b}$ sample, with events categorized into $t\bar{t} + \geq 1b$, $t\bar{t} + \geq 1c$ and $t\bar{t} + \text{light}$ as described in Section 3. The $t\bar{t} + \text{HF}$ background that populates the SR is known from previous studies to be underestimated by the current MC predictions [85]. This mismodeling is corrected by keeping the normalization of these backgrounds unconstrained in the profile-likelihood fit to the $m_{\text{jhad}} + m_{\text{jlep}}$ distribution. To this end, the $t\bar{t} + \geq 1c$ and $t\bar{t} + \text{light}$ contributions are combined and two normalization factors are fit depending on whether in addition to $t\bar{t}$ any b -quarks are present in the event. In this categorization, the combination of the $t\bar{t} + \geq 1c$ and $t\bar{t} + \text{light}$ backgrounds is referred to as $t\bar{t} + 0b$. The resulting background estimates for the SR, CR and VR are presented in Section 8.2.

7 Systematic uncertainties

The predicted signal and background event yields in the SR bins are affected by various sources of systematic uncertainties stemming from instrumentation, the data-driven multijet estimation and theoretical considerations. For the all-hadronic channel, the total uncertainty is dominated by the uncertainty on the multijet background estimate. In the one-lepton channel, the theoretical sources of uncertainty on the background modeling dominate the total uncertainty.

7.1 Experimental uncertainties

The uncertainty in the combined 2015–2018 integrated luminosity is 0.83% [14], obtained using the LUCID-2 detector [11] for the primary luminosity measurements, complemented by measurements using the ID and calorimeters. A systematic variation that might be introduced by the reweighting of simulated samples to match the pileup profile observed in data is estimated by varying the scale factor applied to the pileup distributions. The onset of the H_T trigger used in the all-hadronic channel was studied and potential effects of mismodeling were evaluated. All three of these uncertainties were found to have a negligible impact on the analysis ($< 1\%$ in the all-hadronic channel, and ranking from $< 1\%$ to a few percent depending on the signal in the one-lepton channel).

Slight performance differences between data and simulation in lepton reconstruction, identification and isolation are corrected by the application of scale factors that are estimated from tag-and-probe experiments in data and simulation [64, 66]. The impact of lepton momentum scale corrections is evaluated by $\pm 1\sigma$ scale variations. For resolution uncertainties the lepton energy or momentum is smeared. In total seven (twelve) separate variations for electrons (muons) are considered. The impact of lepton uncertainties is less than 1% in both channels.

The determination of the jet energy scale and resolution is done by combining information from collision data, test beam data and simulation as described in Ref. [70]. Effects from jet flavor composition, single-particle response and pileup are considered. In the one-lepton channel, 29 parameters are evaluated for scale variations, while 13 parameters are evaluated for jet p_T resolution systematic uncertainties. In the all-hadronic channel the variations are simplified since the data-driven background estimation method largely compensates yield changes by different systematic variations and causes most of the systematic uncertainties to be negligibly small. As such, 23 parameters arise from scale variations, while for jet p_T resolution systematic uncertainties 8 parameters are evaluated. The impact of these uncertainties on the final result is small, ranging between $< 1\%$ to about 4% in the all-hadronic channel, and remaining $< 10\%$ in the one-lepton channel.

Uncertainties on the corrections of b -tagging efficiency differences between data and simulation are derived from dedicated flavor-enriched subsets of the data [75]. Also considered are uncertainties due to the mis-tagging of c -jets [77] and light-flavor jets [76]. Additionally, variations to extrapolate the measured uncertainties to the high- p_T region are considered for both channels [86]. The impact of flavor-tagging systematic uncertainties is less than 1% on the final result in the all-hadronic channel, while a larger contribution is observed in the one-lepton channel, reaching values of the order of 10%.

7.2 Modeling uncertainties in background simulations

For the all-hadronic channel, uncertainties in modeling of the $t\bar{t}$ background are included. For the one-lepton channel, uncertainties in modeling the $t\bar{t}$, $t\bar{t}b\bar{b}$, and single top-quark backgrounds are included. All other simulated backgrounds are negligible in both channels and no systematic uncertainties are assigned to them. For the single top-quark background, a 30% normalization uncertainty is applied [87] with an impact ranging between $< 1\%$ and a few percent. Details on the $t\bar{t}$ and $t\bar{t}b\bar{b}$ uncertainties are described below.

7.2.1 $t\bar{t}$ uncertainties

Several uncertainties in the theoretical modeling of the $t\bar{t}$ background samples are considered. In the one-lepton channel the $t\bar{t}$ theory systematic uncertainties apply only on the $t\bar{t} + \text{light}$ and $t\bar{t} + \geq 1c$ background components as they are estimated from the five-flavor scheme $t\bar{t}$ sample, while the $t\bar{t} + \geq 1b$ background has dedicated systematic uncertainties.

Missing higher order contributions in perturbative expansion of the $t\bar{t}$ production cross-section are estimated by adding in quadrature contributions from renormalization and factorization scale variations, which are obtained by independently varying the parameters μ_R and μ_F by a factor 0.5 and 2.0 and taking the envelope. Uncertainties on the choice of PDF set used for event simulation are estimated by using the PDF4LHC and NNPDF error sets following the PDF4LHC prescription [88] and taking the envelope. The initial-state radiation (ISR) modeling is estimated by variations of the strong coupling constant α_S through the VAR3C tune variation. The amount of final-state radiation (FSR) in an event is estimated by varying the factorization scale by factors 0.5 and 2.0 inside PYTHIA8. To assess the uncertainty in the matching of NLO matrix elements to the parton shower, the nominal sample is compared to an alternative sample obtained setting the pthard PYTHIA8 parameter to 1 (the default is 0). This parameter regulates the definition of the vetoed region of the showering, important to avoid holes and overlaps in the phase space filled by POWHEG and PYTHIA8. This recommendation follows the description included in Ref. [89]. The alternative sample was produced using POWHEG interfaced with PYTHIA8.306 using the NNPDF2.3LO PDF set and the A14 set of tuned parameters. The impacts of using a different parton shower and hadronization model were evaluated by comparing the nominal $t\bar{t}$ sample with another event sample produced with the POWHEGBOX v2 generator. For the parton shower variation the NNPDF3.0NLO PDF set was used, while events in the sample used to estimate the impact of the hadronization model were interfaced with HERWIG 7.04 [90, 91], using the H7UE set of tuned parameters [91] and the MMHT2014LO PDF set [92]. The impact of a variation of the h_{damp} parameter is assessed by comparing the nominal samples to an alternative set of samples for which h_{damp} is set to $3m_{\text{top}}$.

All alternative samples used to derive the systematic uncertainties are corrected to match the NNLO in QCD and NLO in EW predictions of the top/antitop-quark p_T and the top-quark mass distribution using the procedure outlined in Section 3.2.1. A systematic uncertainty associated with this reweighting itself is derived from the maximum and minimum 7-point scale variations, independently for the top/antitop-quark p_T and the top-quark mass. The variations are taken into account in the final statistical fit by including them as scale variations on the $t\bar{t}$ background.

To avoid over-constraining the $t\bar{t}$ modeling nuisance parameters in the one-lepton channel, the theoretical systematic uncertainties are treated as uncorrelated among $t\bar{t} + \text{light}$ and $t\bar{t} + \geq 1c$, jet and b -jet multiplicity bins, and between their shape and acceptance components.

The impact of $t\bar{t}$ modeling uncertainties on the final result is found to range between $< 1\%$ and 10%.

7.2.2 $t\bar{t}b\bar{b}$ uncertainties

Theory uncertainties on the $t\bar{t}b\bar{b}$ sample are only applied to the $t\bar{t} + \geq 1b$ component in the one-lepton channel, as all other $t\bar{t}$ components are estimated from the bulk $t\bar{t}$ sample.

The scale, PDF, ISR, and FSR uncertainties for the $t\bar{t}b\bar{b}$ sample are derived in the same way as the bulk $t\bar{t}$ sample. The impacts of using a different parton shower and hadronization model are evaluated by comparing the nominal $t\bar{t}$ sample to another sample produced with the POWHEGBOX v2 generator. For the parton shower variation the NNPDF3.0_{NLO} PDF set was used, while events in the sample estimating the impact of the hadronization model were interfaced with HERWIG 7.1, using the H7.1-DEFAULT set of tuned parameters and the MMHT2014_{LO} PDF set [92].

The matching uncertainty is evaluated by comparing the nominal sample with an alternative sample obtained by setting the pthard PYTHIA8 parameter to 1. The alternative sample was produced using POWHEG interfaced with PYTHIA8.307 using the NNPDF2.3_{LO} PDF set and the A14 set of tuned parameters.

The $t\bar{t}b\bar{b}$ uncertainty nuisance parameters are treated as uncorrelated between the different regions of jet and b -jet multiplicities and are further split up into their shape and acceptance components to avoid over-constraining them in the fit. They constitute the dominant systematic contribution in the one-lepton channel, with an impact on the final results ranging from 1% to about 30%.

7.3 Data-driven background estimation uncertainties

In the all-hadronic channel, the dominant systematic uncertainty originates from the multijet estimation method. Deviations of the ratio between data and SM estimate from unity in the VRs, denoted by $k_{VR} = (\text{data} - \text{MC})/\text{multijet}$, are used to estimate a non-closure systematic uncertainty. These k -factors are a measure of the remaining correlations between 3-tags in the multijet estimation method and are expected to be close to unity. The statistical uncertainties on the k -factors $\sigma_{k_{VR}}$ are added in quadrature so that the final multijet uncertainty is calculated according to:

$$\sigma_{ABCD} = \sqrt{\left(1 - \prod_{VR} k_{VR}\right)^2 + \sum_{VR} \sigma_{k_{VR}}^2} \quad , \quad (5)$$

where the first term under the square root describes the non-closure component of the systematic uncertainty calculated from the k -factors and the second term the statistical uncertainty summed up in quadrature over all four VRs. The statistical component dominates in most regions and is driven by region H in Figure 7 which has the lowest number of events. The computation is done separately for each bin of the SR producing values ranging from 33% to 57%. The uncertainty in each SR mass bin is treated as fully uncorrelated with the other SR mass bins thus yielding a conservative estimate.

8 Statistical analysis and results

Signal hypotheses are evaluated against the data by performing profile-likelihood fits in each analysis channel. The set of nuisance parameters θ that corresponds to the systematic uncertainties is scaled in such a fashion that, before the fit, all individual uncertainties j have $\theta_j = 0$. In addition, the uncertainties of these nuisance parameters σ are scaled to fulfill $\sigma_j = 1$ before fitting. Defining γ as the set of statistical

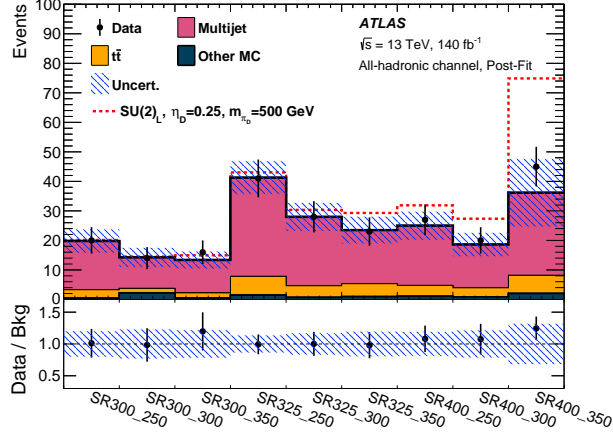


Figure 9: Comparison of the events yields in data and the background prediction after the fit under the background-only hypothesis in all bins of the all-hadronic SR. The dashed line is stacked onto the SM background and shows an example $SU(2)_L$ signal with $\eta_D = 0.25$ and $m_{\pi_D} = 500$ GeV. The uncertainty bands contain all statistical and systematic uncertainties. The horizontal axis labels reflect the different SR bins, with the first number indicating the lower boundary of the leading large- R jet mass bin and the second number the lower boundary of the sub-leading large- R jet mass bin.

uncertainties with γ_i the uncertainty on the number of predicted events of a specific bin i , the set is scaled to be a factor around 1. The profile-likelihood fit is then performed by minimizing the quantity $q(\mu) = -2 \log \mathcal{L}$, where the likelihood \mathcal{L} is defined as

$$\mathcal{L}(\mu, \theta | S, B, N) = \prod_{i \in \text{bins}} \mathcal{P}(N_i | \mu S_i + B_i) \times \mathcal{P}(S_i + B_i | \gamma_i) \prod_{j \in \text{syst.}} \mathcal{G}(\theta_j, \sigma_j) \quad (6)$$

with N being the number of data events, S the predicted number of signal events and B the expected number of background events. Statistical and systematic uncertainties are taken to be Poissonian (\mathcal{P}) and Gaussian (\mathcal{G}) distributed parameters, respectively. The fit is evaluated using the RooFit [93] package with the minimization conducted with the MINUIT2 package [94], which yields the optimal values for μ and the set of parameters θ_i , γ_i and σ_i in a signal plus background fit.

8.1 All-hadronic channel

The fit in the all-hadronic channel is performed over all nine SR bins simultaneously. Since the multijet estimate constrains background to the data, most systematic uncertainties (other than from the multijet estimate) have limited impact on the final result and all systematic uncertainties below 1% are ignored. Surviving uncertainties are kept as nuisance parameters in the fit. Because simulated backgrounds constitute less than 20% of the total SM background in the SR, no CRs are used to scale the simulated estimates.

Figure 9 shows the distributions in all SR bins after fitting. No significant pulls or constraints are observed for the fitted nuisance parameters. The results are also summarized in Table 4. As can be seen the data are very well described by the background-only hypothesis with no significant excess of events above the SM prediction.

Table 4: Observed and predicted event yields after the fit under the background-only hypothesis in all nine all-hadronic SR mass bins. The name of each column corresponds to the SR bins: the leading large- R jet lower mass boundary in GeV is followed by the sub-leading large- R jet lower mass boundary; the same convention is used in Figure 9. The quoted uncertainties contain statistical and systematic components. The total post-fit uncertainty can be smaller than the sum in quadrature of the different components due to correlations resulting from the fit to data.

	SR300_250	SR300_300	SR300_350
V+jets	< 0.01	1.97 ± 0.89	0.28 ± 0.06
Single top	0.12 ± 0.07	0.00 ± 0.03	< 0.01
$t\bar{t} + X$	0.30 ± 0.04	0.21 ± 0.09	0.17 ± 0.04
$t\bar{t}$	2.9 ± 1.9	1.6 ± 1.1	1.78 ± 0.76
Multijet	16.5 ± 4.3	10.5 ± 3.6	11.1 ± 3.1
Total SM	19.8 ± 4.0	14.2 ± 3.3	13.4 ± 2.9
Data	20	14	16

	SR325_250	SR325_300	SR325_350
V+jets	0.74 ± 0.64	0.12 ± 0.18	0.19 ± 0.16
Single top	0.36 ± 0.06	0.12 ± 0.13	0.27 ± 0.15
$t\bar{t} + X$	0.35 ± 0.06	0.44 ± 0.11	0.50 ± 0.07
$t\bar{t}$	6.4 ± 3.6	4.0 ± 2.0	4.4 ± 2.1
Multijet	33.4 ± 6.7	23.3 ± 5.2	18.1 ± 5.0
Total SM	41.2 ± 5.6	28.0 ± 4.8	23.5 ± 4.6
Data	41	28	23

	SR400_250	SR400_300	SR400_350
V+jets	0.71 ± 0.55	< 0.01	1.19 ± 0.30
Single top	< 0.01	0.47 ± 0.08	0.11 ± 0.02
$t\bar{t} + X$	0.34 ± 0.07	0.40 ± 0.07	0.73 ± 0.10
$t\bar{t}$	3.7 ± 1.8	3.1 ± 2.5	6.1 ± 3.9
Multijet	20.2 ± 5.3	14.7 ± 4.6	28 ± 12
Total SM	25.0 ± 4.8	18.6 ± 4.0	36 ± 11
Data	27	20	45

8.2 One-lepton channel

In the one-lepton channel, a profile-likelihood fit is performed to the binned $m_{\text{jhad}} + m_{\text{jlep}}$ spectrum in the six SRs and the six CRs defined based on jet and b -jet multiplicity requirements, simultaneously. As already indicated in Section 6.2, two independent normalization factors are used for the $t\bar{t}$ background depending on whether in addition to $t\bar{t}$ any b -quarks are present in the event. These two normalization factors are denoted by $k(t\bar{t} + 1b)$ and $k(t\bar{t} + 0b)$. To avoid over-constraining the background modeling nuisance parameters, the theoretical systematic uncertainties are treated as uncorrelated among different $t\bar{t}$ flavors, jet and b -jet multiplicity bins, and between their shape and acceptance components.

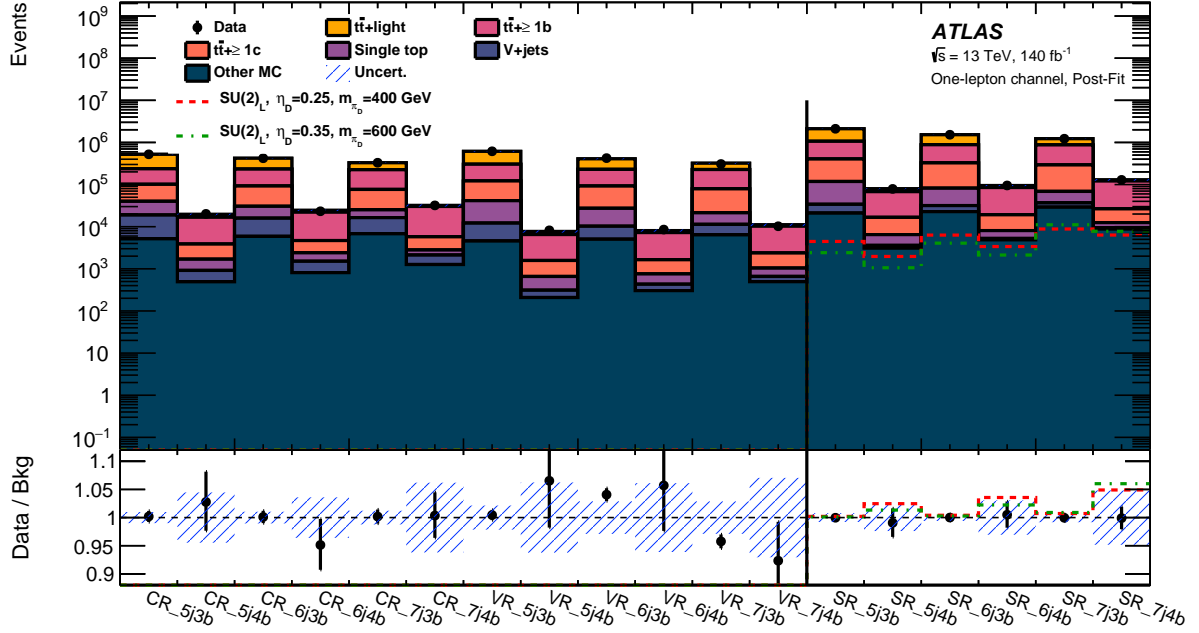


Figure 10: Comparison of the events yields in data and the background prediction in the SRs, CRs, and VRs in the one-lepton channel, after the fit to data in all CRs and SRs under the background-only hypothesis. The uncertainty bands contain all statistical and systematic uncertainties. Two example $SU(2)_L$ signal points are overlaid in the SRs.

The event yields for all SRs, CRs and VRs are shown after a fit to the data under the background-only hypothesis in Figure 10. The corresponding distributions of $m_{\text{jhad}} + m_{\text{jlep}}$ are shown in Figure 11 for all jet and b -jet multiplicity bins of the SR. The SM background estimate is in good agreement with data after the background-only fit. The post-fit normalization factors for the $t\bar{t}$ background components are $k(t\bar{t} + 0b) = 0.92^{+0.09}_{-0.08}$ and $k(t\bar{t} + \geq 1b) = 1.60^{+0.19}_{-0.17}$. No pulls greater than 1σ are observed for the fitted nuisance parameters, with only some constraints in the nuisance parameters describing the theoretical modeling. Data and post-fit background event yields are shown in Table 5. Good agreement between the background prediction and data is observed in all regions.

9 Interpretation

The results are used to set 95% confidence level (CL) upper limits on the dark pion pair production cross-sections following the CL_S technique [95]. Upper limits on the dark pion production cross-sections are shown in Figure 12 for four slices of η_D . The impacts of the different systematic uncertainties, described in Section 7, on the signal strength, defined as the signal cross-section normalized to the theoretical prediction, of two benchmark signals are summarized in Table 6: the analysis is limited by the systematic uncertainty, with dominant contribution from the theoretical sources of uncertainty on the background modeling.

Using the predicted dark pion pair production cross-sections, the limits can be translated into limits on dark pion masses in the two-dimensional $\eta_D - m_{\pi_D}$ plane. The exclusion contour obtained from the all-hadronic channel for the $SU(2)_L$ model is shown in Figure 13(a). No dark pion masses can be excluded for $\eta_D = 0.15$. For $\eta_D = 0.25$ the exclusion covers the mass range $280 \text{ GeV} < m_{\pi_D} < 520 \text{ GeV}$ (expected

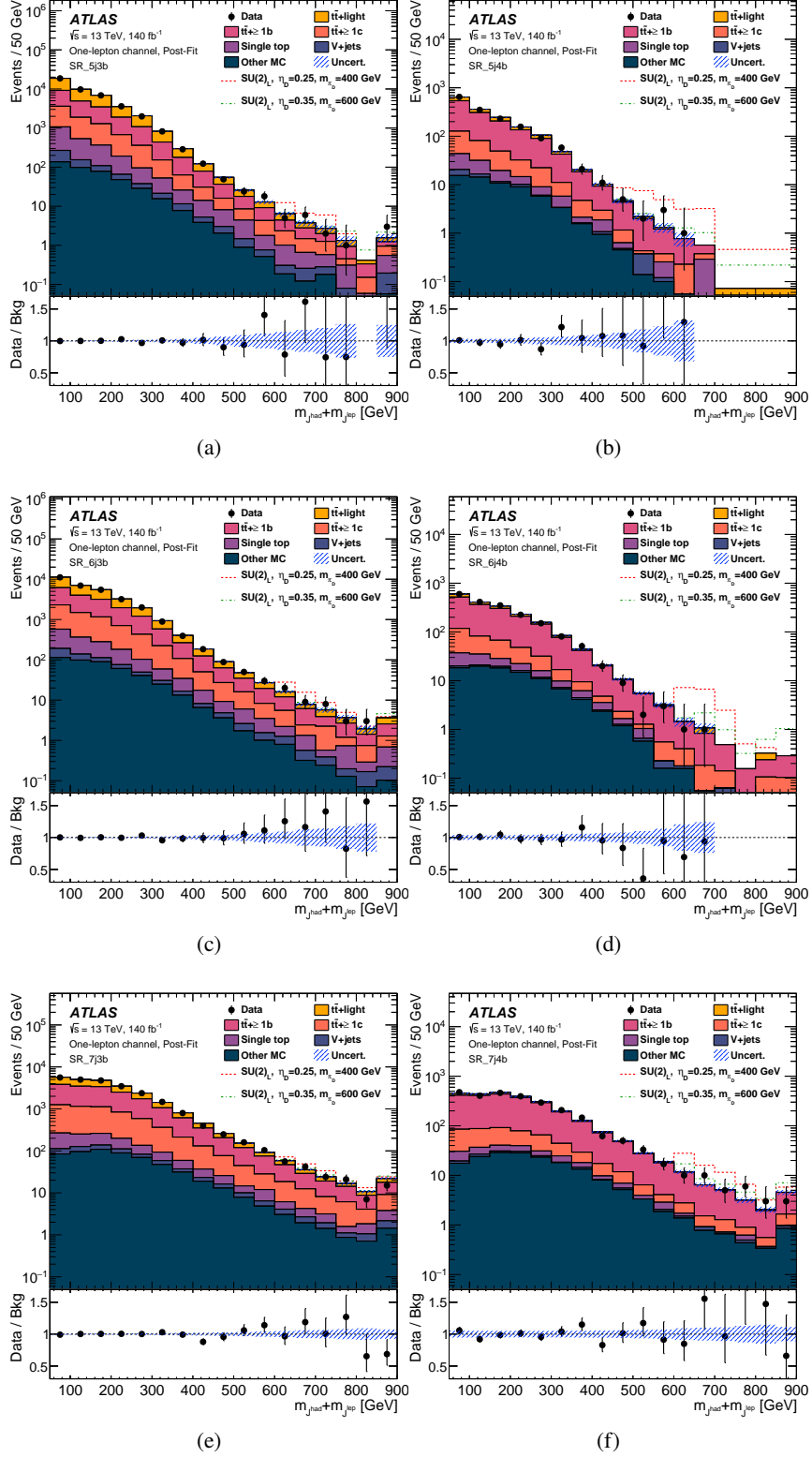


Figure 11: Distributions of $m_{\text{jhad}} + m_{\text{jlep}}$ in (a) SR_5j3b, (b) SR_5j4b, (c) SR_6j3b, (d) SR_6j4b, (e) SR_7j3b, and (f) SR_7j4b, after the fit to data in all CRs and SRs under the background-only hypothesis. Two example $SU(2)_L$ signal point with $\eta_D = 0.25$ and $m_{\pi_D} = 400$ GeV is stacked on top of the background. The uncertainty bands contain all statistical and systematic uncertainties. The dashed line in the ratio panel shows the ratio of signal plus background event yields over just background event yields.

Table 5: Observed and predicted event yields after the fit under the background-only hypothesis in the six SR bins in the one-lepton channel. The name of each column corresponds to the bins described in Section 5.2, identified with the number of jets followed by the number of b -jets. The quoted uncertainties contain statistical and systematic components. The total post-fit uncertainty can be smaller than the sum in quadrature of the different components due to correlations resulting from the fit to data.

	SR_5j3b	SR_5j4b	SR_6j3b
$t\bar{t} + \geq 1b$	12400 ± 2600	1150 ± 180	9400 ± 1800
$t\bar{t} + \geq 1c$	5900 ± 500	230 ± 40	5400 ± 600
$t\bar{t} + \text{light}$	23100 ± 1900	270 ± 70	14300 ± 1200
Single top	1800 ± 500	59 ± 18	1080 ± 330
V+jets	274 ± 30	10.2 ± 1.5	192 ± 22
Other MC	416 ± 15	61 ± 4	465 ± 17
Total SM	10500 ± 100	402 ± 20	8430 ± 110
Data	10462	403	8438

	SR_6j4b	SR_7j3b	SR_7j4b
$t\bar{t} + \geq 1b$	1210 ± 120	9900 ± 2500	1900 ± 400
$t\bar{t} + \geq 1c$	247 ± 45	5400 ± 800	350 ± 90
$t\bar{t} + \text{light}$	220 ± 50	8500 ± 1500	180 ± 50
Single top	59 ± 18	710 ± 220	66 ± 21
V+jets	7.7 ± 1.2	170 ± 20	14.9 ± 1.9
Other MC	99 ± 6	620 ± 40	187 ± 14
Total SM	477 ± 22	6600 ± 120	640 ± 40
Data	465	6598	641

$280 \text{ GeV} < m_{\pi_D} < 540 \text{ GeV}$), while for $\eta_D = 0.35$, dark pions with masses $m_{\pi_D} < 430 \text{ GeV}$ are excluded (expected $m_{\pi_D} < 450 \text{ GeV}$). The exclusion contour obtained from the one-lepton channel for $SU(2)_L$ is shown in Figure 13(b) and is observed to fully cover the all-hadronic limit and significantly extend the probed phase space for this dark meson model. Since the all-hadronic limit is completely contained within the one-lepton limit, there is no expected gain from a combination of the two channels. Dark pion masses with $m_{\pi_D} < 940 \text{ GeV}$ can be excluded for $\eta_D = 0.45$, $m_{\pi_D} < 720 \text{ GeV}$ are excluded for $\eta_D = 0.35$ and for $\eta_D = 0.25$ the mass region $m_{\pi_D} < 740 \text{ GeV}$ is excluded. The results significantly extend the phase space previously excluded through re-interpretation of other collider searches [2]. In the $SU(2)_R$ model, cross sections are significantly smaller than for $SU(2)_L$ and therefore none of the channels have sensitivity to this model with the current data sample.

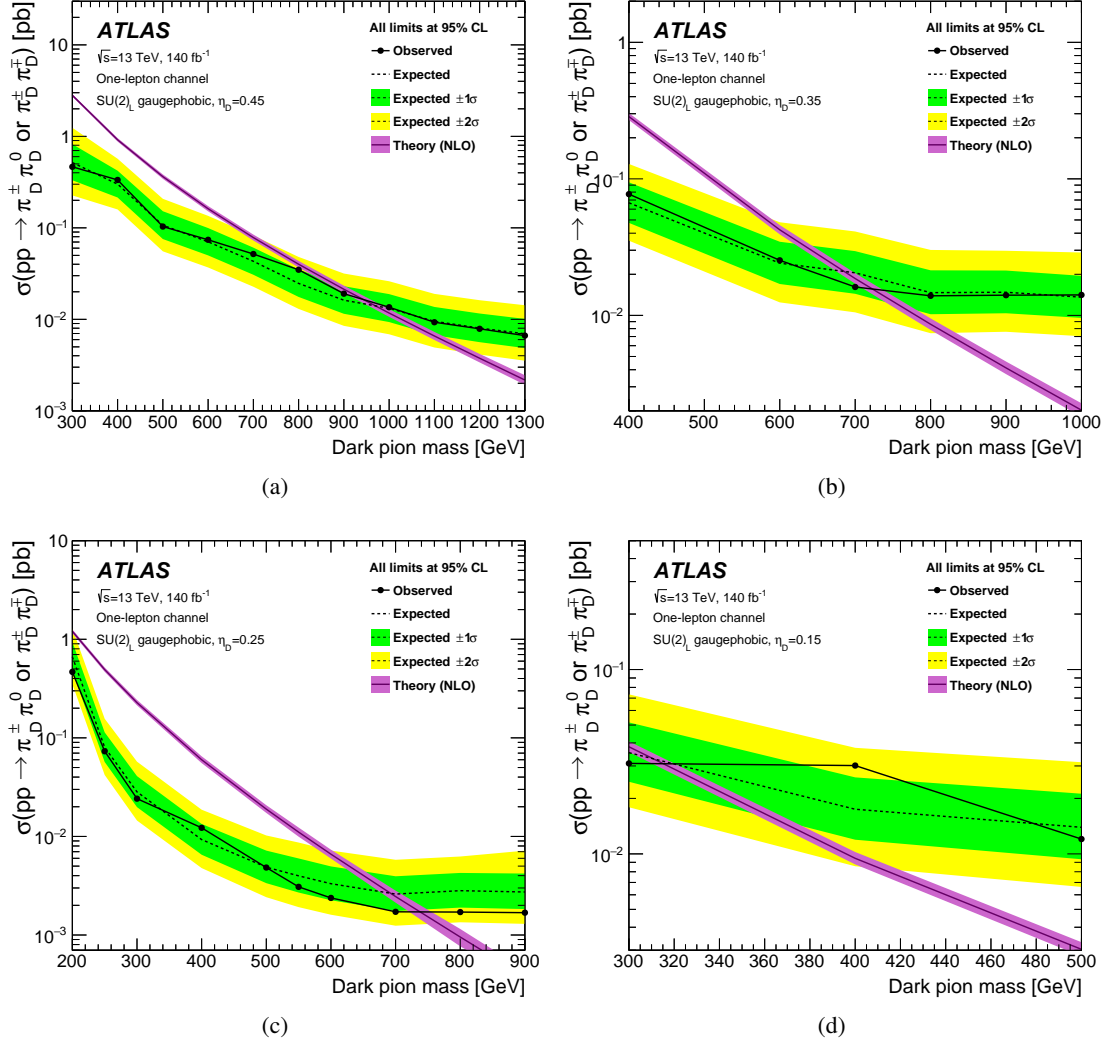


Figure 12: Observed (solid line) and expected (dashed line) limits on the dark pion production cross-section as a function of dark pion mass using the CL_S method for all $SU(2)_L$ models in four slices of η_D : (a) $\eta_D=0.45$, (b) $\eta_D=0.35$, (c) $\eta_D=0.25$, and (d) $\eta_D=0.15$. The surrounding shaded bands correspond to one and two standard deviations around the expected limit. The overlaid theory line shows the theoretical dark pion cross-section prediction [4].

Table 6: Impact of different categories of systematic uncertainty in the one-lepton channel, for two signal benchmarks, relative to the total uncertainty on the fitted signal strength. For each category, the fit is repeated with the corresponding group of nuisance parameters fixed to their best-fit values and the impact for each category is evaluated as the quadrature difference between the signal strength uncertainty in the new fit and in the nominal one, divided by the uncertainty in the nominal fit. The contribution from the statistical uncertainty and the systematic one, further separated into the global instrumental and theoretical uncertainties, are shown. The total systematic uncertainty is different from the sum in quadrature of the different groups due to the correlations among the nuisance parameters in the fit.

Category	$SU(2)_L, \eta_D = 0.25,$	$SU(2)_L, \eta_D = 0.35,$
	$m_{\pi_D} = 400 \text{ GeV}$	$m_{\pi_D} = 700 \text{ GeV}$
Luminosity	0.03	0.05
Pileup	0.05	0.09
Flavor tagging	0.28	0.26
Leptons	0.01	0.04
Jets	0.08	0.14
$t\bar{t} + \geq 1b$	0.26	0.53
$t\bar{t} + \geq 1c$	0.12	0.18
$t\bar{t} + \text{light}$	0.13	0.17
Top p_T NNLO reweighting	0.08	0.09
Single top	0.06	0.06
Statistical	0.28	0.24
Instrumental	0.30	0.30
Theory	0.38	0.63

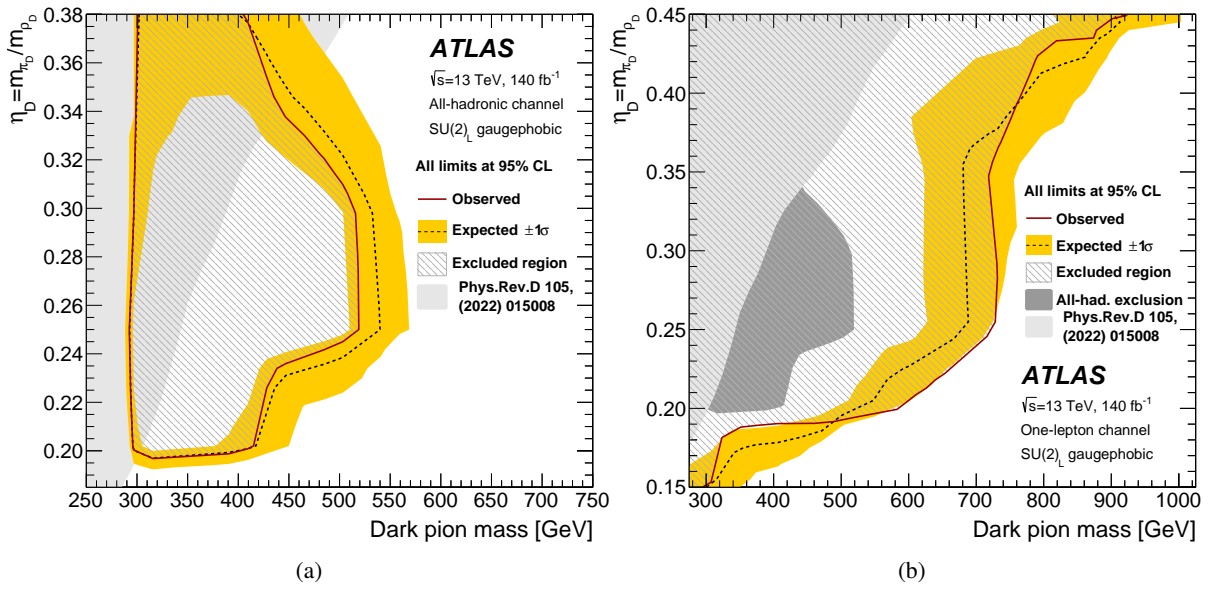


Figure 13: Observed (solid line) and expected (dashed line) exclusion contours at 95% CL in the $\eta_D - m_{\pi_D}$ plane for $SU(2)_L$ signal models in the (a) all-hadronic and (b) one-lepton channel. Masses that are within the contours are excluded, as indicated by the hatched area. An uncertainty band corresponding to the $\pm 1\sigma$ variation on the expected limit is also indicated. The shaded area in (a) and the innermost shaded area in (b) indicates the phase space previously excluded through re-interpretation of other collider searches presented in Ref. [2]. The outermost shaded area in (b) indicates the phase space excluded by the analysis in the all-hadronic channel and is identical to the observed limit shown in (a).

10 Conclusion

Results from a search for dark mesons originating from strongly-coupled, $SU(2)$ dark flavor symmetry conserving models and decaying to top and bottom quarks are reported. The analysis is based on the full Run 2 data sample of proton-proton collisions at $\sqrt{s} = 13$ TeV recorded by the ATLAS detector at the LHC, corresponding to an integrated luminosity of 140 fb^{-1} . The search is performed in the all-hadronic channel, where the event signature results in eight to ten jets of which at least four originate from bottom quarks, and in the one-lepton channel, corresponding to final states with one electron or muon in addition to jets. In the all-hadronic channel, a data-driven technique is used to estimate the predominant multijet background. In the one-lepton channel, the dominant background comes from $t\bar{t}$ production and is estimated from MC simulations.

No excess above the SM background expectation is observed. The strongest exclusion limits are obtained from the one-lepton channel. For $SU(2)_L$ signals with $m_{\pi_D}/m_{\rho_D} = 0.45$, dark pions with masses $m_{\pi_D} < 940$ GeV are excluded, while for $m_{\pi_D}/m_{\rho_D} = 0.25$ the exclusion covers the mass range $m_{\pi_D} < 740$ GeV. These results constitute the first direct collider constraints on this type of model, and significantly extend the phase space previously excluded through re-interpretation of other collider searches.

Acknowledgments

We thank CERN for the very successful operation of the LHC and its injectors, as well as the support staff at CERN and at our institutions worldwide without whom ATLAS could not be operated efficiently.

The crucial computing support from all WLCG partners is acknowledged gratefully, in particular from CERN, the ATLAS Tier-1 facilities at TRIUMF/SFU (Canada), NDGF (Denmark, Norway, Sweden), CC-IN2P3 (France), KIT/GridKA (Germany), INFN-CNAF (Italy), NL-T1 (Netherlands), PIC (Spain), RAL (UK) and BNL (USA), the Tier-2 facilities worldwide and large non-WLCG resource providers. Major contributors of computing resources are listed in Ref. [96].

We gratefully acknowledge the support of ANPCyT, Argentina; YerPhI, Armenia; ARC, Australia; BMWFW and FWF, Austria; ANAS, Azerbaijan; CNPq and FAPESP, Brazil; NSERC, NRC and CFI, Canada; CERN; ANID, Chile; CAS, MOST and NSFC, China; Minciencias, Colombia; MEYS CR, Czech Republic; DNRF and DNSRC, Denmark; IN2P3-CNRS and CEA-DRF/IRFU, France; SRNSFG, Georgia; BMBF, HGF and MPG, Germany; GSRI, Greece; RGC and Hong Kong SAR, China; ISF and Benozziyo Center, Israel; INFN, Italy; MEXT and JSPS, Japan; CNRST, Morocco; NWO, Netherlands; RCN, Norway; MNiSW, Poland; FCT, Portugal; MNE/IFA, Romania; MESTD, Serbia; MSSR, Slovakia; ARIS and MVZI, Slovenia; DSI/NRF, South Africa; MICIU/AEI, Spain; SRC and Wallenberg Foundation, Sweden; SERI, SNSF and Cantons of Bern and Geneva, Switzerland; NSTC, Taipei; TENMAK, Türkiye; STFC/UKRI, United Kingdom; DOE and NSF, United States of America.

Individual groups and members have received support from BCKDF, CANARIE, CRC and DRAC, Canada; CERN-CZ, FORTE and PRIMUS, Czech Republic; COST, ERC, ERDF, Horizon 2020, ICSC-NextGenerationEU and Marie Skłodowska-Curie Actions, European Union; Investissements d’Avenir Labex, Investissements d’Avenir Idex and ANR, France; DFG and AvH Foundation, Germany; Herakleitos, Thales and Aristeia programmes co-financed by EU-ESF and the Greek NSRF, Greece; BSF-NSF and MINERVA, Israel; NCN and NAWA, Poland; La Caixa Banking Foundation, CERCA Programme Generalitat de

Catalunya and PROMETEO and GenT Programmes Generalitat Valenciana, Spain; Göran Gustafssons Stiftelse, Sweden; The Royal Society and Leverhulme Trust, United Kingdom.

In addition, individual members wish to acknowledge support from Armenia: Yerevan Physics Institute (FAPERJ); CERN: European Organization for Nuclear Research (CERN PJA); Chile: Agencia Nacional de Investigación y Desarrollo (FONDECYT 1230812, FONDECYT 1230987, FONDECYT 1240864); China: Chinese Ministry of Science and Technology (MOST-2023YFA1605700), National Natural Science Foundation of China (NSFC - 12175119, NSFC 12275265, NSFC-12075060); Czech Republic: Czech Science Foundation (GACR - 24-11373S), Ministry of Education Youth and Sports (FORTE CZ.02.01.01/00/22_008/0004632), PRIMUS Research Programme (PRIMUS/21/SCI/017); EU: H2020 European Research Council (ERC - 101002463); European Union: European Research Council (ERC - 948254, ERC 101089007), Horizon 2020 Framework Programme (MUCCA - CHIST-ERA-19-XAI-00), European Union, Future Artificial Intelligence Research (FAIR-NextGenerationEU PE00000013), Italian Center for High Performance Computing, Big Data and Quantum Computing (ICSC, NextGenerationEU); France: Agence Nationale de la Recherche (ANR-20-CE31-0013, ANR-21-CE31-0013, ANR-21-CE31-0022, ANR-22-EDIR-0002), Investissements d’Avenir Labex (ANR-11-LABX-0012); Germany: Baden-Württemberg Stiftung (BW Stiftung-Postdoc Eliteprogramme), Deutsche Forschungsgemeinschaft (DFG - 469666862, DFG - CR 312/5-2); Italy: Istituto Nazionale di Fisica Nucleare (ICSC, NextGenerationEU), Ministero dell’Università e della Ricerca (PRIN - 20223N7F8K - PNRR M4.C2.1.1); Japan: Japan Society for the Promotion of Science (JSPS KAKENHI JP22H01227, JSPS KAKENHI JP22H04944, JSPS KAKENHI JP22KK0227, JSPS KAKENHI JP23KK0245); Netherlands: Netherlands Organisation for Scientific Research (NWO Veni 2020 - VI.Veni.202.179); Norway: Research Council of Norway (RCN-314472); Poland: Ministry of Science and Higher Education (IDUB AGH, POB8, D4 no 9722), Polish National Agency for Academic Exchange (PPN/PPO/2020/1/00002/U/00001), Polish National Science Centre (NCN 2021/42/E/ST2/00350, NCN OPUS nr 2022/47/B/ST2/03059, NCN UMO-2019/34/E/ST2/00393, UMO-2020/37/B/ST2/01043, UMO-2021/40/C/ST2/00187, UMO-2022/47/O/ST2/00148, UMO-2023/49/B/ST2/04085); Slovenia: Slovenian Research Agency (ARIS grant J1-3010); Spain: Generalitat Valenciana (Artemisa, FEDER, IDIFEDER/2018/048), Ministry of Science and Innovation (MCIN & NextGenEU PCI2022-135018-2, MICIN & FEDER PID2021-125273NB, RYC2019-028510-I, RYC2020-030254-I, RYC2021-031273-I, RYC2022-038164-I), PROMETEO and GenT Programmes Generalitat Valenciana (CIDEAGENT/2019/027); Sweden: Swedish Research Council (Swedish Research Council 2023-04654, VR 2018-00482, VR 2022-03845, VR 2022-04683, VR 2023-03403, VR grant 2021-03651), Knut and Alice Wallenberg Foundation (KAW 2018.0157, KAW 2018.0458, KAW 2019.0447, KAW 2022.0358); Switzerland: Swiss National Science Foundation (SNSF - PCEFP2_194658); United Kingdom: Leverhulme Trust (Leverhulme Trust RPG-2020-004), Royal Society (NIF-R1-231091); United States of America: U.S. Department of Energy (ECA DE-AC02-76SF00515), Neubauer Family Foundation.

References

- [1] G. D. Kribs and E. T. Neil, *Review of strongly-coupled composite dark matter models and lattice simulations*, *Int. J. Mod. Phys. A* **31** (2016) 1643004, arXiv: [1604.04627 \[hep-ph\]](#).
- [2] J. M. Butterworth, L. Corpe, X. Kong, S. Kulkarni, and M. Thomas, *New sensitivity of LHC measurements to composite dark matter models*, *Phys. Rev. D* **105** (2022) 015008, arXiv: [2105.08494 \[hep-ph\]](#).

- [3] Lattice Strong Dynamics (LSD) Collaboration, *Stealth Dark Matter: Dark scalar baryons through the Higgs portal*, *Phys. Rev. D* **92** (2015) 075030, arXiv: [1503.04203](https://arxiv.org/abs/1503.04203) [[hep-ph](#)].
- [4] G. D. Kribs, A. Martin, B. Ostdiek, and T. Tong, *Dark Mesons at the LHC*, *JHEP* **07** (2019) 133, arXiv: [1809.10184](https://arxiv.org/abs/1809.10184) [[hep-ph](#)].
- [5] G. D. Kribs, A. Martin, and T. Tong, *Effective Theories of Dark Mesons with Custodial Symmetry*, *JHEP* **08** (2019) 020, arXiv: [1809.10183](https://arxiv.org/abs/1809.10183) [[hep-ph](#)].
- [6] ATLAS Collaboration, *Search for new high-mass phenomena in the dilepton final state using 36fb^{-1} of proton–proton collision data at $\sqrt{s} = 13\text{ TeV}$ with the ATLAS detector*, *JHEP* **10** (2017) 182, arXiv: [1707.02424](https://arxiv.org/abs/1707.02424) [[hep-ex](#)].
- [7] CMS Collaboration, *Search for high-mass resonances in dilepton final states in proton–proton collisions at $\sqrt{s} = 13\text{ TeV}$* , *JHEP* **06** (2018) 120, arXiv: [1803.06292](https://arxiv.org/abs/1803.06292) [[hep-ex](#)].
- [8] ATLAS Collaboration, *The ATLAS Experiment at the CERN Large Hadron Collider*, *JINST* **3** (2008) S08003.
- [9] ATLAS Collaboration, *ATLAS Insertable B-Layer: Technical Design Report*, ATLAS-TDR-19; CERN-LHCC-2010-013, 2010, URL: <https://cds.cern.ch/record/1291633>, Addendum: ATLAS-TDR-19-ADD-1; CERN-LHCC-2012-009, 2012, URL: <https://cds.cern.ch/record/1451888>.
- [10] B. Abbott et al., *Production and integration of the ATLAS Insertable B-Layer*, *JINST* **13** (2018) T05008, arXiv: [1803.00844](https://arxiv.org/abs/1803.00844) [[physics.ins-det](#)].
- [11] G. Avoni et al., *The new LUCID-2 detector for luminosity measurement and monitoring in ATLAS*, *JINST* **13** (2018) P07017.
- [12] ATLAS Collaboration, *Performance of the ATLAS trigger system in 2015*, *Eur. Phys. J. C* **77** (2017) 317, arXiv: [1611.09661](https://arxiv.org/abs/1611.09661) [[hep-ex](#)].
- [13] ATLAS Collaboration, *Software and computing for Run 3 of the ATLAS experiment at the LHC*, (2024), arXiv: [2404.06335](https://arxiv.org/abs/2404.06335) [[hep-ex](#)].
- [14] ATLAS Collaboration, *Luminosity determination in pp collisions at $\sqrt{s} = 13\text{ TeV}$ using the ATLAS detector at the LHC*, *Eur. Phys. J. C* **83** (2023) 982, arXiv: [2212.09379](https://arxiv.org/abs/2212.09379) [[hep-ex](#)].
- [15] S. Agostinelli et al., *GEANT4 – a simulation toolkit*, *Nucl. Instrum. Meth. A* **506** (2003) 250.
- [16] ATLAS Collaboration, *The ATLAS Simulation Infrastructure*, *Eur. Phys. J. C* **70** (2010) 823, arXiv: [1005.4568](https://arxiv.org/abs/1005.4568) [[physics.ins-det](#)].
- [17] J. Alwall et al., *The automated computation of tree-level and next-to-leading order differential cross sections, and their matching to parton shower simulations*, *JHEP* **07** (2014) 079, arXiv: [1405.0301](https://arxiv.org/abs/1405.0301) [[hep-ph](#)].
- [18] T. Sjöstrand et al., *An introduction to PYTHIA 8.2*, *Comput. Phys. Commun.* **191** (2015) 159, arXiv: [1410.3012](https://arxiv.org/abs/1410.3012) [[hep-ph](#)].
- [19] ATLAS Collaboration, *ATLAS Pythia 8 tunes to 7 TeV data*, ATL-PHYS-PUB-2014-021, 2014, URL: <https://cds.cern.ch/record/1966419>.
- [20] NNPDF Collaboration, R. D. Ball, et al., *Parton distributions with LHC data*, *Nucl. Phys. B* **867** (2013) 244, arXiv: [1207.1303](https://arxiv.org/abs/1207.1303) [[hep-ph](#)].

- [21] D. J. Lange, *The EvtGen particle decay simulation package*, *Nucl. Instrum. Meth. A* **462** (2001) 152.
- [22] C. Bierlich et al., *A comprehensive guide to the physics and usage of PYTHIA 8.3*, 2022, URL: <https://arxiv.org/abs/2203.11601>.
- [23] S. Frixione, G. Ridolfi, and P. Nason, *A positive-weight next-to-leading-order Monte Carlo for heavy flavour hadroproduction*, *JHEP* **09** (2007) 126, arXiv: [0707.3088](https://arxiv.org/abs/0707.3088) [[hep-ph](#)].
- [24] P. Nason, *A new method for combining NLO QCD with shower Monte Carlo algorithms*, *JHEP* **11** (2004) 040, arXiv: [hep-ph/0409146](https://arxiv.org/abs/hep-ph/0409146).
- [25] S. Frixione, P. Nason, and C. Oleari, *Matching NLO QCD computations with parton shower simulations: the POWHEG method*, *JHEP* **11** (2007) 070, arXiv: [0709.2092](https://arxiv.org/abs/0709.2092) [[hep-ph](#)].
- [26] S. Alioli, P. Nason, C. Oleari, and E. Re, *A general framework for implementing NLO calculations in shower Monte Carlo programs: the POWHEG BOX*, *JHEP* **06** (2010) 043, arXiv: [1002.2581](https://arxiv.org/abs/1002.2581) [[hep-ph](#)].
- [27] NNPDF Collaboration, R. D. Ball, et al., *Parton distributions for the LHC run II*, *JHEP* **04** (2015) 040, arXiv: [1410.8849](https://arxiv.org/abs/1410.8849) [[hep-ph](#)].
- [28] S. Carrazza, S. Forte, Z. Kassabov, J. I. Latorre, and J. Rojo, *An unbiased Hessian representation for Monte Carlo PDFs*, *Eur. Phys. J. C* **75** (2015) 369, arXiv: [1505.06736](https://arxiv.org/abs/1505.06736) [[hep-ph](#)].
- [29] ATLAS Collaboration, *Studies on top-quark Monte Carlo modelling for Top2016*, ATL-PHYS-PUB-2016-020, 2016, URL: <https://cds.cern.ch/record/2216168>.
- [30] M. Beneke, P. Falgari, S. Klein, and C. Schwinn, *Hadronic top-quark pair production with NNLL threshold resummation*, *Nucl. Phys. B* **855** (2012) 695, arXiv: [1109.1536](https://arxiv.org/abs/1109.1536) [[hep-ph](#)].
- [31] M. Cacciari, M. Czakon, M. Mangano, A. Mitov, and P. Nason, *Top-pair production at hadron colliders with next-to-next-to-leading logarithmic soft-gluon resummation*, *Phys. Lett. B* **710** (2012) 612, arXiv: [1111.5869](https://arxiv.org/abs/1111.5869) [[hep-ph](#)].
- [32] P. Bärnreuther, M. Czakon, and A. Mitov, *Percent-Level-Precision Physics at the Tevatron: Next-to-Next-to-Leading Order QCD Corrections to $q\bar{q} \rightarrow t\bar{t} + X$* , *Phys. Rev. Lett.* **109** (2012) 132001, arXiv: [1204.5201](https://arxiv.org/abs/1204.5201) [[hep-ph](#)].
- [33] M. Czakon and A. Mitov, *NNLO corrections to top-pair production at hadron colliders: the all-fermionic scattering channels*, *JHEP* **12** (2012) 054, arXiv: [1207.0236](https://arxiv.org/abs/1207.0236) [[hep-ph](#)].
- [34] M. Czakon and A. Mitov, *NNLO corrections to top pair production at hadron colliders: the quark-gluon reaction*, *JHEP* **01** (2013) 080, arXiv: [1210.6832](https://arxiv.org/abs/1210.6832) [[hep-ph](#)].
- [35] M. Czakon, P. Fiedler, and A. Mitov, *Total Top-Quark Pair-Production Cross Section at Hadron Colliders Through $O(\alpha_S^4)$* , *Phys. Rev. Lett.* **110** (2013) 252004, arXiv: [1303.6254](https://arxiv.org/abs/1303.6254) [[hep-ph](#)].
- [36] M. Czakon and A. Mitov, *Top++: A program for the calculation of the top-pair cross-section at hadron colliders*, *Comput. Phys. Commun.* **185** (2014) 2930, arXiv: [1112.5675](https://arxiv.org/abs/1112.5675) [[hep-ph](#)].

- [37] T. Ježo, J. M. Lindert, N. Moretti, and S. Pozzorini, *New NLOPS predictions for $t\bar{t} + b$ -jet production at the LHC*, *Eur. Phys. J. C* **78** (2018) 502, arXiv: [1802.00426 \[hep-ph\]](#).
- [38] F. Buccioni et al., *OpenLoops 2*, *Eur. Phys. J. C* **79** (2019) 866, arXiv: [1907.13071 \[hep-ph\]](#).
- [39] F. Cascioli, P. Maierhöfer, and S. Pozzorini, *Scattering Amplitudes with Open Loops*, *Phys. Rev. Lett.* **108** (2012) 111601, arXiv: [1111.5206 \[hep-ph\]](#).
- [40] A. Denner, S. Dittmaier, and L. Hofer, *COLLIER: A fortran-based complex one-loop library in extended regularizations*, *Comput. Phys. Commun.* **212** (2017) 220, arXiv: [1604.06792 \[hep-ph\]](#).
- [41] T. Ježo, *Powheg-Box-Res ttbb source code*, 2019, URL: https://gitlab.cern.ch/tjezo/powheg-box-res_ttbb/.
- [42] ATLAS Collaboration, *Measurements of top-quark pair differential cross-sections in the lepton+jets channel in pp collisions at $\sqrt{s} = 8$ TeV using the ATLAS detector*, *Eur. Phys. J. C* **76** (2016) 538, arXiv: [1511.04716 \[hep-ex\]](#).
- [43] M. Czakon et al., *Top-pair production at the LHC through NNLO QCD and NLO EW*, *JHEP* **10** (2017) 186, arXiv: [1705.04105 \[hep-ph\]](#).
- [44] M. Cacciari, G. P. Salam, and G. Soyez, *The anti- k_t jet clustering algorithm*, *JHEP* **04** (2008) 063, arXiv: [0802.1189 \[hep-ph\]](#).
- [45] M. Cacciari, G. P. Salam, and G. Soyez, *FastJet user manual*, *Eur. Phys. J. C* **72** (2012) 1896, arXiv: [1111.6097 \[hep-ph\]](#).
- [46] E. Bothmann et al., *Event generation with Sherpa 2.2*, *SciPost Phys.* **7** (2019) 034, arXiv: [1905.09127 \[hep-ph\]](#).
- [47] T. Gleisberg and S. Höche, *Comix, a new matrix element generator*, *JHEP* **12** (2008) 039, arXiv: [0808.3674 \[hep-ph\]](#).
- [48] S. Schumann and F. Krauss, *A parton shower algorithm based on Catani–Seymour dipole factorisation*, *JHEP* **03** (2008) 038, arXiv: [0709.1027 \[hep-ph\]](#).
- [49] S. Höche, F. Krauss, M. Schönherr, and F. Siegert, *A critical appraisal of NLO+PS matching methods*, *JHEP* **09** (2012) 049, arXiv: [1111.1220 \[hep-ph\]](#).
- [50] S. Höche, F. Krauss, M. Schönherr, and F. Siegert, *QCD matrix elements + parton showers. The NLO case*, *JHEP* **04** (2013) 027, arXiv: [1207.5030 \[hep-ph\]](#).
- [51] S. Catani, F. Krauss, B. R. Webber, and R. Kuhn, *QCD Matrix Elements + Parton Showers*, *JHEP* **11** (2001) 063, arXiv: [hep-ph/0109231](#).
- [52] S. Höche, F. Krauss, S. Schumann, and F. Siegert, *QCD matrix elements and truncated showers*, *JHEP* **05** (2009) 053, arXiv: [0903.1219 \[hep-ph\]](#).
- [53] C. Anastasiou, L. Dixon, K. Melnikov, and F. Petriello, *High-precision QCD at hadron colliders: Electroweak gauge boson rapidity distributions at next-to-next-to leading order*, *Phys. Rev. D* **69** (2004) 094008, arXiv: [hep-ph/0312266](#).
- [54] E. Re, *Single-top Wt -channel production matched with parton showers using the POWHEG method*, *Eur. Phys. J. C* **71** (2011) 1547, arXiv: [1009.2450 \[hep-ph\]](#).

- [55] S. Frixione, E. Laenen, P. Motylinski, C. White, and B. R. Webber, *Single-top hadroproduction in association with a W boson*, **JHEP** **07** (2008) 029, arXiv: [0805.3067 \[hep-ph\]](#).
- [56] R. Frederix, E. Re, and P. Torrielli, *Single-top t-channel hadroproduction in the four-flavour scheme with POWHEG and aMC@NLO*, **JHEP** **09** (2012) 130, arXiv: [1207.5391 \[hep-ph\]](#).
- [57] S. Alioli, P. Nason, C. Oleari, and E. Re, *NLO single-top production matched with shower in POWHEG: s- and t-channel contributions*, **JHEP** **09** (2009) 111, arXiv: [0907.4076 \[hep-ph\]](#), Erratum: **JHEP** **02** (2010) 011.
- [58] R. Frederix, D. Pagani, and M. Zaro, *Large NLO corrections in $t\bar{t}W^\pm$ and $t\bar{t}\bar{t}$ hadroproduction from supposedly subleading EW contributions*, **JHEP** **02** (2018) 031, arXiv: [1711.02116 \[hep-ph\]](#).
- [59] S. Frixione, E. Laenen, P. Motylinski, and B. R. Webber, *Angular correlations of lepton pairs from vector boson and top quark decays in Monte Carlo simulations*, **JHEP** **04** (2007) 081, arXiv: [hep-ph/0702198](#).
- [60] P. Artoisenet, R. Frederix, O. Mattelaer, and R. Rietkerk, *Automatic spin-entangled decays of heavy resonances in Monte Carlo simulations*, **JHEP** **03** (2013) 015, arXiv: [1212.3460 \[hep-ph\]](#).
- [61] H. B. Hartanto, B. Jäger, L. Reina, and D. Wackerroth, *Higgs boson production in association with top quarks in the POWHEG BOX*, **Phys. Rev. D** **91** (2015) 094003, arXiv: [1501.04498 \[hep-ph\]](#).
- [62] D. de Florian et al., *Handbook of LHC Higgs Cross Sections: 4. Deciphering the Nature of the Higgs Sector*, (2017), arXiv: [1610.07922 \[hep-ph\]](#).
- [63] ATLAS Collaboration, *Vertex Reconstruction Performance of the ATLAS Detector at $\sqrt{s} = 13$ TeV*, ATL-PHYS-PUB-2015-026, 2015, URL: <https://cds.cern.ch/record/2037717>.
- [64] ATLAS Collaboration, *Electron and photon performance measurements with the ATLAS detector using the 2015–2017 LHC proton–proton collision data*, **JINST** **14** (2019) P12006, arXiv: [1908.00005 \[hep-ex\]](#).
- [65] ATLAS Collaboration, *Electron reconstruction and identification in the ATLAS experiment using the 2015 and 2016 LHC proton–proton collision data at $\sqrt{s} = 13$ TeV*, **Eur. Phys. J. C** **79** (2019) 639, arXiv: [1902.04655 \[physics.ins-det\]](#).
- [66] ATLAS Collaboration, *Muon reconstruction and identification efficiency in ATLAS using the full Run 2 pp collision data set at $\sqrt{s} = 13$ TeV*, **Eur. Phys. J. C** **81** (2021) 578, arXiv: [2012.00578 \[hep-ex\]](#).
- [67] ATLAS Collaboration, *Jet reconstruction and performance using particle flow with the ATLAS Detector*, **Eur. Phys. J. C** **77** (2017) 466, arXiv: [1703.10485 \[hep-ex\]](#).
- [68] ATLAS Collaboration, *Topological cell clustering in the ATLAS calorimeters and its performance in LHC Run 1*, **Eur. Phys. J. C** **77** (2017) 490, arXiv: [1603.02934 \[hep-ex\]](#).
- [69] ATLAS Collaboration, *Performance of pile-up mitigation techniques for jets in pp collisions at $\sqrt{s} = 8$ TeV using the ATLAS detector*, **Eur. Phys. J. C** **76** (2016) 581, arXiv: [1510.03823 \[hep-ex\]](#).

- [70] ATLAS Collaboration, *Jet energy scale and resolution measured in proton–proton collisions at $\sqrt{s} = 13$ TeV with the ATLAS detector*, *Eur. Phys. J. C* **81** (2021) 689, arXiv: [2007.02645 \[hep-ex\]](#).
- [71] ATLAS Collaboration, *Characterisation and mitigation of beam-induced backgrounds observed in the ATLAS detector during the 2011 proton–proton run*, *JINST* **8** (2013) P07004, arXiv: [1303.0223 \[hep-ex\]](#).
- [72] ATLAS Collaboration, *Selection of jets produced in 13 TeV proton–proton collisions with the ATLAS detector*, ATLAS-CONF-2015-029, 2015, URL: <https://cds.cern.ch/record/2037702>.
- [73] ATLAS Collaboration, *ATLAS flavour-tagging algorithms for the LHC Run 2 pp collision dataset*, *Eur. Phys. J. C* **83** (2023) 681, arXiv: [2211.16345 \[physics.data-an\]](#).
- [74] ATLAS Collaboration, *Optimisation and performance studies of the ATLAS b-tagging algorithms for the 2017-18 LHC run*, ATL-PHYS-PUB-2017-013, 2017, URL: <https://cds.cern.ch/record/2273281>.
- [75] ATLAS Collaboration, *ATLAS b-jet identification performance and efficiency measurement with $t\bar{t}$ events in pp collisions at $\sqrt{s} = 13$ TeV*, *Eur. Phys. J. C* **79** (2019) 970, arXiv: [1907.05120 \[hep-ex\]](#).
- [76] ATLAS Collaboration, *Calibration of the light-flavour jet mistagging efficiency of the b-tagging algorithms with Z+jets events using 139fb^{-1} of ATLAS proton–proton collision data at $\sqrt{s} = 13$ TeV*, *Eur. Phys. J. C* **83** (2023) 728, arXiv: [2301.06319 \[hep-ex\]](#).
- [77] ATLAS Collaboration, *Measurement of the c-jet mistagging efficiency in $t\bar{t}$ events using pp collision data at $\sqrt{s} = 13$ TeV collected with the ATLAS detector*, *Eur. Phys. J. C* **82** (2022) 95, arXiv: [2109.10627 \[hep-ex\]](#).
- [78] B. Nachman, P. Nef, A. Schwartzman, M. Swiatlowski, and C. Wanotayaroj, *Jets from jets: re-clustering as a tool for large radius jet reconstruction and grooming at the LHC*, *JHEP* **02** (2015) 075, arXiv: [1407.2922 \[hep-ph\]](#).
- [79] ATLAS Collaboration, *The performance of the jet trigger for the ATLAS detector during 2011 data taking*, *Eur. Phys. J. C* **76** (2016) 526, arXiv: [1606.07759 \[hep-ex\]](#).
- [80] ATLAS Collaboration, *Performance of the ATLAS muon triggers in Run 2*, *JINST* **15** (2020) P09015, arXiv: [2004.13447 \[physics.ins-det\]](#).
- [81] ATLAS Collaboration, *Performance of electron and photon triggers in ATLAS during LHC Run 2*, *Eur. Phys. J. C* **80** (2020) 47, arXiv: [1909.00761 \[hep-ex\]](#).
- [82] ATLAS Collaboration, *Operation of the ATLAS trigger system in Run 2*, *JINST* **15** (2020) P10004, arXiv: [2007.12539 \[hep-ex\]](#).
- [83] ATLAS Collaboration, *The ATLAS inner detector trigger performance in pp collisions at 13 TeV during LHC Run 2*, *Eur. Phys. J. C* **82** (2022) 206, arXiv: [2107.02485 \[hep-ex\]](#).
- [84] ATLAS Collaboration, *Measurements of $t\bar{t}$ differential cross-sections of highly boosted top quarks decaying to all-hadronic final states in pp collisions at $\sqrt{s} = 13$ TeV using the ATLAS detector*, *Phys. Rev. D* **98** (2018) 012003, arXiv: [1801.02052 \[hep-ex\]](#).

- [85] ATLAS Collaboration, *Measurements of inclusive and differential fiducial cross-sections of $t\bar{t}$ production with additional heavy-flavour jets in proton–proton collisions at $\sqrt{s} = 13$ TeV with the ATLAS detector*, [JHEP **04** \(2019\) 046](#), arXiv: [1811.12113 \[hep-ex\]](#).
- [86] ATLAS Collaboration, *Simulation-based extrapolation of b -tagging calibrations towards high transverse momenta in the ATLAS experiment*, ATL-PHYS-PUB-2021-003, 2021, URL: <https://cds.cern.ch/record/2753444>.
- [87] ATLAS Collaboration, *Search for top-philic heavy resonances in pp collisions at $\sqrt{s} = 13$ TeV with the ATLAS detector*, [Eur. Phys. J. C **84** \(2024\) 157](#), arXiv: [2304.01678 \[hep-ex\]](#).
- [88] M. Botje et al., *The PDF4LHC Working Group Interim Recommendations*, 2011, arXiv: [1101.0538 \[hep-ph\]](#).
- [89] S. Höche, S. Mrenna, S. Payne, C. T. Preuss, and P. Skands, *A Study of QCD Radiation in VBF Higgs Production with Vincia and Pythia*, [SciPost Phys. **12** \(2022\) 010](#), arXiv: [2106.10987 \[hep-ph\]](#).
- [90] M. Bähr et al., *Herwig++ physics and manual*, [Eur. Phys. J. C **58** \(2008\) 639](#), arXiv: [0803.0883 \[hep-ph\]](#).
- [91] J. Bellm et al., *Herwig 7.0/Herwig++ 3.0 release note*, [Eur. Phys. J. C **76** \(2016\) 196](#), arXiv: [1512.01178 \[hep-ph\]](#).
- [92] L. A. Harland-Lang, A. D. Martin, P. Motylinski, and R. S. Thorne, *Parton distributions in the LHC era: MMHT 2014 PDFs*, [Eur. Phys. J. C **75** \(2015\) 204](#), arXiv: [1412.3989 \[hep-ph\]](#).
- [93] W. Verkerke and D. Kirkby, *The RooFit toolkit for data modeling*, 2003, arXiv: [physics/0306116 \[physics.data-an\]](#).
- [94] M. Hatlo et al., *Developments of mathematical software libraries for the LHC experiments*, [IEEE Trans. Nucl. Sci. **52** \(2005\) 2818](#).
- [95] A. L. Read, *Presentation of search results: the CL_S technique*, [J. Phys. G **28** \(2002\) 2693](#).
- [96] ATLAS Collaboration, *ATLAS Computing Acknowledgements*, ATL-SOFT-PUB-2023-001, 2023, URL: <https://cds.cern.ch/record/2869272>.

The ATLAS Collaboration

G. Aad ¹⁰⁴, E. Aakvaag ¹⁷, B. Abbott ¹²³, S. Abdelhameed ^{119a}, K. Abeling ⁵⁶, N.J. Abicht ⁵⁰, S.H. Abidi ³⁰, M. Aboeela ⁴⁵, A. Aboulhorma ^{36e}, H. Abramowicz ¹⁵⁴, H. Abreu ¹⁵³, Y. Abulaiti ¹²⁰, B.S. Acharya ^{70a,70b,k}, A. Ackermann ^{64a}, C. Adam Bourdarios ⁴, L. Adamczyk ^{87a}, S.V. Addepalli ²⁷, M.J. Addison ¹⁰³, J. Adelman ¹¹⁸, A. Adiguzel ^{22c}, T. Adye ¹³⁷, A.A. Affolder ¹³⁹, Y. Afik ⁴⁰, M.N. Agaras ¹³, J. Agarwala ^{74a,74b}, A. Aggarwal ¹⁰², C. Agheorghiesei ^{28c}, F. Ahmadov ^{39,y}, W.S. Ahmed ¹⁰⁶, S. Ahuja ⁹⁷, X. Ai ^{63e}, G. Aielli ^{77a,77b}, A. Aikot ¹⁶⁶, M. Ait Tamlihat ^{36e}, B. Aitbenkikh ^{36a}, M. Akbiyik ¹⁰², T.P.A. Åkesson ¹⁰⁰, A.V. Akimov ³⁸, D. Akiyama ¹⁷¹, N.N. Akolkar ²⁵, S. Aktas ^{22a}, K. Al Houry ⁴², G.L. Alberghi ^{24b}, J. Albert ¹⁶⁸, P. Albicocco ⁵⁴, G.L. Albouy ⁶¹, S. Alderweireldt ⁵³, Z.L. Alegria ¹²⁴, M. Aleksa ³⁷, I.N. Aleksandrov ³⁹, C. Alexa ^{28b}, T. Alexopoulos ¹⁰, F. Alfonsi ^{24b}, M. Algren ⁵⁷, M. Alhroob ¹⁷⁰, B. Ali ¹³⁵, H.M.J. Ali ^{93,s}, S. Ali ³², S.W. Alibocus ⁹⁴, M. Aliev ^{34c}, G. Alimonti ^{72a}, W. Alkahi ⁵⁶, C. Allaire ⁶⁷, B.M.M. Allbrooke ¹⁴⁹, J.F. Allen ⁵³, C.A. Allendes Flores ^{140f}, P.P. Allport ²¹, A. Aloisio ^{73a,73b}, F. Alonso ⁹², C. Alpigiani ¹⁴¹, Z.M.K. Alsolami ⁹³, M. Alvarez Estevez ¹⁰¹, A. Alvarez Fernandez ¹⁰², M. Alves Cardoso ⁵⁷, M.G. Alvigi ^{73a,73b}, M. Aly ¹⁰³, Y. Amaral Coutinho ^{84b}, A. Ambler ¹⁰⁶, C. Amelung ³⁷, M. Amerl ¹⁰³, C.G. Ames ¹¹¹, D. Amidei ¹⁰⁸, B. Amini ⁵⁵, K.J. Amirie ¹⁵⁸, S.P. Amor Dos Santos ^{133a}, K.R. Amos ¹⁶⁶, D. Amperiadou ¹⁵⁵, S. An ⁸⁵, V. Ananiev ¹²⁸, C. Anastopoulos ¹⁴², T. Andeen ¹¹, J.K. Anders ³⁷, A.C. Anderson ⁶⁰, S.Y. Andreato ^{48a,48b}, A. Andreazza ^{72a,72b}, S. Angelidakis ⁹, A. Angerami ⁴², A.V. Anisenkov ³⁸, A. Annovi ^{75a}, C. Antel ⁵⁷, E. Antipov ¹⁴⁸, M. Antonelli ⁵⁴, F. Anulli ^{76a}, M. Aoki ⁸⁵, T. Aoki ¹⁵⁶, M.A. Aparo ¹⁴⁹, L. Aperio Bella ⁴⁹, C. Appelt ¹⁹, A. Apyan ²⁷, S.J. Arbiol Val ⁸⁸, C. Arcangeletti ⁵⁴, A.T.H. Arce ⁵², J-F. Arguin ¹¹⁰, S. Argyropoulos ⁵⁵, J.-H. Arling ⁴⁹, O. Arnaez ⁴, H. Arnold ¹⁴⁸, G. Artoni ^{76a,76b}, H. Asada ¹¹³, K. Asai ¹²¹, S. Asai ¹⁵⁶, N.A. Asbah ³⁷, R.A. Ashby Pickering ¹⁷⁰, K. Assamagan ³⁰, R. Astalos ^{29a}, K.S.V. Astrand ¹⁰⁰, S. Atashi ¹⁶², R.J. Atkin ^{34a}, M. Atkinson ¹⁶⁵, H. Atmani ^{36f}, P.A. Atmasiddha ¹³¹, K. Augsten ¹³⁵, S. Auricchio ^{73a,73b}, A.D. Auriol ²¹, V.A. Austrup ¹⁰³, G. Avolio ³⁷, K. Axiotis ⁵⁷, G. Azuelos ^{110,ad}, D. Babal ^{29b}, H. Bachacou ¹³⁸, K. Bachas ^{155,o}, A. Bachiou ³⁵, F. Backman ^{48a,48b}, A. Badea ⁴⁰, T.M. Baer ¹⁰⁸, P. Bagnaia ^{76a,76b}, M. Bahmani ¹⁹, D. Bahner ⁵⁵, K. Bai ¹²⁶, J.T. Baines ¹³⁷, L. Baines ⁹⁶, O.K. Baker ¹⁷⁵, E. Bakos ¹⁶, D. Bakshi Gupta ⁸, L.E. Balabram Filho ^{84b}, V. Balakrishnan ¹²³, R. Balasubramanian ⁴, E.M. Baldin ³⁸, P. Balek ^{87a}, E. Ballabene ^{24b,24a}, F. Balli ¹³⁸, L.M. Baltes ^{64a}, W.K. Balunas ³³, J. Balz ¹⁰², I. Bamwidhi ^{119b}, E. Banas ⁸⁸, M. Bandieramonte ¹³², A. Bandyopadhyay ²⁵, S. Bansal ²⁵, L. Barak ¹⁵⁴, M. Barakat ⁴⁹, E.L. Barberio ¹⁰⁷, D. Barberis ^{58b,58a}, M. Barbero ¹⁰⁴, M.Z. Barel ¹¹⁷, T. Barillari ¹¹², M-S. Barisits ³⁷, T. Barklow ¹⁴⁶, P. Baron ¹²⁵, D.A. Baron Moreno ¹⁰³, A. Baroncelli ^{63a}, A.J. Barr ¹²⁹, J.D. Barr ⁹⁸, F. Barreiro ¹⁰¹, J. Barreiro Guimarães da Costa ¹⁴, U. Barron ¹⁵⁴, M.G. Barros Teixeira ^{133a}, S. Barsov ³⁸, F. Bartels ^{64a}, R. Bartoldus ¹⁴⁶, A.E. Barton ⁹³, P. Bartos ^{29a}, A. Basan ¹⁰², M. Baselga ⁵⁰, A. Bassalat ^{67,b}, M.J. Basso ^{159a}, S. Bataju ⁴⁵, R. Bate ¹⁶⁷, R.L. Bates ⁶⁰, S. Batlamous ¹⁰¹, B. Batool ¹⁴⁴, M. Battaglia ¹³⁹, D. Battulga ¹⁹, M. Baucé ^{76a,76b}, M. Bauer ⁸⁰, P. Bauer ²⁵, L.T. Bazzano Hurrell ³¹, J.B. Beacham ⁵², T. Beau ¹³⁰, J.Y. Beaucamp ⁹², P.H. Beauchemin ¹⁶¹, P. Bechtel ²⁵, H.P. Beck ^{20,n}, K. Becker ¹⁷⁰, A.J. Beddall ⁸³, V.A. Bednyakov ³⁹, C.P. Bee ¹⁴⁸, L.J. Beemster ¹⁶, T.A. Beermann ³⁷, M. Begalli ^{84d}, M. Beger ³⁰, A. Behera ¹⁴⁸, J.K. Behr ⁴⁹, J.F. Beirer ³⁷, F. Beisiegel ²⁵, M. Belfkir ^{119b}, G. Bella ¹⁵⁴, L. Bellagamba ^{24b}, A. Bellerive ³⁵, P. Bellos ²¹, K. Beloborodov ³⁸, D. Benčekroun ^{36a}, F. Bendebba ^{36a}, Y. Benhammou ¹⁵⁴,

K.C. Benkendorfer [ID62](#), L. Beresford [ID49](#), M. Beretta [ID54](#), E. Bergeaas Kuutmann [ID164](#), N. Berger [ID4](#),
 B. Bergmann [ID135](#), J. Beringer [ID18a](#), G. Bernardi [ID5](#), C. Bernius [ID146](#), F.U. Bernlochner [ID25](#),
 F. Bernon [ID37,104](#), A. Berrocal Guardia [ID13](#), T. Berry [ID97](#), P. Berta [ID136](#), A. Berthold [ID51](#), S. Bethke [ID112](#),
 A. Betti [ID76a,76b](#), A.J. Bevan [ID96](#), N.K. Bhalla [ID55](#), S. Bhatta [ID148](#), D.S. Bhattacharya [ID169](#),
 P. Bhattarai [ID146](#), K.D. Bhide [ID55](#), V.S. Bhopatkar [ID124](#), R.M. Bianchi [ID132](#), G. Bianco [ID24b,24a](#),
 O. Biebel [ID111](#), R. Bielski [ID126](#), M. Biglietti [ID78a](#), C.S. Billingsley [ID45](#), Y. Bimgdi [ID36f](#), M. Bindi [ID56](#),
 A. Bingul [ID22b](#), C. Bini [ID76a,76b](#), G.A. Bird [ID33](#), M. Birman [ID172](#), M. Biros [ID136](#), S. Biryukov [ID149](#),
 T. Bisanz [ID50](#), E. Bisceglie [ID44b,44a](#), J.P. Biswal [ID137](#), D. Biswas [ID144](#), I. Bloch [ID49](#), A. Blue [ID60](#),
 U. Blumenschein [ID96](#), J. Blumenthal [ID102](#), V.S. Bobrovnikov [ID38](#), M. Boehler [ID55](#), B. Boehm [ID169](#),
 D. Bogavac [ID37](#), A.G. Bogdanchikov [ID38](#), L.S. Boggia [ID130](#), C. Bohm [ID48a](#), V. Boisvert [ID97](#),
 P. Bokan [ID37](#), T. Bold [ID87a](#), M. Bomben [ID5](#), M. Bona [ID96](#), M. Boonekamp [ID138](#), C.D. Booth [ID97](#),
 A.G. Borbély [ID60](#), I.S. Bordulev [ID38](#), G. Borissov [ID93](#), D. Bortoletto [ID129](#), D. Boscherini [ID24b](#),
 M. Bosman [ID13](#), J.D. Bossio Sola [ID37](#), K. Bouaouda [ID36a](#), N. Bouchhar [ID166](#), L. Boudet [ID4](#),
 J. Boudreau [ID132](#), E.V. Bouhova-Thacker [ID93](#), D. Boumediene [ID41](#), R. Bouquet [ID58b,58a](#), A. Boveia [ID122](#),
 J. Boyd [ID37](#), D. Boye [ID30](#), I.R. Boyko [ID39](#), L. Bozianu [ID57](#), J. Bracinek [ID21](#), N. Brahimi [ID4](#),
 G. Brandt [ID174](#), O. Brandt [ID33](#), F. Braren [ID49](#), B. Brau [ID105](#), J.E. Brau [ID126](#), R. Brenner [ID172](#),
 L. Brenner [ID117](#), R. Brenner [ID164](#), S. Bressler [ID172](#), G. Brianti [ID79a,79b](#), D. Britton [ID60](#), D. Britzger [ID112](#),
 I. Brock [ID25](#), G. Brooijmans [ID42](#), E.M. Brooks [ID159b](#), E. Brost [ID30](#), L.M. Brown [ID168](#), L.E. Bruce [ID62](#),
 T.L. Bruckler [ID129](#), P.A. Bruckman de Renstrom [ID88](#), B. Brüers [ID49](#), A. Bruni [ID24b](#), G. Bruni [ID24b](#),
 M. Bruschi [ID24b](#), N. Bruscinò [ID76a,76b](#), T. Buanes [ID17](#), Q. Buat [ID141](#), D. Buchin [ID112](#), A.G. Buckley [ID60](#),
 O. Bulekov [ID38](#), B.A. Bullard [ID146](#), S. Burdin [ID94](#), C.D. Burgard [ID50](#), A.M. Burger [ID37](#),
 B. Burghgrave [ID8](#), O. Burlayenko [ID55](#), J. Burleson [ID165](#), J.T.P. Burr [ID33](#), J.C. Burzynski [ID145](#),
 E.L. Busch [ID42](#), V. Büscher [ID102](#), P.J. Bussey [ID60](#), J.M. Butler [ID26](#), C.M. Buttar [ID60](#),
 J.M. Butterworth [ID98](#), W. Buttinger [ID137](#), C.J. Buxo Vazquez [ID109](#), A.R. Buzykaev [ID38](#),
 S. Cabrera Urbán [ID166](#), L. Cadamuro [ID67](#), D. Caforio [ID59](#), H. Cai [ID132](#), Y. Cai [ID14,114c](#), Y. Cai [ID114a](#),
 V.M.M. Cairo [ID37](#), O. Cakir [ID3a](#), N. Calace [ID37](#), P. Calafiura [ID18a](#), G. Calderini [ID130](#), P. Calfayan [ID69](#),
 G. Callea [ID60](#), L.P. Caloba [ID84b](#), D. Calvet [ID41](#), S. Calvet [ID41](#), M. Calvetti [ID75a,75b](#), R. Camacho Toro [ID130](#),
 S. Camarda [ID37](#), D. Camarero Munoz [ID27](#), P. Camarri [ID77a,77b](#), M.T. Camerlingo [ID73a,73b](#),
 D. Cameron [ID37](#), C. Camincher [ID168](#), M. Campanelli [ID98](#), A. Camplani [ID43](#), V. Canale [ID73a,73b](#),
 A.C. Canbay [ID3a](#), E. Canonero [ID97](#), J. Cantero [ID166](#), Y. Cao [ID165](#), F. Capocasa [ID27](#), M. Capua [ID44b,44a](#),
 A. Carbone [ID72a,72b](#), R. Cardarelli [ID77a](#), J.C.J. Cardenas [ID8](#), G. Carducci [ID44b,44a](#), T. Carli [ID37](#),
 G. Carlino [ID73a](#), J.I. Carlotto [ID13](#), B.T. Carlson [ID132,p](#), E.M. Carlson [ID168,159a](#), J. Carmignani [ID94](#),
 L. Carminati [ID72a,72b](#), A. Carnelli [ID138](#), M. Carnesale [ID76a,76b](#), S. Caron [ID116](#), E. Carquin [ID140f](#),
 I.B. Carr [ID107](#), S. Carrá [ID72a](#), G. Carratta [ID24b,24a](#), A.M. Carroll [ID126](#), T.M. Carter [ID53](#),
 M.P. Casado [ID13,h](#), M. Caspar [ID49](#), F.L. Castillo [ID4](#), L. Castillo Garcia [ID13](#), V. Castillo Gimenez [ID166](#),
 N.F. Castro [ID133a,133e](#), A. Catinaccio [ID37](#), J.R. Catmore [ID128](#), T. Cavaliere [ID4](#), V. Cavaliere [ID30](#),
 N. Cavalli [ID24b,24a](#), L.J. Caviedes Betancourt [ID23b](#), Y.C. Cekmecelioglu [ID49](#), E. Celebi [ID83](#), S. Cella [ID37](#),
 F. Celli [ID129](#), M.S. Centonze [ID71a,71b](#), V. Cepaitis [ID57](#), K. Cerny [ID125](#), A.S. Cerqueira [ID84a](#),
 A. Cerri [ID149](#), L. Cerrito [ID77a,77b](#), F. Cerutti [ID18a](#), B. Cervato [ID144](#), A. Cervelli [ID24b](#), G. Cesarini [ID54](#),
 S.A. Cetin [ID83](#), D. Chakraborty [ID118](#), J. Chan [ID18a](#), W.Y. Chan [ID156](#), J.D. Chapman [ID33](#), E. Chapon [ID138](#),
 B. Chargeishvili [ID152b](#), D.G. Charlton [ID21](#), M. Chatterjee [ID20](#), C. Chauhan [ID136](#), Y. Che [ID114a](#),
 S. Chekanov [ID6](#), S.V. Chekulaev [ID159a](#), G.A. Chelkov [ID39,a](#), A. Chen [ID108](#), B. Chen [ID154](#), B. Chen [ID168](#),
 H. Chen [ID114a](#), H. Chen [ID30](#), J. Chen [ID63c](#), J. Chen [ID145](#), M. Chen [ID129](#), S. Chen [ID89](#), S.J. Chen [ID114a](#),
 X. Chen [ID63c](#), X. Chen [ID15,ac](#), Y. Chen [ID63a](#), C.L. Cheng [ID173](#), H.C. Cheng [ID65a](#), S. Cheong [ID146](#),
 A. Cheplakov [ID39](#), E. Cheremushkina [ID49](#), E. Cherepanova [ID117](#), R. Cherkaoui El Moursli [ID36e](#),
 E. Cheu [ID7](#), K. Cheung [ID66](#), L. Chevalier [ID138](#), V. Chiarella [ID54](#), G. Chiarelli [ID75a](#), N. Chiedde [ID104](#),
 G. Chiodini [ID71a](#), A.S. Chisholm [ID21](#), A. Chitan [ID28b](#), M. Chitishvili [ID166](#), M.V. Chizhov [ID39,q](#),

K. Choi ¹¹, Y. Chou ¹⁴¹, E.Y.S. Chow ¹¹⁶, K.L. Chu ¹⁷², M.C. Chu ^{65a}, X. Chu ^{14,114c},
 Z. Chubinidze ⁵⁴, J. Chudoba ¹³⁴, J.J. Chwastowski ⁸⁸, D. Cieri ¹¹², K.M. Ciesla ^{87a},
 V. Cindro ⁹⁵, A. Ciocio ^{18a}, F. Cirotto ^{73a,73b}, Z.H. Citron ¹⁷², M. Citterio ^{72a}, D.A. Ciubotaru ^{28b},
 A. Clark ⁵⁷, P.J. Clark ⁵³, N. Clarke Hall ⁹⁸, C. Clarry ¹⁵⁸, J.M. Clavijo Columbie ⁴⁹,
 S.E. Clawson ⁴⁹, C. Clement ^{48a,48b}, Y. Coadou ¹⁰⁴, M. Cobal ^{70a,70c}, A. Coccaro ^{58b},
 R.F. Coelho Barrue ^{133a}, R. Coelho Lopes De Sa ¹⁰⁵, S. Coelli ^{72a}, B. Cole ⁴², J. Collot ⁶¹,
 P. Conde Muiño ^{133a,133g}, M.P. Connell ^{34c}, S.H. Connell ^{34c}, E.I. Conroy ¹²⁹, F. Conventi ^{73a,ae},
 H.G. Cooke ²¹, A.M. Cooper-Sarkar ¹²⁹, F.A. Corchia ^{24b,24a}, A. Cordeiro Oudot Choi ¹³⁰,
 L.D. Corpe ⁴¹, M. Corradi ^{76a,76b}, F. Corriveau ^{106,x}, A. Cortes-Gonzalez ¹⁹, M.J. Costa ¹⁶⁶,
 F. Costanza ⁴, D. Costanzo ¹⁴², B.M. Cote ¹²², J. Couthures ⁴, G. Cowan ⁹⁷, K. Cranmer ¹⁷³,
 L. Cremer ⁵⁰, D. Cremonini ^{24b,24a}, S. Crépe-Renaudin ⁶¹, F. Crescioli ¹³⁰, M. Cristinziani ¹⁴⁴,
 M. Cristoforetti ^{79a,79b}, V. Croft ¹¹⁷, J.E. Crosby ¹²⁴, G. Crosetti ^{44b,44a}, A. Cueto ¹⁰¹, H. Cui ⁹⁸,
 Z. Cui ⁷, W.R. Cunningham ⁶⁰, F. Curcio ¹⁶⁶, J.R. Curran ⁵³, P. Czodrowski ³⁷,
 M.J. Da Cunha Sargedas De Sousa ^{58b,58a}, J.V. Da Fonseca Pinto ^{84b}, C. Da Via ¹⁰³,
 W. Dabrowski ^{87a}, T. Dado ³⁷, S. Dahbi ¹⁵¹, T. Dai ¹⁰⁸, D. Dal Santo ²⁰, C. Dallapiccola ¹⁰⁵,
 M. Dam ⁴³, G. D'amen ³⁰, V. D'Amico ¹¹¹, J. Damp ¹⁰², J.R. Dandoy ³⁵, D. Dannheim ³⁷,
 M. Danninger ¹⁴⁵, V. Dao ¹⁴⁸, G. Darbo ^{58b}, S.J. Das ^{30,af}, F. Dattola ⁴⁹, S. D'Auria ^{72a,72b},
 A. D'avano ^{73a,73b}, C. David ^{34a}, T. Davidek ¹³⁶, I. Dawson ⁹⁶, H.A. Day-hall ¹³⁵, K. De ⁸,
 R. De Asmundis ^{73a}, N. De Biase ⁴⁹, S. De Castro ^{24b,24a}, N. De Groot ¹¹⁶, P. de Jong ¹¹⁷,
 H. De la Torre ¹¹⁸, A. De Maria ^{114a}, A. De Salvo ^{76a}, U. De Sanctis ^{77a,77b}, F. De Santis ^{71a,71b},
 A. De Santo ¹⁴⁹, J.B. De Vivie De Regie ⁶¹, J. Debevc ⁹⁵, D.V. Dedovich ³⁹, J. Degens ⁹⁴,
 A.M. Deiana ⁴⁵, F. Del Corso ^{24b,24a}, J. Del Peso ¹⁰¹, L. Delagrangé ¹³⁰, F. Deliot ¹³⁸,
 C.M. Delitzsch ⁵⁰, M. Della Pietra ^{73a,73b}, D. Della Volpe ⁵⁷, A. Dell'Acqua ³⁷,
 L. Dell'Asta ^{72a,72b}, M. Delmastro ⁴, P.A. Delsart ⁶¹, S. Demers ¹⁷⁵, M. Demichev ³⁹,
 S.P. Denisov ³⁸, L. D'Eramo ⁴¹, D. Derendarz ⁸⁸, F. Derue ¹³⁰, P. Dervan ⁹⁴, K. Desch ²⁵,
 C. Deutsch ²⁵, F.A. Di Bello ^{58b,58a}, A. Di Ciaccio ^{77a,77b}, L. Di Ciaccio ⁴,
 A. Di Domenico ^{76a,76b}, C. Di Donato ^{73a,73b}, A. Di Girolamo ³⁷, G. Di Gregorio ³⁷,
 A. Di Luca ^{79a,79b}, B. Di Micco ^{78a,78b}, R. Di Nardo ^{78a,78b}, K.F. Di Petrillo ⁴⁰,
 M. Diamantopoulou ³⁵, F.A. Dias ¹¹⁷, T. Dias Do Vale ¹⁴⁵, M.A. Diaz ^{140a,140b},
 F.G. Diaz Capriles ²⁵, A.R. Didenko ³⁹, M. Didenko ¹⁶⁶, E.B. Diehl ¹⁰⁸, S. Díez Cornell ⁴⁹,
 C. Díez Pardos ¹⁴⁴, C. Dimitriadi ¹⁶⁴, A. Dimitrievska ²¹, J. Dingfelder ²⁵, T. Dingley ¹²⁹,
 I-M. Dinu ^{28b}, S.J. Dittmeier ^{64b}, F. Dittus ³⁷, M. Divisek ¹³⁶, B. Dixit ⁹⁴, F. Djama ¹⁰⁴,
 T. Djobava ^{152b}, C. Doglioni ^{103,100}, A. Dohalova ^{29a}, J. Dolejsi ¹³⁶, Z. Dolezal ¹³⁶,
 K. Domijan ^{87a}, K.M. Dona ⁴⁰, M. Donadelli ^{84d}, B. Dong ¹⁰⁹, J. Donini ⁴¹,
 A. D'Onofrio ^{73a,73b}, M. D'Onofrio ⁹⁴, J. Dopke ¹³⁷, A. Doria ^{73a}, N. Dos Santos Fernandes ^{133a},
 P. Dougan ¹⁰³, M.T. Dova ⁹², A.T. Doyle ⁶⁰, M.A. Draguet ¹²⁹, E. Dreyer ¹⁷²,
 I. Drivas-koulouris ¹⁰, M. Drnevich ¹²⁰, M. Drozdova ⁵⁷, D. Du ^{63a}, T.A. du Pree ¹¹⁷,
 F. Dubinin ³⁸, M. Dubovsky ^{29a}, E. Duchovni ¹⁷², G. Duckeck ¹¹¹, O.A. Ducu ^{28b}, D. Duda ⁵³,
 A. Dudarev ³⁷, E.R. Duden ²⁷, M. D'uffizi ¹⁰³, L. Duflot ⁶⁷, M. Dührssen ³⁷, I. Duminica ^{28g},
 A.E. Dumitriu ^{28b}, M. Dunford ^{64a}, S. Dungs ⁵⁰, K. Dunne ^{48a,48b}, A. Duperrin ¹⁰⁴,
 H. Duran Yildiz ^{3a}, M. Düren ⁵⁹, A. Durglishvili ^{152b}, B.L. Dwyer ¹¹⁸, G.I. Dyckes ^{18a},
 M. Dyndal ^{87a}, B.S. Dziedzic ³⁷, Z.O. Earnshaw ¹⁴⁹, G.H. Eberwein ¹²⁹, B. Eckerova ^{29a},
 S. Eggebrecht ⁵⁶, E. Egidio Purcino De Souza ^{84e}, L.F. Ehrke ⁵⁷, G. Eigen ¹⁷, K. Einsweiler ^{18a},
 T. Ekelof ¹⁶⁴, P.A. Ekman ¹⁰⁰, S. El Farkh ^{36b}, Y. El Ghazali ^{63a}, H. El Jarrari ³⁷,
 A. El Moussaouy ^{36a}, V. Ellajosyula ¹⁶⁴, M. Ellert ¹⁶⁴, F. Ellinghaus ¹⁷⁴, N. Ellis ³⁷,
 J. Elmsheuser ³⁰, M. Elsayy ^{119a}, M. Elsing ³⁷, D. Emelianov ¹³⁷, Y. Enari ⁸⁵, I. Ene ^{18a},
 S. Epari ¹³, P.A. Erland ⁸⁸, D. Ernani Martins Neto ⁸⁸, M. Errenst ¹⁷⁴, M. Escalier ⁶⁷,

C. Escobar ¹⁶⁶, E. Etzion ¹⁵⁴, G. Evans ^{133a}, H. Evans ⁶⁹, L.S. Evans ⁹⁷, A. Ezhilov ³⁸,
 S. Ezzarqtouni ^{36a}, F. Fabbri ^{24b,24a}, L. Fabbri ^{24b,24a}, G. Facini ⁹⁸, V. Fadeyev ¹³⁹,
 R.M. Fakhrutdinov ³⁸, D. Fakoudis ¹⁰², S. Falciano ^{76a}, L.F. Falda Ulhoa Coelho ³⁷,
 F. Fallavollita ¹¹², G. Falsetti ^{44b,44a}, J. Faltova ¹³⁶, C. Fan ¹⁶⁵, K.Y. Fan ^{65b}, Y. Fan ¹⁴,
 Y. Fang ^{14,114c}, M. Fanti ^{72a,72b}, M. Faraj ^{70a,70b}, Z. Farazpay ⁹⁹, A. Farbin ⁸, A. Farilla ^{78a},
 T. Farooque ¹⁰⁹, S.M. Farrington ⁵³, F. Fassi ^{36e}, D. Fassouliotis ⁹, M. Faucci Giannelli ^{77a,77b},
 W.J. Fawcett ³³, L. Fayard ⁶⁷, P. Federic ¹³⁶, P. Federicova ¹³⁴, O.L. Fedin ^{38,a}, M. Feickert ¹⁷³,
 L. Feligioni ¹⁰⁴, D.E. Fellers ¹²⁶, C. Feng ^{63b}, Z. Feng ¹¹⁷, M.J. Fenton ¹⁶², L. Ferencz ⁴⁹,
 R.A.M. Ferguson ⁹³, S.I. Fernandez Luengo ^{140f}, P. Fernandez Martinez ¹³, M.J.V. Fernoux ¹⁰⁴,
 J. Ferrando ⁹³, A. Ferrari ¹⁶⁴, P. Ferrari ^{117,116}, R. Ferrari ^{74a}, D. Ferrere ⁵⁷, C. Ferretti ¹⁰⁸,
 D. Fiacco ^{76a,76b}, F. Fiedler ¹⁰², P. Fiedler ¹³⁵, A. Filipčič ⁹⁵, E.K. Filmer ¹, F. Filthaut ¹¹⁶,
 M.C.N. Fiolhais ^{133a,133c,c}, L. Fiorini ¹⁶⁶, W.C. Fisher ¹⁰⁹, T. Fitschen ¹⁰³, P.M. Fitzhugh ¹³⁸,
 I. Fleck ¹⁴⁴, P. Fleischmann ¹⁰⁸, T. Flick ¹⁷⁴, M. Flores ^{34d,aa}, L.R. Flores Castillo ^{65a},
 L. Flores Sanz De Acedo ³⁷, F.M. Follega ^{79a,79b}, N. Fomin ³³, J.H. Foo ¹⁵⁸, A. Formica ¹³⁸,
 A.C. Forti ¹⁰³, E. Fortin ³⁷, A.W. Fortman ^{18a}, M.G. Foti ^{18a}, L. Fountas ^{9,1}, D. Fournier ⁶⁷,
 H. Fox ⁹³, P. Francavilla ^{75a,75b}, S. Francescato ⁶², S. Franchellucci ⁵⁷, M. Franchini ^{24b,24a},
 S. Franchino ^{64a}, D. Francis ³⁷, L. Franco ¹¹⁶, V. Franco Lima ³⁷, L. Franconi ⁴⁹, M. Franklin ⁶²,
 G. Frattari ²⁷, Y.Y. Frid ¹⁵⁴, J. Friend ⁶⁰, N. Fritzsche ³⁷, A. Froch ⁵⁵, D. Froidevaux ³⁷,
 J.A. Frost ¹²⁹, Y. Fu ^{63a}, S. Fuenzalida Garrido ^{140f}, M. Fujimoto ¹⁰⁴, K.Y. Fung ^{65a},
 E. Furtado De Simas Filho ^{84e}, M. Furukawa ¹⁵⁶, J. Fuster ¹⁶⁶, A. Gaa ⁵⁶, A. Gabrielli ^{24b,24a},
 A. Gabrielli ¹⁵⁸, P. Gadow ³⁷, G. Gagliardi ^{58b,58a}, L.G. Gagnon ^{18a}, S. Gaid ¹⁶³,
 S. Galantzan ¹⁵⁴, J. Gallagher ¹, E.J. Gallas ¹²⁹, B.J. Gallop ¹³⁷, K.K. Gan ¹²², S. Ganguly ¹⁵⁶,
 Y. Gao ⁵³, F.M. Garay Walls ^{140a,140b}, B. Garcia ³⁰, C. García ¹⁶⁶, A. Garcia Alonso ¹¹⁷,
 A.G. Garcia Caffaro ¹⁷⁵, J.E. García Navarro ¹⁶⁶, M. Garcia-Sciveres ^{18a}, G.L. Gardner ¹³¹,
 R.W. Gardner ⁴⁰, N. Garelli ¹⁶¹, D. Garg ⁸¹, R.B. Garg ¹⁴⁶, J.M. Gargan ⁵³, C.A. Garner ¹⁵⁸,
 C.M. Garvey ^{34a}, V.K. Gassmann ¹⁶¹, G. Gaudio ^{74a}, V. Gautam ¹³, P. Gauzzi ^{76a,76b},
 J. Gavranovic ⁹⁵, I.L. Gavrilenko ³⁸, A. Gavriluk ³⁸, C. Gay ¹⁶⁷, G. Gaycken ¹²⁶,
 E.N. Gazis ¹⁰, A.A. Geanta ^{28b}, C.M. Gee ¹³⁹, A. Gekow ¹²², C. Gemme ^{58b}, M.H. Genest ⁶¹,
 A.D. Gentry ¹¹⁵, S. George ⁹⁷, W.F. George ²¹, T. Geralis ⁴⁷, P. Gessinger-Befurt ³⁷,
 M.E. Geyik ¹⁷⁴, M. Ghani ¹⁷⁰, K. Ghorbanian ⁹⁶, A. Ghosal ¹⁴⁴, A. Ghosh ¹⁶², A. Ghosh ⁷,
 B. Giacobbe ^{24b}, S. Giagu ^{76a,76b}, T. Giani ¹¹⁷, A. Giannini ^{63a}, S.M. Gibson ⁹⁷, M. Gignac ¹³⁹,
 D.T. Gil ^{87b}, A.K. Gilbert ^{87a}, B.J. Gilbert ⁴², D. Gillberg ³⁵, G. Gilles ¹¹⁷, L. Ginabat ¹³⁰,
 D.M. Gingrich ^{2,ad}, M.P. Giordani ^{70a,70c}, P.F. Giraud ¹³⁸, G. Giugliarelli ^{70a,70c}, D. Giugni ^{72a},
 F. Giuli ³⁷, I. Gkialas ^{9,i}, L.K. Gladilin ³⁸, C. Glasman ¹⁰¹, G.R. Gledhill ¹²⁶, G. Glemža ⁴⁹,
 M. Glisic ¹²⁶, I. Gnesi ^{44b}, Y. Go ³⁰, M. Goblirsch-Kolb ³⁷, B. Gocke ⁵⁰, D. Godin ¹¹⁰,
 B. Gokturk ^{22a}, S. Goldfarb ¹⁰⁷, T. Golling ⁵⁷, M.G.D. Gololo ^{34g}, D. Golubkov ³⁸,
 J.P. Gombas ¹⁰⁹, A. Gomes ^{133a,133b}, G. Gomes Da Silva ¹⁴⁴, A.J. Gomez Delegido ¹⁶⁶,
 R. Gonçalves ^{133a}, L. Gonella ²¹, A. Gongadze ^{152c}, F. Gonnella ²¹, J.L. Gonski ¹⁴⁶,
 R.Y. González Andana ⁵³, S. González de la Hoz ¹⁶⁶, R. Gonzalez Lopez ⁹⁴,
 C. Gonzalez Renteria ^{18a}, M.V. Gonzalez Rodrigues ⁴⁹, R. Gonzalez Suarez ¹⁶⁴,
 S. Gonzalez-Sevilla ⁵⁷, L. Goossens ³⁷, B. Gorini ³⁷, E. Gorini ^{71a,71b}, A. Gorišek ⁹⁵,
 T.C. Gosart ¹³¹, A.T. Goshaw ⁵², M.I. Gostkin ³⁹, S. Goswami ¹²⁴, C.A. Gottardo ³⁷,
 S.A. Gotz ¹¹¹, M. Goughri ^{36b}, V. Goumarre ⁴⁹, A.G. Goussiou ¹⁴¹, N. Govender ^{34c},
 R.P. Grabarczyk ¹²⁹, I. Grabowska-Bold ^{87a}, K. Graham ³⁵, E. Gramstad ¹²⁸,
 S. Grancagnolo ^{71a,71b}, C.M. Grant ^{1,138}, P.M. Gravila ^{28f}, F.G. Gravili ^{71a,71b}, H.M. Gray ^{18a},
 M. Greco ^{71a,71b}, M.J. Green ¹, C. Grefe ²⁵, A.S. Grefsrud ¹⁷, I.M. Gregor ⁴⁹, K.T. Greif ¹⁶²,
 P. Grenier ¹⁴⁶, S.G. Grewe ¹¹², A.A. Grillo ¹³⁹, K. Grimm ³², S. Grinstein ^{13,t}, J.-F. Grivaz ⁶⁷,

E. Gross ¹⁷², J. Grosse-Knetter ⁵⁶, L. Guan ¹⁰⁸, J.G.R. Guerrero Rojas ¹⁶⁶, G. Guerrieri ³⁷,
 R. Gugel ¹⁰², J.A.M. Guhit ¹⁰⁸, A. Guida ¹⁹, E. Guilloton ¹⁷⁰, S. Guindon ³⁷, F. Guo ^{14,114c},
 J. Guo ^{63c}, L. Guo ⁴⁹, Y. Guo ¹⁰⁸, R. Gupta ¹³², S. Gurbuz ²⁵, S.S. Gurdasani ⁵⁵,
 G. Gustavino ^{76a,76b}, P. Gutierrez ¹²³, L.F. Gutierrez Zagazeta ¹³¹, M. Gutsche ⁵¹,
 C. Gutschow ⁹⁸, C. Gwenlan ¹²⁹, C.B. Gwilliam ⁹⁴, E.S. Haaland ¹²⁸, A. Haas ¹²⁰,
 M. Habedank ⁴⁹, C. Haber ^{18a}, H.K. Hadavand ⁸, A. Hadeif ⁵¹, S. Hadzic ¹¹², A.I. Hagan ⁹³,
 J.J. Hahn ¹⁴⁴, E.H. Haines ⁹⁸, M. Haleem ¹⁶⁹, J. Haley ¹²⁴, J.J. Hall ¹⁴², G.D. Hallewell ¹⁰⁴,
 L. Halser ²⁰, K. Hamano ¹⁶⁸, M. Hamer ²⁵, G.N. Hamity ⁵³, E.J. Hampshire ⁹⁷, J. Han ^{63b},
 K. Han ^{63a}, L. Han ^{114a}, L. Han ^{63a}, S. Han ^{18a}, Y.F. Han ¹⁵⁸, K. Hanagaki ⁸⁵, M. Hance ¹³⁹,
 D.A. Hangal ⁴², H. Hanif ¹⁴⁵, M.D. Hank ¹³¹, J.B. Hansen ⁴³, P.H. Hansen ⁴³, D. Harada ⁵⁷,
 T. Harenberg ¹⁷⁴, S. Harkusha ³⁸, M.L. Harris ¹⁰⁵, Y.T. Harris ²⁵, J. Harrison ¹³,
 N.M. Harrison ¹²², P.F. Harrison ¹⁷⁰, N.M. Hartman ¹¹², N.M. Hartmann ¹¹¹, R.Z. Hasan ^{97,137},
 Y. Hasegawa ¹⁴³, F. Haslbeck ¹²⁹, S. Hassan ¹⁷, R. Hauser ¹⁰⁹, C.M. Hawkes ²¹,
 R.J. Hawkings ³⁷, Y. Hayashi ¹⁵⁶, D. Hayden ¹⁰⁹, C. Hayes ¹⁰⁸, R.L. Hayes ¹¹⁷, C.P. Hays ¹²⁹,
 J.M. Hays ⁹⁶, H.S. Hayward ⁹⁴, F. He ^{63a}, M. He ^{14,114c}, Y. He ⁴⁹, Y. He ⁹⁸, N.B. Heatley ⁹⁶,
 V. Hedberg ¹⁰⁰, A.L. Heggelund ¹²⁸, N.D. Hehir ^{96,*}, C. Heidegger ⁵⁵, K.K. Heidegger ⁵⁵,
 J. Heilman ³⁵, S. Heim ⁴⁹, T. Heim ^{18a}, J.G. Heinlein ¹³¹, J.J. Heinrich ¹²⁶, L. Heinrich ^{112,ab},
 J. Hejbal ¹³⁴, A. Held ¹⁷³, S. Hellesund ¹⁷, C.M. Helling ¹⁶⁷, S. Hellman ^{48a,48b},
 R.C.W. Henderson ⁹³, L. Henkelmann ³³, A.M. Henriques Correia ³⁷, H. Herde ¹⁰⁰,
 Y. Hernández Jiménez ¹⁴⁸, L.M. Herrmann ²⁵, T. Herrmann ⁵¹, G. Herten ⁵⁵, R. Hertenberger ¹¹¹,
 L. Hervas ³⁷, M.E. Hespings ¹⁰², N.P. Hessey ^{159a}, M. Hidaoui ^{36b}, N. Hidic ¹³⁶, E. Hill ¹⁵⁸,
 S.J. Hillier ²¹, J.R. Hinds ¹⁰⁹, F. Hinterkeuser ²⁵, M. Hirose ¹²⁷, S. Hirose ¹⁶⁰,
 D. Hirschbuehl ¹⁷⁴, T.G. Hitchings ¹⁰³, B. Hiti ⁹⁵, J. Hobbs ¹⁴⁸, R. Hobincu ^{28e}, N. Hod ¹⁷²,
 M.C. Hodgkinson ¹⁴², B.H. Hodgkinson ¹²⁹, A. Hoecker ³⁷, D.D. Hofer ¹⁰⁸, J. Hofer ¹⁶⁶,
 T. Holm ²⁵, M. Holzbock ³⁷, L.B.A.H. Hommels ³³, B.P. Honan ¹⁰³, J.J. Hong ⁶⁹, J. Hong ^{63c},
 T.M. Hong ¹³², B.H. Hooberman ¹⁶⁵, W.H. Hopkins ⁶, M.C. Hoppesch ¹⁶⁵, Y. Horii ¹¹³,
 M.E. Horstmann ¹¹², S. Hou ¹⁵¹, A.S. Howard ⁹⁵, J. Howarth ⁶⁰, J. Hoya ⁶, M. Hrabovsky ¹²⁵,
 A. Hrynevich ⁴⁹, T. Hryn'ova ⁴, P.J. Hsu ⁶⁶, S.-C. Hsu ¹⁴¹, T. Hsu ⁶⁷, M. Hu ^{18a}, Q. Hu ^{63a},
 S. Huang ^{65b}, X. Huang ^{14,114c}, Y. Huang ¹⁴², Y. Huang ¹⁰², Y. Huang ¹⁴, Z. Huang ¹⁰³,
 Z. Hubacek ¹³⁵, M. Huebner ²⁵, F. Huegging ²⁵, T.B. Huffman ¹²⁹, C.A. Hugli ⁴⁹,
 M. Huhtinen ³⁷, S.K. Huiberts ¹⁷, R. Hulsken ¹⁰⁶, N. Huseynov ^{12,f}, J. Huston ¹⁰⁹, J. Huth ⁶²,
 R. Hyneman ¹⁴⁶, G. Iacobucci ⁵⁷, G. Iakovidis ³⁰, L. Iconomidou-Fayard ⁶⁷, J.P. Iddon ³⁷,
 P. Iengo ^{73a,73b}, R. Iguchi ¹⁵⁶, Y. Iiyama ¹⁵⁶, T. Iizawa ¹²⁹, Y. Ikegami ⁸⁵, N. Ilic ¹⁵⁸,
 H. Imam ^{84c}, G. Inacio Goncalves ^{84d}, M. Ince Lezki ⁵⁷, T. Ingebretsen Carlson ^{48a,48b},
 J.M. Inglis ⁹⁶, G. Introzzi ^{74a,74b}, M. Iodice ^{78a}, V. Ippolito ^{76a,76b}, R.K. Irwin ⁹⁴, M. Ishino ¹⁵⁶,
 W. Islam ¹⁷³, C. Issever ^{19,49}, S. Istin ^{22a,ah}, H. Ito ¹⁷¹, R. Iuppa ^{79a,79b}, A. Ivina ¹⁷²,
 J.M. Izen ⁴⁶, V. Izzo ^{73a}, P. Jacka ¹³⁴, P. Jackson ¹, C.S. Jagfeld ¹¹¹, G. Jain ^{159a}, P. Jain ⁴⁹,
 K. Jakobs ⁵⁵, T. Jakoubek ¹⁷², J. Jamieson ⁶⁰, W. Jang ¹⁵⁶, M. Javurkova ¹⁰⁵, P. Jawahar ¹⁰³,
 L. Jeanty ¹²⁶, J. Jejelava ^{152a,z}, P. Jenni ^{55,e}, C.E. Jessiman ³⁵, C. Jia ^{63b}, J. Jia ¹⁴⁸, X. Jia ^{14,114c},
 Z. Jia ^{114a}, C. Jiang ⁵³, S. Jiggins ⁴⁹, J. Jimenez Pena ¹³, S. Jin ^{114a}, A. Jinaru ^{28b},
 O. Jinnouchi ¹⁵⁷, P. Johansson ¹⁴², K.A. Johns ⁷, J.W. Johnson ¹³⁹, F.A. Jolly ⁴⁹,
 D.M. Jones ¹⁴⁹, E. Jones ⁴⁹, K.S. Jones ⁸, P. Jones ³³, R.W.L. Jones ⁹³, T.J. Jones ⁹⁴,
 H.L. Joos ^{56,37}, R. Joshi ¹²², J. Jovicevic ¹⁶, X. Ju ^{18a}, J.J. Junggeburth ¹⁰⁵, T. Junkermann ^{64a},
 A. Juste Rozas ^{13,t}, M.K. Juzek ⁸⁸, S. Kabana ^{140e}, A. Kaczmarzka ⁸⁸, M. Kado ¹¹²,
 H. Kagan ¹²², M. Kagan ¹⁴⁶, A. Kahn ¹³¹, C. Kahra ¹⁰², T. Kaji ¹⁵⁶, E. Kajomovitz ¹⁵³,
 N. Kakati ¹⁷², I. Kalaitzidou ⁵⁵, C.W. Kalderon ³⁰, N.J. Kang ¹³⁹, D. Kar ^{34g}, K. Karava ¹²⁹,
 M.J. Kareem ^{159b}, E. Karentzos ⁵⁵, O. Karkout ¹¹⁷, S.N. Karpov ³⁹, Z.M. Karpova ³⁹,

V. Kartvelishvili ⁹³, A.N. Karyukhin ³⁸, E. Kasimi ¹⁵⁵, J. Katzy ⁴⁹, S. Kaur ³⁵, K. Kawade ¹⁴³, M.P. Kawale ¹²³, C. Kawamoto ⁸⁹, T. Kawamoto ^{63a}, E.F. Kay ³⁷, F.I. Kaya ¹⁶¹, S. Kazakos ¹⁰⁹, V.F. Kazanin ³⁸, Y. Ke ¹⁴⁸, J.M. Keaveney ^{34a}, R. Keeler ¹⁶⁸, G.V. Kehris ⁶², J.S. Keller ³⁵, A.S. Kelly ⁹⁸, J.J. Kempster ¹⁴⁹, P.D. Kennedy ¹⁰², O. Kepka ¹³⁴, B.P. Kerridge ¹³⁷, S. Kersten ¹⁷⁴, B.P. Kerševan ⁹⁵, L. Keszeghova ^{29a}, S. Kitabchi Haghghat ¹⁵⁸, R.A. Khan ¹³², A. Khanov ¹²⁴, A.G. Kharlamov ³⁸, T. Kharlamova ³⁸, E.E. Khoda ¹⁴¹, M. Kholodenko ^{133a}, T.J. Khoo ¹⁹, G. Khoriauli ¹⁶⁹, J. Khubua ^{152b,*}, Y.A.R. Khwaira ¹³⁰, B. Kibirige ^{34g}, D. Kim ⁶, D.W. Kim ^{48a,48b}, Y.K. Kim ⁴⁰, N. Kimura ⁹⁸, M.K. Kingston ⁵⁶, A. Kirchhoff ⁵⁶, C. Kirfel ²⁵, F. Kirfel ²⁵, J. Kirk ¹³⁷, A.E. Kiryunin ¹¹², S. Kita ¹⁶⁰, C. Kitsaki ¹⁰, O. Kivernyk ²⁵, M. Klassen ¹⁶¹, C. Klein ³⁵, L. Klein ¹⁶⁹, M.H. Klein ⁴⁵, S.B. Klein ⁵⁷, U. Klein ⁹⁴, P. Klimek ³⁷, A. Klimentov ³⁰, T. Klioutchnikova ³⁷, P. Kluit ¹¹⁷, S. Kluth ¹¹², E. Kneringer ⁸⁰, T.M. Knight ¹⁵⁸, A. Knue ⁵⁰, D. Kobylanski ¹⁷², S.F. Koch ¹²⁹, M. Kocian ¹⁴⁶, P. Kodyš ¹³⁶, D.M. Koeck ¹²⁶, P.T. Koenig ²⁵, T. Koffas ³⁵, O. Kolay ⁵¹, I. Koletsou ⁴, T. Komarek ⁸⁸, K. Köneke ⁵⁵, A.X.Y. Kong ¹, T. Kono ¹²¹, N. Konstantinidis ⁹⁸, P. Kontaxakis ⁵⁷, B. Konya ¹⁰⁰, R. Kopeliansky ⁴², S. Koperny ^{87a}, K. Korcyl ⁸⁸, K. Kordas ^{155,d}, A. Korn ⁹⁸, S. Korn ⁵⁶, I. Korolkov ¹³, N. Korotkova ³⁸, B. Kortman ¹¹⁷, O. Kortner ¹¹², S. Kortner ¹¹², W.H. Kostecka ¹¹⁸, V.V. Kostyukhin ¹⁴⁴, A. Kotsokechagia ³⁷, A. Kotwal ⁵², A. Koulouris ³⁷, A. Kourkoumeli-Charalampidi ^{74a,74b}, C. Kourkoumelis ⁹, E. Kourlitis ^{112,ab}, O. Kovanda ¹²⁶, R. Kowalewski ¹⁶⁸, W. Kozanecki ¹²⁶, A.S. Kozhin ³⁸, V.A. Kramarenko ³⁸, G. Kramberger ⁹⁵, P. Kramer ¹⁰², M.W. Krasny ¹³⁰, A. Krasznahorkay ³⁷, A.C. Kraus ¹¹⁸, J.W. Kraus ¹⁷⁴, J.A. Kremer ⁴⁹, T. Kresse ⁵¹, L. Kretschmann ¹⁷⁴, J. Kretzschmar ⁹⁴, K. Kreul ¹⁹, P. Krieger ¹⁵⁸, M. Krivos ¹³⁶, K. Krizka ²¹, K. Kroeninger ⁵⁰, H. Kroha ¹¹², J. Kroll ¹³⁴, J. Kroll ¹³¹, K.S. Krowpman ¹⁰⁹, U. Kruchonak ³⁹, H. Krüger ²⁵, N. Krumnack ⁸², M.C. Kruse ⁵², O. Kuchinskaia ³⁸, S. Kuday ^{3a}, S. Kuehn ³⁷, R. Kuesters ⁵⁵, T. Kuhl ⁴⁹, V. Kukhtin ³⁹, Y. Kulchitsky ^{38,a}, S. Kuleshov ^{140d,140b}, M. Kumar ^{34g}, N. Kumari ⁴⁹, P. Kumari ^{159b}, A. Kupco ¹³⁴, T. Kupfer ⁵⁰, A. Kupich ³⁸, O. Kuprash ⁵⁵, H. Kurashige ⁸⁶, L.L. Kurchaninov ^{159a}, O. Kurdysh ⁶⁷, Y.A. Kurochkin ³⁸, A. Kurova ³⁸, M. Kuze ¹⁵⁷, A.K. Kvam ¹⁰⁵, J. Kvitá ¹²⁵, T. Kwan ¹⁰⁶, N.G. Kyriacou ¹⁰⁸, L.A.O. Laatu ¹⁰⁴, C. Lacasta ¹⁶⁶, F. Lacava ^{76a,76b}, H. Lacker ¹⁹, D. Lacour ¹³⁰, N.N. Lad ⁹⁸, E. Ladygin ³⁹, A. Lafarge ⁴¹, B. Laforge ¹³⁰, T. Lagouri ¹⁷⁵, F.Z. Lahbabi ^{36a}, S. Lai ⁵⁶, J.E. Lambert ¹⁶⁸, S. Lammers ⁶⁹, W. Lampl ⁷, C. Lampoudis ^{155,d}, G. Lamprinoudis ¹⁰², A.N. Lancaster ¹¹⁸, E. Lançon ³⁰, U. Landgraf ⁵⁵, M.P.J. Landon ⁹⁶, V.S. Lang ⁵⁵, O.K.B. Langrekken ¹²⁸, A.J. Lankford ¹⁶², F. Lanni ³⁷, K. Lantzsch ²⁵, A. Lanza ^{74a}, M. Lanzac Berrocal ¹⁶⁶, J.F. Laporte ¹³⁸, T. Lari ^{72a}, F. Lasagni Manghi ^{24b}, M. Lassnig ³⁷, V. Latonova ¹³⁴, A. Laurier ¹⁵³, S.D. Lawlor ¹⁴², Z. Lawrence ¹⁰³, R. Lazaridou ¹⁷⁰, M. Lazzaroni ^{72a,72b}, B. Le ¹⁰³, H.D.M. Le ¹⁰⁹, E.M. Le Boulicaut ¹⁷⁵, L.T. Le Pottier ^{18a}, B. Leban ^{24b,24a}, A. Lebedev ⁸², M. LeBlanc ¹⁰³, F. Ledroit-Guillon ⁶¹, S.C. Lee ¹⁵¹, S. Lee ^{48a,48b}, T.F. Lee ⁹⁴, L.L. Leeuw ^{34c}, H.P. Lefebvre ⁹⁷, M. Lefebvre ¹⁶⁸, C. Leggett ^{18a}, G. Lehmann Miotto ³⁷, M. Leigh ⁵⁷, W.A. Leight ¹⁰⁵, W. Leinonen ¹¹⁶, A. Leisos ^{155,r}, M.A.L. Leite ^{84c}, C.E. Leitgeb ¹⁹, R. Leitner ¹³⁶, K.J.C. Leney ⁴⁵, T. Lenz ²⁵, S. Leone ^{75a}, C. Leonidopoulos ⁵³, A. Leopold ¹⁴⁷, R. Les ¹⁰⁹, C.G. Lester ³³, M. Levchenko ³⁸, J. Levêque ⁴, L.J. Levinson ¹⁷², G. Levrini ^{24b,24a}, M.P. Lewicki ⁸⁸, C. Lewis ¹⁴¹, D.J. Lewis ⁴, L. Lewitt ¹⁴², A. Li ³⁰, B. Li ^{63b}, C. Li ^{63a}, C-Q. Li ¹¹², H. Li ^{63a}, H. Li ^{63b}, H. Li ^{114a}, H. Li ¹⁵, H. Li ^{63b}, J. Li ^{63c}, K. Li ¹⁴, L. Li ^{63c}, M. Li ^{14,114c}, S. Li ^{14,114c}, S. Li ^{63d,63c}, T. Li ⁵, X. Li ¹⁰⁶, Z. Li ¹²⁹, Z. Li ¹⁵⁶, Z. Li ^{14,114c}, Z. Li ^{63a}, S. Liang ^{14,114c}, Z. Liang ¹⁴, M. Liberatore ¹³⁸, B. Liberti ^{77a}, K. Lie ^{65c}, J. Lieber Marin ^{84e}, H. Lien ⁶⁹, H. Lin ¹⁰⁸, K. Lin ¹⁰⁹, R.E. Lindley ⁷, J.H. Lindon ², J. Ling ⁶², E. Lipeles ¹³¹, A. Lipniacka ¹⁷, A. Lister ¹⁶⁷, J.D. Little ⁶⁹, B. Liu ¹⁴, B.X. Liu ^{114b},

D. Liu ^{63d,63c}, E.H.L. Liu ²¹, J.B. Liu ^{63a}, J.K.K. Liu ³³, K. Liu ^{63d}, K. Liu ^{63d,63c}, M. Liu ^{63a},
 M.Y. Liu ^{63a}, P. Liu ¹⁴, Q. Liu ^{63d,141,63c}, X. Liu ^{63a}, X. Liu ^{63b}, Y. Liu ^{114b,114c}, Y.L. Liu ^{63b},
 Y.W. Liu ^{63a}, S.L. Lloyd ⁹⁶, E.M. Lobodzinska ⁴⁹, P. Loch ⁷, T. Lohse ¹⁹, K. Lohwasser ¹⁴²,
 E. Loiacono ⁴⁹, M. Lokajicek ^{134,*}, J.D. Lomas ²¹, J.D. Long ¹⁶⁵, I. Longarini ¹⁶²,
 R. Longo ¹⁶⁵, I. Lopez Paz ⁶⁸, A. Lopez Solis ⁴⁹, N.A. Lopez-canelas ⁷, N. Lorenzo Martinez ⁴,
 A.M. Lory ¹¹¹, M. Losada ^{119a}, G. Löschcke Centeno ¹⁴⁹, O. Loseva ³⁸, X. Lou ^{48a,48b},
 X. Lou ^{14,114c}, A. Lounis ⁶⁷, P.A. Love ⁹³, G. Lu ^{14,114c}, M. Lu ⁶⁷, S. Lu ¹³¹, Y.J. Lu ⁶⁶,
 H.J. Lubatti ¹⁴¹, C. Luci ^{76a,76b}, F.L. Lucio Alves ^{114a}, F. Luehring ⁶⁹, O. Lukianchuk ⁶⁷,
 O. Lundberg ¹⁴⁷, B. Lund-Jensen ^{147,*}, N.A. Luongo ⁶, M.S. Lutz ³⁷, A.B. Lux ²⁶, D. Lynn ³⁰,
 R. Lysak ¹³⁴, E. Lytken ¹⁰⁰, V. Lyubushkin ³⁹, T. Lyubushkina ³⁹, M.M. Lyukova ¹⁴⁸,
 M.Firdaus M. Soberi ⁵³, H. Ma ³⁰, K. Ma ^{63a}, L.L. Ma ^{63b}, W. Ma ^{63a}, Y. Ma ¹²⁴,
 J.C. MacDonald ¹⁰², P.C. Machado De Abreu Farias ^{84e}, R. Madar ⁴¹, T. Madula ⁹⁸, J. Maeda ⁸⁶,
 T. Maeno ³⁰, H. Maguire ¹⁴², V. Maiboroda ¹³⁸, A. Maio ^{133a,133b,133d}, K. Maj ^{87a},
 O. Majersky ⁴⁹, S. Majewski ¹²⁶, N. Makovec ⁶⁷, V. Maksimovic ¹⁶, B. Malaescu ¹³⁰,
 Pa. Malecki ⁸⁸, V.P. Maleev ³⁸, F. Malek ^{61,m}, M. Mali ⁹⁵, D. Malito ⁹⁷, U. Mallik ^{81,*},
 S. Maltezos ¹⁰, S. Malyukov ³⁹, J. Mamuzic ¹³, G. Mancini ⁵⁴, M.N. Mancini ²⁷, G. Manco ^{74a,74b},
 J.P. Mandalia ⁹⁶, S.S. Mandarray ¹⁴⁹, I. Mandić ⁹⁵, L. Manhaes de Andrade Filho ^{84a},
 I.M. Maniatis ¹⁷², J. Manjarres Ramos ⁹¹, D.C. Mankad ¹⁷², A. Mann ¹¹¹, S. Manzoni ³⁷,
 L. Mao ^{63c}, X. Mapekula ^{34c}, A. Marantis ^{155,r}, G. Marchiori ⁵, M. Marcisovsky ¹³⁴,
 C. Marcon ^{72a}, M. Marinescu ²¹, S. Marium ⁴⁹, M. Marjanovic ¹²³, A. Markhoos ⁵⁵,
 M. Markovitch ⁶⁷, E.J. Marshall ⁹³, Z. Marshall ^{18a}, S. Marti-Garcia ¹⁶⁶, J. Martin ⁹⁸,
 T.A. Martin ¹³⁷, V.J. Martin ⁵³, B. Martin dit Latour ¹⁷, L. Martinelli ^{76a,76b}, M. Martinez ^{13,t},
 P. Martinez Agullo ¹⁶⁶, V.I. Martinez Outschoorn ¹⁰⁵, P. Martinez Suarez ¹³, S. Martin-Haugh ¹³⁷,
 G. Martinovicova ¹³⁶, V.S. Martoiu ^{28b}, A.C. Martyniuk ⁹⁸, A. Marzin ³⁷, D. Mascione ^{79a,79b},
 L. Masetti ¹⁰², J. Masik ¹⁰³, A.L. Maslennikov ³⁸, P. Massarotti ^{73a,73b}, P. Mastrandrea ^{75a,75b},
 A. Mastroberardino ^{44b,44a}, T. Masubuchi ¹²⁷, T.T. Mathew ¹²⁶, T. Mathisen ¹⁶⁴, J. Matousek ¹³⁶,
 J. Maurer ^{28b}, T. Maurin ⁶⁰, A.J. Maury ⁶⁷, B. Maček ⁹⁵, D.A. Maximov ³⁸, A.E. May ¹⁰³,
 R. Mazini ¹⁵¹, I. Maznas ¹¹⁸, M. Mazza ¹⁰⁹, S.M. Mazza ¹³⁹, E. Mazzeo ^{72a,72b}, C. Mc Ginn ³⁰,
 J.P. Mc Gowan ¹⁶⁸, S.P. Mc Kee ¹⁰⁸, C.C. McCracken ¹⁶⁷, E.F. McDonald ¹⁰⁷,
 A.E. McDougall ¹¹⁷, J.A. Mcfayden ¹⁴⁹, R.P. McGovern ¹³¹, R.P. Mckenzie ^{34g},
 T.C. McLachlan ⁴⁹, D.J. McLaughlin ⁹⁸, S.J. McMahon ¹³⁷, C.M. Mcpartland ⁹⁴,
 R.A. McPherson ^{168,x}, S. Mehlhase ¹¹¹, A. Mehta ⁹⁴, D. Melini ¹⁶⁶, B.R. Mellado Garcia ^{34g},
 A.H. Melo ⁵⁶, F. Meloni ⁴⁹, A.M. Mendes Jacques Da Costa ¹⁰³, H.Y. Meng ¹⁵⁸, L. Meng ⁹³,
 S. Menke ¹¹², M. Mentink ³⁷, E. Meoni ^{44b,44a}, G. Mercado ¹¹⁸, S. Merianos ¹⁵⁵,
 C. Merlassino ^{70a,70c}, L. Merola ^{73a,73b}, C. Meroni ^{72a,72b}, J. Metcalfe ⁶, A.S. Mete ⁶,
 E. Meuser ¹⁰², C. Meyer ⁶⁹, J-P. Meyer ¹³⁸, R.P. Middleton ¹³⁷, L. Mijović ⁵³,
 G. Mikenberg ¹⁷², M. Mikestikova ¹³⁴, M. Mikuž ⁹⁵, H. Mildner ¹⁰², A. Milic ³⁷,
 D.W. Miller ⁴⁰, E.H. Miller ¹⁴⁶, L.S. Miller ³⁵, A. Milov ¹⁷², D.A. Milstead ^{48a,48b}, T. Min ^{114a},
 A.A. Minaenko ³⁸, I.A. Minashvili ^{152b}, L. Mince ⁶⁰, A.I. Mincer ¹²⁰, B. Mindur ^{87a},
 M. Mineev ³⁹, Y. Mino ⁸⁹, L.M. Mir ¹³, M. Miralles Lopez ⁶⁰, M. Mironova ^{18a},
 M.C. Missio ¹¹⁶, A. Mitra ¹⁷⁰, V.A. Mitsou ¹⁶⁶, Y. Mitsumori ¹¹³, O. Miu ¹⁵⁸,
 P.S. Miyagawa ⁹⁶, T. Mkrtchyan ^{64a}, M. Mlinarevic ⁹⁸, T. Mlinarevic ⁹⁸, M. Mlynarikova ³⁷,
 S. Mobius ²⁰, P. Mogg ¹¹¹, M.H. Mohamed Farook ¹¹⁵, A.F. Mohammed ^{14,114c}, S. Mohapatra ⁴²,
 G. Mokgatitwane ^{34g}, L. Moleri ¹⁷², B. Mondal ¹⁴⁴, S. Mondal ¹³⁵, K. Mönig ⁴⁹,
 E. Monnier ¹⁰⁴, L. Monsonis Romero ¹⁶⁶, J. Montejo Berlingen ¹³, A. Montella ^{48a,48b},
 M. Montella ¹²², F. Montekali ^{78a,78b}, F. Monticelli ⁹², S. Monzani ^{70a,70c}, A. Morancho Tarda ⁴³,
 N. Morange ⁶⁷, A.L. Moreira De Carvalho ⁴⁹, M. Moreno Llácer ¹⁶⁶, C. Moreno Martinez ⁵⁷,

J.M. Moreno Perez^{23b}, P. Morettini^{58b}, S. Morgenstern³⁷, M. Morii⁶², M. Morinaga¹⁵⁶, F. Morodei^{76a,76b}, L. Morvaj³⁷, P. Moschovakos³⁷, B. Moser¹²⁹, M. Mosidze^{152b}, T. Moskalets⁴⁵, P. Moskvitina¹¹⁶, J. Moss^{32j}, P. Moszkowicz^{87a}, A. Moussa^{36d}, E.J.W. Moyse¹⁰⁵, O. Mtintsilana^{34g}, S. Muanza¹⁰⁴, J. Mueller¹³², D. Muenstermann⁹³, R. Müller³⁷, G.A. Mullier¹⁶⁴, A.J. Mullin³³, J.J. Mullin¹³¹, D.P. Mungo¹⁵⁸, D. Munoz Perez¹⁶⁶, F.J. Munoz Sanchez¹⁰³, M. Murin¹⁰³, W.J. Murray^{170,137}, M. Muškinja⁹⁵, C. Mwewa³⁰, A.G. Myagkov^{38a}, A.J. Myers⁸, G. Myers¹⁰⁸, M. Myska¹³⁵, B.P. Nachman^{18a}, O. Nackenhorst⁵⁰, K. Nagai¹²⁹, K. Nagano⁸⁵, R. Nagasaka¹⁵⁶, J.L. Nagle^{30,af}, E. Nagy¹⁰⁴, A.M. Nairz³⁷, Y. Nakahama⁸⁵, K. Nakamura⁸⁵, K. Nakkalil⁵, H. Nanjo¹²⁷, E.A. Narayanan¹¹⁵, I. Naryshkin³⁸, L. Nasella^{72a,72b}, M. Naseri³⁵, S. Nasri^{119b}, C. Nass²⁵, G. Navarro^{23a}, J. Navarro-Gonzalez¹⁶⁶, R. Nayak¹⁵⁴, A. Nayaz¹⁹, P.Y. Nechaeva³⁸, S. Nechaeva^{24b,24a}, F. Nechansky¹³⁴, L. Nedic¹²⁹, T.J. Neep²¹, A. Negri^{74a,74b}, M. Negrini^{24b}, C. Nellist¹¹⁷, C. Nelson¹⁰⁶, K. Nelson¹⁰⁸, S. Nemecek¹³⁴, M. Nessi^{37,g}, M.S. Neubauer¹⁶⁵, F. Neuhaus¹⁰², J. Neundorff⁴⁹, J. Newell⁹⁴, P.R. Newman²¹, C.W. Ng¹³², Y.W.Y. Ng⁴⁹, B. Ngair^{119a}, H.D.N. Nguyen¹¹⁰, R.B. Nickerson¹²⁹, R. Nicolaidou¹³⁸, J. Nielsen¹³⁹, M. Niemeyer⁵⁶, J. Niermann⁵⁶, N. Nikiforou³⁷, V. Nikolaenko^{38,a}, I. Nikolic-Audit¹³⁰, K. Nikolopoulos²¹, P. Nilsson³⁰, I. Ninca⁴⁹, G. Ninio¹⁵⁴, A. Nisati^{76a}, N. Nishu², R. Nisius¹¹², J-E. Nitschke⁵¹, E.K. Nkadimeng^{34g}, T. Nobe¹⁵⁶, T. Nommensen¹⁵⁰, M.B. Norfolk¹⁴², B.J. Norman³⁵, M. Noury^{36a}, J. Novak⁹⁵, T. Novak⁹⁵, L. Novotny¹³⁵, R. Novotny¹¹⁵, L. Nozka¹²⁵, K. Ntekas¹⁶², N.M.J. Nunes De Moura Junior^{84b}, J. Ocariz¹³⁰, A. Ochi⁸⁶, I. Ochoa^{133a}, S. Oerdek^{49,u}, J.T. Offermann⁴⁰, A. Ogrodnik¹³⁶, A. Oh¹⁰³, C.C. Ohm¹⁴⁷, H. Oide⁸⁵, R. Oishi¹⁵⁶, M.L. Ojeda³⁷, Y. Okumura¹⁵⁶, L.F. Oleiro Seabra^{133a}, I. Oleksiyuk⁵⁷, S.A. Olivares Pino^{140d}, G. Oliveira Correa¹³, D. Oliveira Damazio³⁰, J.L. Oliver¹⁶², Ö.O. Öncel⁵⁵, A.P. O'Neill²⁰, A. Onofre^{133a,133e}, P.U.E. Onyisi¹¹, M.J. Oreglia⁴⁰, G.E. Orellana⁹², D. Orestano^{78a,78b}, N. Orlando¹³, R.S. Orr¹⁵⁸, L.M. Osojnak¹³¹, R. Ospanov^{63a}, G. Otero y Garzon³¹, H. Otono⁹⁰, P.S. Ott^{64a}, G.J. Ottino^{18a}, M. Ouchrif^{36d}, F. Ould-Saada¹²⁸, T. Ovsianikova¹⁴¹, M. Owen⁶⁰, R.E. Owen¹³⁷, V.E. Ozcan^{22a}, F. Ozturk⁸⁸, N. Ozturk⁸, S. Ozturk⁸³, H.A. Pacey¹²⁹, A. Pacheco Pages¹³, C. Padilla Aranda¹³, G. Padovano^{76a,76b}, S. Pagan Griso^{18a}, G. Palacino⁶⁹, A. Palazzo^{71a,71b}, J. Pampel²⁵, J. Pan¹⁷⁵, T. Pan^{65a}, D.K. Panchal¹¹, C.E. Pandini¹¹⁷, J.G. Panduro Vazquez¹³⁷, H.D. Pandya¹, H. Pang¹⁵, P. Pani⁴⁹, G. Panizzo^{70a,70c}, L. Panwar¹³⁰, L. Paolozzi⁵⁷, S. Parajuli¹⁶⁵, A. Paramonov⁶, C. Paraskevopoulos⁵⁴, D. Paredes Hernandez^{65b}, A. Pareti^{74a,74b}, K.R. Park⁴², T.H. Park¹⁵⁸, M.A. Parker³³, F. Parodi^{58b,58a}, E.W. Parrish¹¹⁸, V.A. Parrish⁵³, J.A. Parsons⁴², U. Parzefall⁵⁵, B. Pascual Dias¹¹⁰, L. Pascual Dominguez¹⁰¹, E. Pasqualucci^{76a}, S. Passaggio^{58b}, F. Pastore⁹⁷, P. Patel⁸⁸, U.M. Patel⁵², J.R. Pater¹⁰³, T. Pauly³⁷, C.I. Pazos¹⁶¹, J. Pearkes¹⁴⁶, M. Pedersen¹²⁸, R. Pedro^{133a}, S.V. Peleganchuk³⁸, O. Penc³⁷, E.A. Pender⁵³, S. Peng¹⁵, G.D. Penn¹⁷⁵, K.E. Pensi¹¹¹, M. Penzin³⁸, B.S. Peralva^{84d}, A.P. Pereira Peixoto¹⁴¹, L. Pereira Sanchez¹⁴⁶, D.V. Perepelitsa^{30,af}, G. Perera¹⁰⁵, E. Perez Codina^{159a}, M. Perganti¹⁰, H. Pernegger³⁷, S. Perrella^{76a,76b}, O. Perrin⁴¹, K. Peters⁴⁹, R.F.Y. Peters¹⁰³, B.A. Petersen³⁷, T.C. Petersen⁴³, E. Petit¹⁰⁴, V. Petousis¹³⁵, C. Petridou^{155,d}, T. Petru¹³⁶, A. Petrukhin¹⁴⁴, M. Pettee^{18a}, A. Petukhov³⁸, K. Petukhova³⁷, R. Pezoa^{140f}, L. Pezzotti³⁷, G. Pezzullo¹⁷⁵, A.J. Pflieger³⁷, T.M. Pham¹⁷³, T. Pham¹⁰⁷, P.W. Phillips¹³⁷, G. Piacquadio¹⁴⁸, E. Pianori^{18a}, F. Piazza¹²⁶, R. Piegai³¹, D. Pietreanu^{28b}, A.D. Pilkington¹⁰³, M. Pinamonti^{70a,70c}, J.L. Pinfeld², B.C. Pinheiro Pereira^{133a}, J. Pinol Bel¹³, A.E. Pinto Pinoargote^{138,138}, L. Pintucci^{70a,70c}, K.M. Piper¹⁴⁹, A. Pirttikoski⁵⁷, D.A. Pizzi³⁵, L. Pizzimento^{65b}, A. Pizzini¹¹⁷, M.-A. Pleier³⁰, V. Pleskot¹³⁶, E. Plotnikova³⁹,

G. Poddar ⁹⁶, R. Poettgen ¹⁰⁰, L. Poggioli ¹³⁰, I. Pokharel ⁵⁶, S. Polacek ¹³⁶, G. Polesello ^{74a}, A. Poley ^{145,159a}, A. Polini ^{24b}, C.S. Pollard ¹⁷⁰, Z.B. Pollock ¹²², E. Pompa Pacchi ^{76a,76b}, N.I. Pond ⁹⁸, D. Ponomarenko ⁶⁹, L. Pontecorvo ³⁷, S. Popa ^{28a}, G.A. Popeneciu ^{28d}, A. Poreba ³⁷, D.M. Portillo Quintero ^{159a}, S. Pospisil ¹³⁵, M.A. Postill ¹⁴², P. Postolache ^{28c}, K. Potamianos ¹⁷⁰, P.A. Potepa ^{87a}, I.N. Potrap ³⁹, C.J. Potter ³³, H. Potti ¹⁵⁰, J. Poveda ¹⁶⁶, M.E. Pozo Astigarraga ³⁷, A. Prades Ibanez ^{77a,77b}, J. Pretel ¹⁶⁸, D. Price ¹⁰³, M. Primavera ^{71a}, L. Primomo ^{70a,70c}, M.A. Principe Martin ¹⁰¹, R. Privara ¹²⁵, T. Procter ⁶⁰, M.L. Proffitt ¹⁴¹, N. Proklova ¹³¹, K. Prokofiev ^{65c}, G. Proto ¹¹², J. Proudfoot ⁶, M. Przybycien ^{87a}, W.W. Przygoda ^{87b}, A. Psallidas ⁴⁷, J.E. Puddefoot ¹⁴², D. Pudzha ⁵⁵, D. Pyatiizbyantseva ³⁸, J. Qian ¹⁰⁸, D. Qichen ¹⁰³, Y. Qin ¹³, T. Qiu ⁵³, A. Quadt ⁵⁶, M. Queitsch-Maitland ¹⁰³, G. Quetant ⁵⁷, R.P. Quinn ¹⁶⁷, G. Rabanal Bolanos ⁶², D. Rafanoharana ⁵⁵, F. Raffaelli ^{77a,77b}, F. Ragusa ^{72a,72b}, J.L. Rainbolt ⁴⁰, J.A. Raine ⁵⁷, S. Rajagopalan ³⁰, E. Ramakoti ³⁸, L. Rambelli ^{58b,58a}, I.A. Ramirez-Berend ³⁵, K. Ran ^{49,114c}, D.S. Rankin ¹³¹, N.P. Rapheeha ^{34g}, H. Rasheed ^{28b}, V. Raskina ¹³⁰, D.F. Rassloff ^{64a}, A. Rastogi ^{18a}, S. Rave ¹⁰², S. Ravera ^{58b,58a}, B. Ravina ⁵⁶, I. Ravinovich ¹⁷², M. Raymond ³⁷, A.L. Read ¹²⁸, N.P. Readioff ¹⁴², D.M. Rebuzzi ^{74a,74b}, G. Redlinger ³⁰, A.S. Reed ¹¹², K. Reeves ²⁷, J.A. Reidelsturz ¹⁷⁴, D. Reikher ¹²⁶, A. Rej ⁵⁰, C. Rembser ³⁷, M. Renda ^{28b}, F. Renner ⁴⁹, A.G. Rennie ¹⁶², A.L. Rescia ⁴⁹, S. Resconi ^{72a}, M. Ressegotti ^{58b,58a}, S. Rettie ³⁷, J.G. Reyes Rivera ¹⁰⁹, E. Reynolds ^{18a}, O.L. Rezanova ³⁸, P. Reznicek ¹³⁶, H. Riani ^{36d}, N. Ribaric ⁵², E. Ricci ^{79a,79b}, R. Richter ¹¹², S. Richter ^{48a,48b}, E. Richter-Was ^{87b}, M. Ridel ¹³⁰, S. Ridouani ^{36d}, P. Rieck ¹²⁰, P. Riedler ³⁷, E.M. Riefel ^{48a,48b}, J.O. Rieger ¹¹⁷, M. Rijssenbeek ¹⁴⁸, M. Rimoldi ³⁷, L. Rinaldi ^{24b,24a}, P. Rincke ^{56,164}, T.T. Rinn ³⁰, M.P. Rinnagel ¹¹¹, G. Ripellino ¹⁶⁴, I. Riu ¹³, J.C. Rivera Vergara ¹⁶⁸, F. Rizatdinova ¹²⁴, E. Rizvi ⁹⁶, B.R. Roberts ^{18a}, S.S. Roberts ¹³⁹, S.H. Robertson ^{106,x}, D. Robinson ³³, M. Robles Manzano ¹⁰², A. Robson ⁶⁰, A. Rocchi ^{77a,77b}, C. Roda ^{75a,75b}, S. Rodriguez Bosca ³⁷, Y. Rodriguez Garcia ^{23a}, A. Rodriguez Rodriguez ⁵⁵, A.M. Rodríguez Vera ¹¹⁸, S. Roe ³⁷, J.T. Roemer ³⁷, A.R. Roepe-Gier ¹³⁹, O. Røhne ¹²⁸, R.A. Rojas ¹⁰⁵, C.P.A. Roland ¹³⁰, J. Roloff ³⁰, A. Romaniouk ³⁸, E. Romano ^{74a,74b}, M. Romano ^{24b}, A.C. Romero Hernandez ¹⁶⁵, N. Rompotis ⁹⁴, L. Roos ¹³⁰, S. Rosati ^{76a}, B.J. Rosser ⁴⁰, E. Rossi ¹²⁹, E. Rossi ^{73a,73b}, L.P. Rossi ⁶², L. Rossini ⁵⁵, R. Rosten ¹²², M. Rotaru ^{28b}, B. Rottler ⁵⁵, C. Rougier ⁹¹, D. Rousseau ⁶⁷, D. Rousso ⁴⁹, A. Roy ¹⁶⁵, S. Roy-Garand ¹⁵⁸, A. Rozanov ¹⁰⁴, Z.M.A. Rozario ⁶⁰, Y. Rozen ¹⁵³, A. Rubio Jimenez ¹⁶⁶, A.J. Ruby ⁹⁴, V.H. Ruelas Rivera ¹⁹, T.A. Ruggeri ¹, A. Ruggiero ¹²⁹, A. Ruiz-Martinez ¹⁶⁶, A. Rummler ³⁷, Z. Rurikova ⁵⁵, N.A. Rusakovich ³⁹, H.L. Russell ¹⁶⁸, G. Russo ^{76a,76b}, J.P. Rutherford ⁷, S. Rutherford Colmenares ³³, M. Rybar ¹³⁶, E.B. Rye ¹²⁸, A. Ryzhov ⁴⁵, J.A. Sabater Iglesias ⁵⁷, H.F.W. Sadrozinski ¹³⁹, F. Safai Tehrani ^{76a}, B. Safarzadeh Samani ¹³⁷, S. Saha ¹, M. Sahinsoy ⁸³, A. Saibel ¹⁶⁶, M. Saimpert ¹³⁸, M. Saito ¹⁵⁶, T. Saito ¹⁵⁶, A. Sala ^{72a,72b}, D. Salamani ³⁷, A. Salnikov ¹⁴⁶, J. Salt ¹⁶⁶, A. Salvador Salas ¹⁵⁴, D. Salvatore ^{44b,44a}, F. Salvatore ¹⁴⁹, A. Salzburger ³⁷, D. Sammel ⁵⁵, E. Sampson ⁹³, D. Sampsonidis ^{155,d}, D. Sampsonidou ¹²⁶, J. Sánchez ¹⁶⁶, V. Sanchez Sebastian ¹⁶⁶, H. Sandaker ¹²⁸, C.O. Sander ⁴⁹, J.A. Sandesara ¹⁰⁵, M. Sandhoff ¹⁷⁴, C. Sandoval ^{23b}, L. Sanfilippo ^{64a}, D.P.C. Sankey ¹³⁷, T. Sano ⁸⁹, A. Sansoni ⁵⁴, L. Santi ^{37,76b}, C. Santoni ⁴¹, H. Santos ^{133a,133b}, A. Santra ¹⁷², E. Sanzani ^{24b,24a}, K.A. Saoucha ¹⁶³, J.G. Saraiva ^{133a,133d}, J. Sardain ⁷, O. Sasaki ⁸⁵, K. Sato ¹⁶⁰, C. Sauer ^{64b}, E. Sauvan ⁴, P. Savard ^{158,ad}, R. Sawada ¹⁵⁶, C. Sawyer ¹³⁷, L. Sawyer ⁹⁹, C. Sbarra ^{24b}, A. Sbrizzi ^{24b,24a}, T. Scanlon ⁹⁸, J. Schaarschmidt ¹⁴¹, U. Schäfer ¹⁰², A.C. Schaffer ^{67,45}, D. Schaile ¹¹¹, R.D. Schamberger ¹⁴⁸, C. Scharf ¹⁹, M.M. Schefer ²⁰, V.A. Schegelsky ³⁸, D. Scheirich ¹³⁶, M. Schernau ¹⁶², C. Scheulen ⁵⁶, C. Schiavi ^{58b,58a}, M. Schioppa ^{44b,44a}, B. Schlag ^{146,1}, K.E. Schleicher ⁵⁵,

S. Schlenker , J. Schmeing , M.A. Schmidt , K. Schmieden , C. Schmitt ,
 N. Schmitt , S. Schmitt , L. Schoeffel , A. Schoening , P.G. Scholer , E. Schopf ,
 M. Schott , J. Schovancova , S. Schramm , T. Schroer , H-C. Schultz-Coulon ,
 M. Schumacher , B.A. Schumm , Ph. Schune , A.J. Schuy , H.R. Schwartz ,
 A. Schwartzman , T.A. Schwarz , Ph. Schwemling , R. Schwienhorst ,
 F.G. Sciacca , A. Sciandra , G. Sciolla , F. Scuri , C.D. Sebastiani , K. Sedlaczek ,
 S.C. Seidel , A. Seiden , B.D. Seidlitz , C. Seitz , J.M. Seixas , G. Sekhniaidze ,
 L. Selem , N. Semprini-Cesari , D. Sengupta , V. Senthilkumar , L. Serin ,
 M. Sessa , H. Severini , F. Sforza , A. Sfyrla , Q. Sha , E. Shabalina ,
 A.H. Shah , R. Shaheen , J.D. Shahinian , D. Shaked Renous , L.Y. Shan ,
 M. Shapiro , A. Sharma , A.S. Sharma , P. Sharma , P.B. Shatalov , K. Shaw ,
 S.M. Shaw , Q. Shen , D.J. Sheppard , P. Sherwood , L. Shi , X. Shi ,
 S. Shimizu , C.O. Shimmin , J.D. Shinner , I.P.J. Shipsey , S. Shirabe ,
 M. Shiyakova , M.J. Shochet , D.R. Shope , B. Shrestha , S. Shrestha ,
 M.J. Shroff , P. Sicho , A.M. Sickles , E. Sideras Haddad , A.C. Sidley ,
 A. Sidoti , F. Siegert , Dj. Sijacki , F. Sili , J.M. Silva , I. Silva Ferreira ,
 M.V. Silva Oliveira , S.B. Silverstein , S. Simion , R. Simoniello , E.L. Simpson ,
 H. Simpson , L.R. Simpson , N.D. Simpson , S. Simsek , S. Sindhu , P. Sinervo ,
 S. Singh , S. Sinha , S. Sinha , M. Sioli , I. Siral , E. Sitnikova ,
 J. Sjölin , A. Skaf , E. Skorda , P. Skubic , M. Slawinska , V. Smakhtin ,
 B.H. Smart , S.Yu. Smirnov , Y. Smirnov , L.N. Smirnova , O. Smirnova ,
 A.C. Smith , D.R. Smith , E.A. Smith , J.L. Smith , R. Smith , M. Smizanska ,
 K. Smolek , A.A. Snesarev , H.L. Snoek , S. Snyder , R. Sobie , A. Soffer ,
 C.A. Solans Sanchez , E.Yu. Soldatov , U. Soldevila , A.A. Solodkov , S. Solomon ,
 A. Soloshenko , K. Solovieva , O.V. Solovyanov , P. Sommer , A. Sonay ,
 W.Y. Song , A. Sopczak , A.L. Soppio , F. Sopkova , J.D. Sorenson ,
 I.R. Sotarriva Alvarez , V. Sothilingam , O.J. Soto Sandoval , S. Sottocornola ,
 R. Soualah , Z. Soumami , D. South , N. Soybelman , S. Spagnolo ,
 M. Spalla , D. Sperlich , G. Spigo , B. Spisso , D.P. Spiteri , M. Spousta ,
 E.J. Staats , R. Stamen , A. Stampeki , E. Stanecka , W. Stanek-Maslouska ,
 M.V. Stange , B. Stanislaus , M.M. Stanitzki , B. Stapf , E.A. Starchenko ,
 G.H. Stark , J. Stark , P. Staroba , P. Starovoitov , S. Stärz , R. Staszewski ,
 G. Stavropoulos , A. Stefl , P. Steinberg , B. Stelzer , H.J. Stelzer ,
 O. Stelzer-Chilton , H. Stenzel , T.J. Stevenson , G.A. Stewart , J.R. Stewart ,
 M.C. Stockton , G. Stoicea , M. Stolarski , S. Stonjek , A. Straessner ,
 J. Strandberg , S. Strandberg , M. Stratmann , M. Strauss , T. Strebler ,
 P. Strizenec , R. Ströhmer , D.M. Strom , R. Stroynowski , A. Strubig ,
 S.A. Stucci , B. Stugu , J. Stupak , N.A. Styles , D. Su , S. Su ,
 X. Su , D. Suchy , K. Sugizaki , V.V. Sulin , M.J. Sullivan , D.M.S. Sultan ,
 L. Sultanliyeva , S. Sultansoy , T. Sumida , S. Sun , O. Sunneborn Gudnadottir ,
 N. Sur , M.R. Sutton , H. Suzuki , M. Svatos , M. Swiatlowski , T. Swirski ,
 I. Sykora , M. Sykora , T. Sykora , D. Ta , K. Tackmann , A. Taffard ,
 R. Tafirout , J.S. Tafoya Vargas , Y. Takubo , M. Talby , A.A. Talyshev ,
 K.C. Tam , N.M. Tamir , A. Tanaka , J. Tanaka , R. Tanaka , M. Tanasini ,
 Z. Tao , S. Tapia Araya , S. Tapprogge , A. Tarek Abouelfadl Mohamed ,
 S. Tarem , K. Tariq , G. Tarna , G.F. Tartarelli , M.J. Tartarin , P. Tas ,
 M. Tasevsky , E. Tassi , A.C. Tate , G. Tateno , Y. Tayalati , G.N. Taylor ,

W. Taylor ^{159b}, R. Teixeira De Lima ¹⁴⁶, P. Teixeira-Dias ⁹⁷, J.J. Teoh ¹⁵⁸, K. Terashi ¹⁵⁶,
 J. Terron ¹⁰¹, S. Terzo ¹³, M. Testa ⁵⁴, R.J. Teuscher ^{158,x}, A. Thaler ⁸⁰, O. Theiner ⁵⁷,
 T. Thevenaux-Pelzer ¹⁰⁴, O. Thielmann ¹⁷⁴, D.W. Thomas ⁹⁷, J.P. Thomas ²¹, E.A. Thompson ^{18a},
 P.D. Thompson ²¹, E. Thomson ¹³¹, R.E. Thornberry ⁴⁵, C. Tian ^{63a}, Y. Tian ⁵⁶,
 V. Tikhomirov ^{38,a}, Yu.A. Tikhonov ³⁸, S. Timoshenko ³⁸, D. Timoshyn ¹³⁶, E.X.L. Ting ¹,
 P. Tipton ¹⁷⁵, A. Tishelman-Charny ³⁰, S.H. Tlou ^{34g}, K. Todome ¹⁵⁷, S. Todorova-Nova ¹³⁶,
 S. Todt ⁵¹, L. Toffolin ^{70a,70c}, M. Togawa ⁸⁵, J. Tojo ⁹⁰, S. Tokár ^{29a}, K. Tokushuku ⁸⁵,
 O. Toldaiev ⁶⁹, M. Tomoto ^{85,113}, L. Tompkins ^{146,1}, K.W. Topolnicki ^{87b}, E. Torrence ¹²⁶,
 H. Torres ⁹¹, E. Torró Pastor ¹⁶⁶, M. Toscani ³¹, C. Toscirci ⁴⁰, M. Tost ¹¹, D.R. Tovey ¹⁴²,
 I.S. Trandafir ^{28b}, T. Trefzger ¹⁶⁹, A. Tricoli ³⁰, I.M. Trigger ^{159a}, S. Trincaz-Duvoid ¹³⁰,
 D.A. Trischuk ²⁷, B. Trocmé ⁶¹, A. Tropina ³⁹, L. Truong ^{34c}, M. Trzebinski ⁸⁸, A. Trzupek ⁸⁸,
 F. Tsai ¹⁴⁸, M. Tsai ¹⁰⁸, A. Tsiamis ¹⁵⁵, P.V. Tsiareshka ³⁸, S. Tsigaridas ^{159a}, A. Tsigiriotis ^{155,r},
 V. Tsiskaridze ¹⁵⁸, E.G. Tskhadadze ^{152a}, M. Tsopoulou ¹⁵⁵, Y. Tsujikawa ⁸⁹, I.I. Tsukerman ³⁸,
 V. Tsulaia ^{18a}, S. Tsuno ⁸⁵, K. Tsuru ¹²¹, D. Tsybychev ¹⁴⁸, Y. Tu ^{65b}, A. Tudorache ^{28b},
 V. Tudorache ^{28b}, A.N. Tuna ⁶², S. Turchikhin ^{58b,58a}, I. Turk Cakir ^{3a}, R. Turra ^{72a},
 T. Turtuvshin ³⁹, P.M. Tuts ⁴², S. Tzamarias ^{155,d}, E. Tzovara ¹⁰², F. Ukegawa ¹⁶⁰,
 P.A. Ulloa Poblete ^{140c,140b}, E.N. Umaka ³⁰, G. Unal ³⁷, A. Undrus ³⁰, G. Unel ¹⁶², J. Urban ^{29b},
 P. Urrejola ^{140a}, G. Usai ⁸, R. Ushioda ¹⁵⁷, M. Usman ¹¹⁰, F. Ustuner ⁵³, Z. Uysal ⁸³,
 V. Vacek ¹³⁵, B. Vachon ¹⁰⁶, T. Vafeiadis ³⁷, A. Vaitkus ⁹⁸, C. Valderanis ¹¹¹,
 E. Valdes Santurio ^{48a,48b}, M. Valente ^{159a}, S. Valentinetti ^{24b,24a}, A. Valero ¹⁶⁶,
 E. Valiente Moreno ¹⁶⁶, A. Vallier ⁹¹, J.A. Valls Ferrer ¹⁶⁶, D.R. Van Arneman ¹¹⁷,
 T.R. Van Daalen ¹⁴¹, A. Van Der Graaf ⁵⁰, P. Van Gemmeren ⁶, M. Van Rijnbach ³⁷,
 S. Van Stroud ⁹⁸, I. Van Vulpen ¹¹⁷, P. Vana ¹³⁶, M. Vanadia ^{77a,77b}, W. Vandelli ³⁷,
 E.R. Vandewall ¹²⁴, D. Vannicola ¹⁵⁴, L. Vannoli ⁵⁴, R. Vari ^{76a}, E.W. Varnes ⁷, C. Varni ^{18b},
 T. Varol ¹⁵¹, D. Varouchas ⁶⁷, L. Varriale ¹⁶⁶, K.E. Varvell ¹⁵⁰, M.E. Vasile ^{28b}, L. Vaslin ⁸⁵,
 G.A. Vasquez ¹⁶⁸, A. Vasyukov ³⁹, L.M. Vaughan ¹²⁴, R. Vavricka ¹⁰², T. Vazquez Schroeder ³⁷,
 J. Veatch ³², V. Vecchio ¹⁰³, M.J. Veen ¹⁰⁵, I. Veliscek ³⁰, L.M. Veloce ¹⁵⁸, F. Veloso ^{133a,133c},
 S. Veneziano ^{76a}, A. Ventura ^{71a,71b}, S. Ventura Gonzalez ¹³⁸, A. Verbytskyi ¹¹²,
 M. Verducci ^{75a,75b}, C. Vergis ⁹⁶, M. Verissimo De Araujo ^{84b}, W. Verkerke ¹¹⁷,
 J.C. Vermeulen ¹¹⁷, C. Vernieri ¹⁴⁶, M. Vessella ¹⁰⁵, M.C. Vetterli ^{145,ad}, A. Vgenopoulos ¹⁰²,
 N. Viaux Maira ^{140f}, T. Vickey ¹⁴², O.E. Vickey Boeriu ¹⁴², G.H.A. Viehhauser ¹²⁹, L. Vigani ^{64b},
 M. Vigil ¹¹², M. Villa ^{24b,24a}, M. Villaplana Perez ¹⁶⁶, E.M. Villhauer ⁵³, E. Vilucchi ⁵⁴,
 M.G. Vincter ³⁵, A. Visibile ¹¹⁷, C. Vittori ³⁷, I. Vivarelli ^{24b,24a}, E. Voevodina ¹¹², F. Vogel ¹¹¹,
 J.C. Voigt ⁵¹, P. Vokac ¹³⁵, Yu. Volkotrub ^{87b}, J. Von Ahnen ⁴⁹, E. Von Toerne ²⁵,
 B. Vormwald ³⁷, V. Vorobel ¹³⁶, K. Vorobev ³⁸, M. Vos ¹⁶⁶, K. Voss ¹⁴⁴, M. Vozak ¹¹⁷,
 L. Vozdecky ¹²³, N. Vranjes ¹⁶, M. Vranjes Milosavljevic ¹⁶, M. Vreeswijk ¹¹⁷, N.K. Vu ^{63d,63c},
 R. Vuillermet ³⁷, O. Vujinovic ¹⁰², I. Vukotic ⁴⁰, I.K. Vyas ³⁵, S. Wada ¹⁶⁰, C. Wagner ¹⁰⁵,
 J.M. Wagner ^{18a}, W. Wagner ¹⁷⁴, S. Wahdan ¹⁷⁴, H. Wahlberg ⁹², J. Walder ¹³⁷, R. Walker ¹¹¹,
 W. Walkowiak ¹⁴⁴, A. Wall ¹³¹, E.J. Wallin ¹⁰⁰, T. Wamorkar ⁶, A.Z. Wang ¹³⁹, C. Wang ¹⁰²,
 C. Wang ¹¹, H. Wang ^{18a}, J. Wang ^{65c}, P. Wang ⁹⁸, R. Wang ⁶², R. Wang ⁶, S.M. Wang ¹⁵¹,
 S. Wang ^{63b}, S. Wang ¹⁴, T. Wang ^{63a}, W.T. Wang ⁸¹, W. Wang ¹⁴, X. Wang ^{114a}, X. Wang ¹⁶⁵,
 X. Wang ^{63c}, Y. Wang ^{63d}, Y. Wang ^{114a}, Y. Wang ^{63a}, Z. Wang ¹⁰⁸, Z. Wang ^{63d,52,63c},
 Z. Wang ¹⁰⁸, A. Warburton ¹⁰⁶, R.J. Ward ²¹, N. Warrack ⁶⁰, S. Waterhouse ⁹⁷, A.T. Watson ²¹,
 H. Watson ⁵³, M.F. Watson ²¹, E. Watton ^{60,137}, G. Watts ¹⁴¹, B.M. Waugh ⁹⁸, J.M. Webb ⁵⁵,
 C. Weber ³⁰, H.A. Weber ¹⁹, M.S. Weber ²⁰, S.M. Weber ^{64a}, C. Wei ^{63a}, Y. Wei ⁵⁵,
 A.R. Weidberg ¹²⁹, E.J. Weik ¹²⁰, J. Weingarten ⁵⁰, C. Weiser ⁵⁵, C.J. Wells ⁴⁹, T. Wenaus ³⁰,
 B. Wendland ⁵⁰, T. Wengler ³⁷, N.S. Wenke ¹¹², N. Wermes ²⁵, M. Wessels ^{64a}, A.M. Wharton ⁹³,

A.S. White ⁶², A. White ⁸, M.J. White ¹, D. Whiteson ¹⁶², L. Wickremasinghe ¹²⁷, W. Wiedenmann ¹⁷³, M. Wielers ¹³⁷, C. Wiglesworth ⁴³, D.J. Wilbern ¹²³, H.G. Wilkens ³⁷, J.J.H. Wilkinson ³³, D.M. Williams ⁴², H.H. Williams ¹³¹, S. Williams ³³, S. Willocq ¹⁰⁵, B.J. Wilson ¹⁰³, P.J. Windischhofer ⁴⁰, F.I. Winkel ³¹, F. Winklmeier ¹²⁶, B.T. Winter ⁵⁵, J.K. Winter ¹⁰³, M. Wittgen ¹⁴⁶, M. Wobisch ⁹⁹, T. Wojtkowski ⁶¹, Z. Wolffs ¹¹⁷, J. Wollrath ¹⁶², M.W. Wolter ⁸⁸, H. Wolters ^{133a,133c}, M.C. Wong ¹³⁹, E.L. Woodward ⁴², S.D. Worm ⁴⁹, B.K. Wosiek ⁸⁸, K.W. Woźniak ⁸⁸, S. Wozniowski ⁵⁶, K. Wraight ⁶⁰, C. Wu ²¹, M. Wu ^{114b}, M. Wu ¹¹⁶, S.L. Wu ¹⁷³, X. Wu ⁵⁷, Y. Wu ^{63a}, Z. Wu ⁴, J. Wuerzinger ^{112,ab}, T.R. Wyatt ¹⁰³, B.M. Wynne ⁵³, S. Xella ⁴³, L. Xia ^{114a}, M. Xia ¹⁵, M. Xie ^{63a}, S. Xin ^{14,114c}, A. Xiong ¹²⁶, J. Xiong ^{18a}, D. Xu ¹⁴, H. Xu ^{63a}, L. Xu ^{63a}, R. Xu ¹³¹, T. Xu ¹⁰⁸, Y. Xu ¹⁵, Z. Xu ⁵³, Z. Xu ^{114a}, B. Yabsley ¹⁵⁰, S. Yacoob ^{34a}, Y. Yamaguchi ⁸⁵, E. Yamashita ¹⁵⁶, H. Yamauchi ¹⁶⁰, T. Yamazaki ^{18a}, Y. Yamazaki ⁸⁶, J. Yan ^{63c}, S. Yan ⁶⁰, Z. Yan ¹⁰⁵, H.J. Yang ^{63c,63d}, H.T. Yang ^{63a}, S. Yang ^{63a}, T. Yang ^{65c}, X. Yang ³⁷, X. Yang ¹⁴, Y. Yang ⁴⁵, Y. Yang ^{63a}, Z. Yang ^{63a}, W.-M. Yao ^{18a}, H. Ye ^{114a}, H. Ye ⁵⁶, J. Ye ¹⁴, S. Ye ³⁰, X. Ye ^{63a}, Y. Yeh ⁹⁸, I. Yeletsikh ³⁹, B. Yeo ^{18b}, M.R. Yexley ⁹⁸, T.P. Yildirim ¹²⁹, P. Yin ⁴², K. Yorita ¹⁷¹, S. Younas ^{28b}, C.J.S. Young ³⁷, C. Young ¹⁴⁶, C. Yu ^{14,114c}, Y. Yu ^{63a}, J. Yuan ^{14,114c}, M. Yuan ¹⁰⁸, R. Yuan ^{63d,63c}, L. Yue ⁹⁸, M. Zaazoua ^{63a}, B. Zabinski ⁸⁸, E. Zaid ⁵³, Z.K. Zak ⁸⁸, T. Zakareishvili ¹⁶⁶, S. Zambito ⁵⁷, J.A. Zamora Saa ^{140d,140b}, J. Zang ¹⁵⁶, D. Zanzi ⁵⁵, O. Zaplatilek ¹³⁵, C. Zeitnitz ¹⁷⁴, H. Zeng ¹⁴, J.C. Zeng ¹⁶⁵, D.T. Zenger Jr ²⁷, O. Zenin ³⁸, T. Ženiš ^{29a}, S. Zenz ⁹⁶, S. Zerradi ^{36a}, D. Zerwas ⁶⁷, M. Zhai ^{14,114c}, D.F. Zhang ¹⁴², J. Zhang ^{63b}, J. Zhang ⁶, K. Zhang ^{14,114c}, L. Zhang ^{63a}, L. Zhang ^{114a}, P. Zhang ^{14,114c}, R. Zhang ¹⁷³, S. Zhang ¹⁰⁸, S. Zhang ⁹¹, T. Zhang ¹⁵⁶, X. Zhang ^{63c}, X. Zhang ^{63b}, Y. Zhang ^{63c}, Y. Zhang ⁹⁸, Y. Zhang ^{114a}, Z. Zhang ^{18a}, Z. Zhang ^{63b}, Z. Zhang ⁶⁷, H. Zhao ¹⁴¹, T. Zhao ^{63b}, Y. Zhao ¹³⁹, Z. Zhao ^{63a}, Z. Zhao ^{63a}, A. Zhemchugov ³⁹, J. Zheng ^{114a}, K. Zheng ¹⁶⁵, X. Zheng ^{63a}, Z. Zheng ¹⁴⁶, D. Zhong ¹⁶⁵, B. Zhou ¹⁰⁸, H. Zhou ⁷, N. Zhou ^{63c}, Y. Zhou ¹⁵, Y. Zhou ^{114a}, Y. Zhou ⁷, C.G. Zhu ^{63b}, J. Zhu ¹⁰⁸, X. Zhu ^{63d}, Y. Zhu ^{63c}, Y. Zhu ^{63a}, X. Zhuang ¹⁴, K. Zhukov ⁶⁹, N.I. Zimine ³⁹, J. Zinsser ^{64b}, M. Ziolkowski ¹⁴⁴, L. Živković ¹⁶, A. Zoccoli ^{24b,24a}, K. Zoch ⁶², T.G. Zorbas ¹⁴², O. Zormpa ⁴⁷, W. Zou ⁴², L. Zwalinski ³⁷.

¹Department of Physics, University of Adelaide, Adelaide; Australia.

²Department of Physics, University of Alberta, Edmonton AB; Canada.

³(^a)Department of Physics, Ankara University, Ankara; (^b)Division of Physics, TOBB University of Economics and Technology, Ankara; Türkiye.

⁴LAPP, Université Savoie Mont Blanc, CNRS/IN2P3, Annecy; France.

⁵APC, Université Paris Cité, CNRS/IN2P3, Paris; France.

⁶High Energy Physics Division, Argonne National Laboratory, Argonne IL; United States of America.

⁷Department of Physics, University of Arizona, Tucson AZ; United States of America.

⁸Department of Physics, University of Texas at Arlington, Arlington TX; United States of America.

⁹Physics Department, National and Kapodistrian University of Athens, Athens; Greece.

¹⁰Physics Department, National Technical University of Athens, Zografou; Greece.

¹¹Department of Physics, University of Texas at Austin, Austin TX; United States of America.

¹²Institute of Physics, Azerbaijan Academy of Sciences, Baku; Azerbaijan.

¹³Institut de Física d'Altes Energies (IFAE), Barcelona Institute of Science and Technology, Barcelona; Spain.

¹⁴Institute of High Energy Physics, Chinese Academy of Sciences, Beijing; China.

¹⁵Physics Department, Tsinghua University, Beijing; China.

- ¹⁶Institute of Physics, University of Belgrade, Belgrade; Serbia.
- ¹⁷Department for Physics and Technology, University of Bergen, Bergen; Norway.
- ¹⁸(^a)Physics Division, Lawrence Berkeley National Laboratory, Berkeley CA;(^b)University of California, Berkeley CA; United States of America.
- ¹⁹Institut für Physik, Humboldt Universität zu Berlin, Berlin; Germany.
- ²⁰Albert Einstein Center for Fundamental Physics and Laboratory for High Energy Physics, University of Bern, Bern; Switzerland.
- ²¹School of Physics and Astronomy, University of Birmingham, Birmingham; United Kingdom.
- ²²(^a)Department of Physics, Bogazici University, Istanbul;(^b)Department of Physics Engineering, Gaziantep University, Gaziantep;(^c)Department of Physics, Istanbul University, Istanbul; Türkiye.
- ²³(^a)Facultad de Ciencias y Centro de Investigaciones, Universidad Antonio Nariño, Bogotá;(^b)Departamento de Física, Universidad Nacional de Colombia, Bogotá; Colombia.
- ²⁴(^a)Dipartimento di Fisica e Astronomia A. Righi, Università di Bologna, Bologna;(^b)INFN Sezione di Bologna; Italy.
- ²⁵Physikalisches Institut, Universität Bonn, Bonn; Germany.
- ²⁶Department of Physics, Boston University, Boston MA; United States of America.
- ²⁷Department of Physics, Brandeis University, Waltham MA; United States of America.
- ²⁸(^a)Transilvania University of Brasov, Brasov;(^b)Horia Hulubei National Institute of Physics and Nuclear Engineering, Bucharest;(^c)Department of Physics, Alexandru Ioan Cuza University of Iasi, Iasi;(^d)National Institute for Research and Development of Isotopic and Molecular Technologies, Physics Department, Cluj-Napoca;(^e)National University of Science and Technology Politehnica, Bucharest;(^f)West University in Timisoara, Timisoara;(^g)Faculty of Physics, University of Bucharest, Bucharest; Romania.
- ²⁹(^a)Faculty of Mathematics, Physics and Informatics, Comenius University, Bratislava;(^b)Department of Subnuclear Physics, Institute of Experimental Physics of the Slovak Academy of Sciences, Kosice; Slovak Republic.
- ³⁰Physics Department, Brookhaven National Laboratory, Upton NY; United States of America.
- ³¹Universidad de Buenos Aires, Facultad de Ciencias Exactas y Naturales, Departamento de Física, y CONICET, Instituto de Física de Buenos Aires (IFIBA), Buenos Aires; Argentina.
- ³²California State University, CA; United States of America.
- ³³Cavendish Laboratory, University of Cambridge, Cambridge; United Kingdom.
- ³⁴(^a)Department of Physics, University of Cape Town, Cape Town;(^b)iThemba Labs, Western Cape;(^c)Department of Mechanical Engineering Science, University of Johannesburg, Johannesburg;(^d)National Institute of Physics, University of the Philippines Diliman (Philippines);(^e)University of South Africa, Department of Physics, Pretoria;(^f)University of Zululand, KwaDlangezwa;(^g)School of Physics, University of the Witwatersrand, Johannesburg; South Africa.
- ³⁵Department of Physics, Carleton University, Ottawa ON; Canada.
- ³⁶(^a)Faculté des Sciences Ain Chock, Université Hassan II de Casablanca;(^b)Faculté des Sciences, Université Ibn-Tofail, Kénitra;(^c)Faculté des Sciences Semailia, Université Cadi Ayyad, LPHEA-Marrakech;(^d)LPMR, Faculté des Sciences, Université Mohamed Premier, Oujda;(^e)Faculté des sciences, Université Mohammed V, Rabat;(^f)Institute of Applied Physics, Mohammed VI Polytechnic University, Ben Guerir; Morocco.
- ³⁷CERN, Geneva; Switzerland.
- ³⁸Affiliated with an institute covered by a cooperation agreement with CERN.
- ³⁹Affiliated with an international laboratory covered by a cooperation agreement with CERN.
- ⁴⁰Enrico Fermi Institute, University of Chicago, Chicago IL; United States of America.
- ⁴¹LPC, Université Clermont Auvergne, CNRS/IN2P3, Clermont-Ferrand; France.
- ⁴²Nevis Laboratory, Columbia University, Irvington NY; United States of America.

- ⁴³Niels Bohr Institute, University of Copenhagen, Copenhagen; Denmark.
- ⁴⁴(^a)Dipartimento di Fisica, Università della Calabria, Rende; (^b)INFN Gruppo Collegato di Cosenza, Laboratori Nazionali di Frascati; Italy.
- ⁴⁵Physics Department, Southern Methodist University, Dallas TX; United States of America.
- ⁴⁶Physics Department, University of Texas at Dallas, Richardson TX; United States of America.
- ⁴⁷National Centre for Scientific Research "Demokritos", Agia Paraskevi; Greece.
- ⁴⁸(^a)Department of Physics, Stockholm University; (^b)Oskar Klein Centre, Stockholm; Sweden.
- ⁴⁹Deutsches Elektronen-Synchrotron DESY, Hamburg and Zeuthen; Germany.
- ⁵⁰Fakultät Physik, Technische Universität Dortmund, Dortmund; Germany.
- ⁵¹Institut für Kern- und Teilchenphysik, Technische Universität Dresden, Dresden; Germany.
- ⁵²Department of Physics, Duke University, Durham NC; United States of America.
- ⁵³SUPA - School of Physics and Astronomy, University of Edinburgh, Edinburgh; United Kingdom.
- ⁵⁴INFN e Laboratori Nazionali di Frascati, Frascati; Italy.
- ⁵⁵Physikalisches Institut, Albert-Ludwigs-Universität Freiburg, Freiburg; Germany.
- ⁵⁶II. Physikalisches Institut, Georg-August-Universität Göttingen, Göttingen; Germany.
- ⁵⁷Département de Physique Nucléaire et Corpusculaire, Université de Genève, Genève; Switzerland.
- ⁵⁸(^a)Dipartimento di Fisica, Università di Genova, Genova; (^b)INFN Sezione di Genova; Italy.
- ⁵⁹II. Physikalisches Institut, Justus-Liebig-Universität Giessen, Giessen; Germany.
- ⁶⁰SUPA - School of Physics and Astronomy, University of Glasgow, Glasgow; United Kingdom.
- ⁶¹LPSC, Université Grenoble Alpes, CNRS/IN2P3, Grenoble INP, Grenoble; France.
- ⁶²Laboratory for Particle Physics and Cosmology, Harvard University, Cambridge MA; United States of America.
- ⁶³(^a)Department of Modern Physics and State Key Laboratory of Particle Detection and Electronics, University of Science and Technology of China, Hefei; (^b)Institute of Frontier and Interdisciplinary Science and Key Laboratory of Particle Physics and Particle Irradiation (MOE), Shandong University, Qingdao; (^c)School of Physics and Astronomy, Shanghai Jiao Tong University, Key Laboratory for Particle Astrophysics and Cosmology (MOE), SKLPPC, Shanghai; (^d)Tsung-Dao Lee Institute, Shanghai; (^e)School of Physics and Microelectronics, Zhengzhou University; China.
- ⁶⁴(^a)Kirchhoff-Institut für Physik, Ruprecht-Karls-Universität Heidelberg, Heidelberg; (^b)Physikalisches Institut, Ruprecht-Karls-Universität Heidelberg, Heidelberg; Germany.
- ⁶⁵(^a)Department of Physics, Chinese University of Hong Kong, Shatin, N.T., Hong Kong; (^b)Department of Physics, University of Hong Kong, Hong Kong; (^c)Department of Physics and Institute for Advanced Study, Hong Kong University of Science and Technology, Clear Water Bay, Kowloon, Hong Kong; China.
- ⁶⁶Department of Physics, National Tsing Hua University, Hsinchu; Taiwan.
- ⁶⁷IJCLab, Université Paris-Saclay, CNRS/IN2P3, 91405, Orsay; France.
- ⁶⁸Centro Nacional de Microelectrónica (IMB-CNM-CSIC), Barcelona; Spain.
- ⁶⁹Department of Physics, Indiana University, Bloomington IN; United States of America.
- ⁷⁰(^a)INFN Gruppo Collegato di Udine, Sezione di Trieste, Udine; (^b)ICTP, Trieste; (^c)Dipartimento Politecnico di Ingegneria e Architettura, Università di Udine, Udine; Italy.
- ⁷¹(^a)INFN Sezione di Lecce; (^b)Dipartimento di Matematica e Fisica, Università del Salento, Lecce; Italy.
- ⁷²(^a)INFN Sezione di Milano; (^b)Dipartimento di Fisica, Università di Milano, Milano; Italy.
- ⁷³(^a)INFN Sezione di Napoli; (^b)Dipartimento di Fisica, Università di Napoli, Napoli; Italy.
- ⁷⁴(^a)INFN Sezione di Pavia; (^b)Dipartimento di Fisica, Università di Pavia, Pavia; Italy.
- ⁷⁵(^a)INFN Sezione di Pisa; (^b)Dipartimento di Fisica E. Fermi, Università di Pisa, Pisa; Italy.
- ⁷⁶(^a)INFN Sezione di Roma; (^b)Dipartimento di Fisica, Sapienza Università di Roma, Roma; Italy.
- ⁷⁷(^a)INFN Sezione di Roma Tor Vergata; (^b)Dipartimento di Fisica, Università di Roma Tor Vergata, Roma; Italy.

- ^{78(a)}INFN Sezione di Roma Tre; ^(b)Dipartimento di Matematica e Fisica, Università Roma Tre, Roma; Italy.
- ^{79(a)}INFN-TIFPA; ^(b)Università degli Studi di Trento, Trento; Italy.
- ⁸⁰Universität Innsbruck, Department of Astro and Particle Physics, Innsbruck; Austria.
- ⁸¹University of Iowa, Iowa City IA; United States of America.
- ⁸²Department of Physics and Astronomy, Iowa State University, Ames IA; United States of America.
- ⁸³Istinye University, Sariyer, Istanbul; Türkiye.
- ^{84(a)}Departamento de Engenharia Elétrica, Universidade Federal de Juiz de Fora (UFJF), Juiz de Fora; ^(b)Universidade Federal do Rio De Janeiro COPPE/EE/IF, Rio de Janeiro; ^(c)Instituto de Física, Universidade de São Paulo, São Paulo; ^(d)Rio de Janeiro State University, Rio de Janeiro; ^(e)Federal University of Bahia, Bahia; Brazil.
- ⁸⁵KEK, High Energy Accelerator Research Organization, Tsukuba; Japan.
- ⁸⁶Graduate School of Science, Kobe University, Kobe; Japan.
- ^{87(a)}AGH University of Krakow, Faculty of Physics and Applied Computer Science, Krakow; ^(b)Marian Smoluchowski Institute of Physics, Jagiellonian University, Krakow; Poland.
- ⁸⁸Institute of Nuclear Physics Polish Academy of Sciences, Krakow; Poland.
- ⁸⁹Faculty of Science, Kyoto University, Kyoto; Japan.
- ⁹⁰Research Center for Advanced Particle Physics and Department of Physics, Kyushu University, Fukuoka ; Japan.
- ⁹¹L2IT, Université de Toulouse, CNRS/IN2P3, UPS, Toulouse; France.
- ⁹²Instituto de Física La Plata, Universidad Nacional de La Plata and CONICET, La Plata; Argentina.
- ⁹³Physics Department, Lancaster University, Lancaster; United Kingdom.
- ⁹⁴Oliver Lodge Laboratory, University of Liverpool, Liverpool; United Kingdom.
- ⁹⁵Department of Experimental Particle Physics, Jožef Stefan Institute and Department of Physics, University of Ljubljana, Ljubljana; Slovenia.
- ⁹⁶School of Physics and Astronomy, Queen Mary University of London, London; United Kingdom.
- ⁹⁷Department of Physics, Royal Holloway University of London, Egham; United Kingdom.
- ⁹⁸Department of Physics and Astronomy, University College London, London; United Kingdom.
- ⁹⁹Louisiana Tech University, Ruston LA; United States of America.
- ¹⁰⁰Fysiska institutionen, Lunds universitet, Lund; Sweden.
- ¹⁰¹Departamento de Física Teórica C-15 and CIAFF, Universidad Autónoma de Madrid, Madrid; Spain.
- ¹⁰²Institut für Physik, Universität Mainz, Mainz; Germany.
- ¹⁰³School of Physics and Astronomy, University of Manchester, Manchester; United Kingdom.
- ¹⁰⁴CPPM, Aix-Marseille Université, CNRS/IN2P3, Marseille; France.
- ¹⁰⁵Department of Physics, University of Massachusetts, Amherst MA; United States of America.
- ¹⁰⁶Department of Physics, McGill University, Montreal QC; Canada.
- ¹⁰⁷School of Physics, University of Melbourne, Victoria; Australia.
- ¹⁰⁸Department of Physics, University of Michigan, Ann Arbor MI; United States of America.
- ¹⁰⁹Department of Physics and Astronomy, Michigan State University, East Lansing MI; United States of America.
- ¹¹⁰Group of Particle Physics, University of Montreal, Montreal QC; Canada.
- ¹¹¹Fakultät für Physik, Ludwig-Maximilians-Universität München, München; Germany.
- ¹¹²Max-Planck-Institut für Physik (Werner-Heisenberg-Institut), München; Germany.
- ¹¹³Graduate School of Science and Kobayashi-Maskawa Institute, Nagoya University, Nagoya; Japan.
- ^{114(a)}Department of Physics, Nanjing University, Nanjing; ^(b)School of Science, Shenzhen Campus of Sun Yat-sen University; ^(c)University of Chinese Academy of Science (UCAS), Beijing; China.
- ¹¹⁵Department of Physics and Astronomy, University of New Mexico, Albuquerque NM; United States of

America.

¹¹⁶Institute for Mathematics, Astrophysics and Particle Physics, Radboud University/Nikhef, Nijmegen; Netherlands.

¹¹⁷Nikhef National Institute for Subatomic Physics and University of Amsterdam, Amsterdam; Netherlands.

¹¹⁸Department of Physics, Northern Illinois University, DeKalb IL; United States of America.

¹¹⁹^(a)New York University Abu Dhabi, Abu Dhabi; ^(b)United Arab Emirates University, Al Ain; United Arab Emirates.

¹²⁰Department of Physics, New York University, New York NY; United States of America.

¹²¹Ochanomizu University, Otsuka, Bunkyo-ku, Tokyo; Japan.

¹²²Ohio State University, Columbus OH; United States of America.

¹²³Homer L. Dodge Department of Physics and Astronomy, University of Oklahoma, Norman OK; United States of America.

¹²⁴Department of Physics, Oklahoma State University, Stillwater OK; United States of America.

¹²⁵Palacký University, Joint Laboratory of Optics, Olomouc; Czech Republic.

¹²⁶Institute for Fundamental Science, University of Oregon, Eugene, OR; United States of America.

¹²⁷Graduate School of Science, Osaka University, Osaka; Japan.

¹²⁸Department of Physics, University of Oslo, Oslo; Norway.

¹²⁹Department of Physics, Oxford University, Oxford; United Kingdom.

¹³⁰LPNHE, Sorbonne Université, Université Paris Cité, CNRS/IN2P3, Paris; France.

¹³¹Department of Physics, University of Pennsylvania, Philadelphia PA; United States of America.

¹³²Department of Physics and Astronomy, University of Pittsburgh, Pittsburgh PA; United States of America.

¹³³^(a)Laboratório de Instrumentação e Física Experimental de Partículas - LIP, Lisboa; ^(b)Departamento de Física, Faculdade de Ciências, Universidade de Lisboa, Lisboa; ^(c)Departamento de Física, Universidade de Coimbra, Coimbra; ^(d)Centro de Física Nuclear da Universidade de Lisboa, Lisboa; ^(e)Departamento de Física, Universidade do Minho, Braga; ^(f)Departamento de Física Teórica y del Cosmos, Universidad de Granada, Granada (Spain); ^(g)Departamento de Física, Instituto Superior Técnico, Universidade de Lisboa, Lisboa; Portugal.

¹³⁴Institute of Physics of the Czech Academy of Sciences, Prague; Czech Republic.

¹³⁵Czech Technical University in Prague, Prague; Czech Republic.

¹³⁶Charles University, Faculty of Mathematics and Physics, Prague; Czech Republic.

¹³⁷Particle Physics Department, Rutherford Appleton Laboratory, Didcot; United Kingdom.

¹³⁸IRFU, CEA, Université Paris-Saclay, Gif-sur-Yvette; France.

¹³⁹Santa Cruz Institute for Particle Physics, University of California Santa Cruz, Santa Cruz CA; United States of America.

¹⁴⁰^(a)Departamento de Física, Pontificia Universidad Católica de Chile, Santiago; ^(b)Millennium Institute for Subatomic physics at high energy frontier (SAPHIR), Santiago; ^(c)Instituto de Investigación Multidisciplinario en Ciencia y Tecnología, y Departamento de Física, Universidad de La Serena; ^(d)Universidad Andres Bello, Department of Physics, Santiago; ^(e)Instituto de Alta Investigación, Universidad de Tarapacá, Arica; ^(f)Departamento de Física, Universidad Técnica Federico Santa María, Valparaíso; Chile.

¹⁴¹Department of Physics, University of Washington, Seattle WA; United States of America.

¹⁴²Department of Physics and Astronomy, University of Sheffield, Sheffield; United Kingdom.

¹⁴³Department of Physics, Shinshu University, Nagano; Japan.

¹⁴⁴Department Physik, Universität Siegen, Siegen; Germany.

¹⁴⁵Department of Physics, Simon Fraser University, Burnaby BC; Canada.

- ¹⁴⁶SLAC National Accelerator Laboratory, Stanford CA; United States of America.
- ¹⁴⁷Department of Physics, Royal Institute of Technology, Stockholm; Sweden.
- ¹⁴⁸Departments of Physics and Astronomy, Stony Brook University, Stony Brook NY; United States of America.
- ¹⁴⁹Department of Physics and Astronomy, University of Sussex, Brighton; United Kingdom.
- ¹⁵⁰School of Physics, University of Sydney, Sydney; Australia.
- ¹⁵¹Institute of Physics, Academia Sinica, Taipei; Taiwan.
- ¹⁵²^(a)E. Andronikashvili Institute of Physics, Iv. Javakhishvili Tbilisi State University, Tbilisi; ^(b)High Energy Physics Institute, Tbilisi State University, Tbilisi; ^(c)University of Georgia, Tbilisi; Georgia.
- ¹⁵³Department of Physics, Technion, Israel Institute of Technology, Haifa; Israel.
- ¹⁵⁴Raymond and Beverly Sackler School of Physics and Astronomy, Tel Aviv University, Tel Aviv; Israel.
- ¹⁵⁵Department of Physics, Aristotle University of Thessaloniki, Thessaloniki; Greece.
- ¹⁵⁶International Center for Elementary Particle Physics and Department of Physics, University of Tokyo, Tokyo; Japan.
- ¹⁵⁷Department of Physics, Tokyo Institute of Technology, Tokyo; Japan.
- ¹⁵⁸Department of Physics, University of Toronto, Toronto ON; Canada.
- ¹⁵⁹^(a)TRIUMF, Vancouver BC; ^(b)Department of Physics and Astronomy, York University, Toronto ON; Canada.
- ¹⁶⁰Division of Physics and Tomonaga Center for the History of the Universe, Faculty of Pure and Applied Sciences, University of Tsukuba, Tsukuba; Japan.
- ¹⁶¹Department of Physics and Astronomy, Tufts University, Medford MA; United States of America.
- ¹⁶²Department of Physics and Astronomy, University of California Irvine, Irvine CA; United States of America.
- ¹⁶³University of Sharjah, Sharjah; United Arab Emirates.
- ¹⁶⁴Department of Physics and Astronomy, University of Uppsala, Uppsala; Sweden.
- ¹⁶⁵Department of Physics, University of Illinois, Urbana IL; United States of America.
- ¹⁶⁶Instituto de Física Corpuscular (IFIC), Centro Mixto Universidad de Valencia - CSIC, Valencia; Spain.
- ¹⁶⁷Department of Physics, University of British Columbia, Vancouver BC; Canada.
- ¹⁶⁸Department of Physics and Astronomy, University of Victoria, Victoria BC; Canada.
- ¹⁶⁹Fakultät für Physik und Astronomie, Julius-Maximilians-Universität Würzburg, Würzburg; Germany.
- ¹⁷⁰Department of Physics, University of Warwick, Coventry; United Kingdom.
- ¹⁷¹Waseda University, Tokyo; Japan.
- ¹⁷²Department of Particle Physics and Astrophysics, Weizmann Institute of Science, Rehovot; Israel.
- ¹⁷³Department of Physics, University of Wisconsin, Madison WI; United States of America.
- ¹⁷⁴Fakultät für Mathematik und Naturwissenschaften, Fachgruppe Physik, Bergische Universität Wuppertal, Wuppertal; Germany.
- ¹⁷⁵Department of Physics, Yale University, New Haven CT; United States of America.
- ^a Also Affiliated with an institute covered by a cooperation agreement with CERN.
- ^b Also at An-Najah National University, Nablus; Palestine.
- ^c Also at Borough of Manhattan Community College, City University of New York, New York NY; United States of America.
- ^d Also at Center for Interdisciplinary Research and Innovation (CIRI-AUTH), Thessaloniki; Greece.
- ^e Also at CERN, Geneva; Switzerland.
- ^f Also at CMD-AC UNEC Research Center, Azerbaijan State University of Economics (UNEC); Azerbaijan.
- ^g Also at Département de Physique Nucléaire et Corpusculaire, Université de Genève, Genève; Switzerland.

- h* Also at Departament de Física de la Universitat Autònoma de Barcelona, Barcelona; Spain.
- i* Also at Department of Financial and Management Engineering, University of the Aegean, Chios; Greece.
- j* Also at Department of Physics, California State University, Sacramento; United States of America.
- k* Also at Department of Physics, King's College London, London; United Kingdom.
- l* Also at Department of Physics, Stanford University, Stanford CA; United States of America.
- m* Also at Department of Physics, Stellenbosch University; South Africa.
- n* Also at Department of Physics, University of Fribourg, Fribourg; Switzerland.
- o* Also at Department of Physics, University of Thessaly; Greece.
- p* Also at Department of Physics, Westmont College, Santa Barbara; United States of America.
- q* Also at Faculty of Physics, Sofia University, 'St. Kliment Ohridski', Sofia; Bulgaria.
- r* Also at Hellenic Open University, Patras; Greece.
- s* Also at Imam Mohammad Ibn Saud Islamic University; Saudi Arabia.
- t* Also at Institució Catalana de Recerca i Estudis Avançats, ICREA, Barcelona; Spain.
- u* Also at Institut für Experimentalphysik, Universität Hamburg, Hamburg; Germany.
- v* Also at Institute for Nuclear Research and Nuclear Energy (INRNE) of the Bulgarian Academy of Sciences, Sofia; Bulgaria.
- w* Also at Institute of Applied Physics, Mohammed VI Polytechnic University, Ben Guerir; Morocco.
- x* Also at Institute of Particle Physics (IPP); Canada.
- y* Also at Institute of Physics, Azerbaijan Academy of Sciences, Baku; Azerbaijan.
- z* Also at Institute of Theoretical Physics, Ilia State University, Tbilisi; Georgia.
- aa* Also at National Institute of Physics, University of the Philippines Diliman (Philippines); Philippines.
- ab* Also at Technical University of Munich, Munich; Germany.
- ac* Also at The Collaborative Innovation Center of Quantum Matter (CICQM), Beijing; China.
- ad* Also at TRIUMF, Vancouver BC; Canada.
- ae* Also at Università di Napoli Parthenope, Napoli; Italy.
- af* Also at University of Colorado Boulder, Department of Physics, Colorado; United States of America.
- ag* Also at Washington College, Chestertown, MD; United States of America.
- ah* Also at Yeditepe University, Physics Department, Istanbul; Türkiye.
- * Deceased